Trace Level Impurity Quantitation and the Reduction of Calibration Uncertainty for Secondary Ion Mass Spectrometry Analysis of Niobium Superconducting Radio Frequency Materials

Jonathan Angle

Dissertation submitted to the faculty of the Virginia Polytechnic Institute and State University in partial fulfillment of the requirements for the degree of

Doctor of Philosophy

In

Materials Science and Engineering

Michael J. Kelley, Chair
Fred A. Stevie
Charles E. Reece
William T. Reynolds Jr.
Mitsuhiro Murayama

March 14, 2022
Blacksburg, Virginia, USA

Keywords: Materials Characterization, SIMS, SRF, Nitrogen Doping, Oxygen Alloying

Trace Level Impurity Quantitation and the Reduction of Calibration Uncertainty for Secondary Ion Mass Spectrometry Analysis of Niobium Superconducting Radio Frequency Materials

ABSTRACT

Over the last decade, the interstitial alloying of niobium has proven to be essential for enabling superconducting radiofrequency (SRF) cavities to operate more efficiently at high accelerating gradients. The discovery of "nitrogen doping" was the first readily accessible avenue of interstitial alloying in which researchers saw an increase in cavity performance. However, the serendipitous nature of the discovery led to additional research to fundamentally understand the physics behind the increase in cavity performance. This knowledge gap is bridged by materials characterization. Secondary ion mass spectrometry (SIMS) is a characterization technique which has become a staple of SRF cavity characterization that details elemental concentration profiles as a function of depth into the niobium surface with submicron resolution.

SIMS has been widely used by the semiconductor industry for decades but has found less application in other fields due to the difficulty to produce reproducible data for polycrystalline materials. Much effort has been given to reduce the uncertainty of SIMS results to as low as 1% - 2% for single crystals. However, less attention has been given to polycrystalline materials with uncertainty values reported between 40% - 50% The sources of uncertainty were found to be deterministic in nature and therefore could be mitigated to produce reliable results. This dissertation documents the efforts to reduce SIMS method uncertainty which has been further used to solve mysteries regarding the characterization of SRF cavities which include predictive modeling of oxygen diffusion as well as the identification of contaminants resulting from cavity furnace treatments.

Trace Level Impurity Quantitation and the Reduction of Calibration Uncertainty for Secondary Ion Mass Spectrometry Analysis of Niobium Superconducting Radio Frequency Materials

General Audience Abstract

Particle accelerators find many uses in society in which their complexity depends on their intended purpose. These purposes vary from projecting an image as in cathode ray tube (CRT) TVs, to creating high energy x-rays for life saving cancer treatments, to researching the very fundamental principles of science and physics. The later uses particle accelerators which are very large, spanning multiple miles, and run at extremely high energies. To keep operational costs reasonable, these instruments need to run as efficiently as possible. Therefore, superconducting radiofrequency (SRF) niobium cavities are used and are responsible for propulsion of charged particles.

Although, niobium SRF cavities can pass incredibly high currents with very little surface resistance, these high-end particle accelerators push the operational boundaries of efficiency. To improve the efficiency of these cavities, an optimal concentration of impurities, such as oxygen and nitrogen, are added to the niobium surface. The addition of an impurity level that is too high or too low causes the resistance to increase which translates to higher operational costs. Therefore, it is important to accurately determine the concentration of impurities within the niobium and with high depth resolution.

Secondary ion mass spectrometry is a characterization method that uses a primary ion beam to impact the surface of a material to remove atoms at the very surface. The ejected atoms are then ionized into a secondary beam which can then be detected to determine the concentration and to identify the species which was removed. Historically, this instrument has yielded results with 40% - 50% uncertainty for polycrystalline metals, such as niobium, which do not sputter evenly. With SRF cavity performance depending on accurate quantitation of impurities, a more robust method is needed. Therefore, this dissertation identifies issues which cause high uncertainties for polycrystalline materials and in addition offers mitigation strategies to reduce uncertainty to below 10%. These methods were then applied to solve real problems aimed to improve the production of niobium SRF cavities.

Dedicated To:

Life is seldom a clear path forward. I have found this to be true in my own. Looking back, I see so many people who have offered their wisdom, love, friendship, and guidance in helping me to achieve my dreams. It is important to me that I express my gratitude to many responsible for becoming the engineer and man I am today.

I would like to thank my advisor Dr. Michael Kelley. I have not just learned from you what it means to be a good engineer, but you have helped me to improve my communication skills as well as to become more efficient with my time. Most important of all you have shown me what a mentor should look like. I can only hope that one day I can inspire and teach a generation of learners as effectively as you have taught me.

I would also like to thank Dr. Charlie Reece and Fred Stevie. The mentorship you two have provided me is truly invaluable. I have become much more effective as a researcher and SIMS analyst thanks you your weekly commitments to our project.

I would like to name previous professors who strongly influenced me, Dr. Cindy Burkhardt, and Dr. Francis Webster. I have never experienced such enthusiasm for a student's success as I have from these two. It was their belief in me that convinced me to consider graduate school. I owe them so much. I would also like to thank my previous advisor Dr. Johan Foster for taking me under his wing. His advice helped me to survive during a difficult time in grad school.

I could have never wished for a more supportive family. I am truly blessed to have this level of love and encouragement. I was taught valuable life lessons and without the guidance of my family, I'm not sure I could have made it this far. Specifically, I want to thank my mother and father, Cindy and Garry Angle, my stepmother Barbara Angle, and my brother Patrick Angle for always being in my corner.

To Kassandra Nucamendi. You have been here through the ups and downs of graduate school and helped me in keeping a level head during my time here. Your continual encouragement gives me the strength to keep pursing my wildest dreams. Thank you for being a part of this journey.

I want to thank friends and colleagues. There are many more than I can list in this space, but I would like to note a special few who have positively influenced me during my time here at Virginia Tech: Jarret Wright, Roberto McAlister Council Troche, Alex Wensley, Jay Tuggle, Priya Venkatraman, John Will, Eric Lechner and Hesham Elmkharram. I will treasure this phase of my life largely thanks to the positive influences you have had on me.

Contents

Table of Figures

List of Tables

Attributions

Several scientists collaborated on this project which resulted in published articles found in chapters 5 and 6 of this dissertation. At the time of this dissertation presentation, the submission of chapter 7 was in progress. Each collaborator attended weekly meetings to offer intellectual contributions and provided edits for each experimental chapter. The collaborators are listed below:

Jonathan W. Angle- M.S. in Materials Science and Engineering from Virginia Tech, 2018. Ph. D. student in Materials Science and Engineering from Virginia Tech. Primary analyst and author of experimental work.

Michael J. Kelley- Ph. D. in Materials Engineering from Rensselaer Polytechnic Institute, 1966. Professor at William and Mary and Virginia Tech. Applied Research Program Manager at Jefferson Laboratory. Primary source of guidance and advisor to Jonathan W. Angle.

Charles E. Reece- Ph. D. in Physics from Cornell University, 1983. Senior Scientist and SRF group leader at the Thomas Jefferson National Accelerator Facility (JLab).

Fred A. Stevie- M.S. from Vanderbilt University, 1970. Senior Researcher at the Analytical Instrumentation Facility. Characterization expert specialization in Secondary Ion Mass Spectrometry (SIMS), X-ray Photoelectron Spectroscopy (XPS), and Focused Ion Beam (FIB).

Eric M. Lechner- Ph. D. in Physics from Temple University, 2019. Postdoctoral Researcher at the Thomas Jefferson National Accelerator Facility (JLab).

Ari D. Palczewski - Ph. D. in experimental physics from Iowa State University, 2010. Staff Scientist at the Thomas Jefferson National Accelerator Facility (JLab).

Specific contributions for each chapter are as follows:

Chapter 5: Mr. Angle performed the SIMS, EBSD and profilometry analyses and was the primary author for the chapter. Dr. Reece, and Dr. Palczewski provided the electropolished niobium witness samples and implant standards. Mr. Stevie provided guidance on SIMS tuning and conditions as well as suggested conditions for implant standard fabrication. Dr. Kelley assisted with the planning of experiments, data interpretation, and acted as the primary editor for the work.

Chapter 6: Mr. Angle performed the SIMS, FIB, EBSD and profilometry analyses and was the primary author for the chapter. Additionally, Mr. Angle designed the new sample holders in Fusion 360 and performed the simulations associated with this work. Dr. Reece, Dr. Palczewski, and Dr. Lechner provided the electropolished niobium witness samples. Dr. Palczewski was responsible for manufacturing the new sample holder. Mr. Stevie provided the silicon implant standard as well as yielded guidance on the SIMS and FIB conditions used in this project. Dr. Kelley assisted with the planning of experiments, data interpretation, and acted as the primary editor for the work.

Chapter 7: Mr. Angle performed the SIMS and XPS analyses and was the primary author for the chapter. Dr. Lechner performed the SEM and EBSD analysis in this project. Dr. Reece, Dr. Palczewski, and Dr. Lechner Dr. Reece, and Dr. Palczewski coordinated the nitrogen doping and production of witness samples used for this work. Mr. Stevie provided guidance on the SIMS conditions for mass spectral analysis as well as participated in interpreting the results. Dr. Kelley assisted with the planning of experiments, data interpretation, and acted as the primary editor for the work.

Chapter 1: Introduction

Surface properties are important in the selection process of materials for various applications. Consider a hypothetical base material used for boat construction. Ideally, it would be strong, ductile, and cost effective, but perhaps the most significant attribute would be its resistance to corrosion. Aluminum would be a logical choice as it satisfies these requirements. Corrosion resistance in aluminum is the result of a naturally occurring oxide layer at the surface which protects the metal from further oxidation by water, salts, and most acids. Titanium and niobium are similar in that a natural oxide layer exists. Titanium that has been anodized is useful in environments where abrasion is inevitable. Niobium is an excellent superconductor. The recent discovery that the dissolution of the oxide layer and subsequent diffusion of oxygen atoms beneath the surface will enhance the efficiency of its superconductive properties make it the new standard in particle acceleration.

Materials can be further engineered to improve their surface characteristics, but this requires accurate characterization of those properties. Techniques for analysis can vary from visual examination to electron microscopy, measurement of surface roughness, or determination of surface chemical structure with x-ray photoelectron spectroscopy (XPS) or secondary ion mass spectrometry (SIMS). These methods are often complimentary and not considered mutually exclusive. For example, XPS can be uniquely used to non-destructively identify bonding characteristics of a surface, which can be useful for determining oxide layer speciation (i.e. TiO vs. TiO_2). However, x-ray beams are not easy to focus, limiting lateral resolution. Additionally, the detection limit of this technique is limited to roughly 0.1 atomic % or 1000 parts per million (ppm). Analysis via SIMS can

often be challenging and is generally a destructive technique. However, SIMS uses an ion beam which can be focused and is capable of part per billion (ppb) detection limits.

This dissertation largely focuses on using SIMS to investigate the surface concentration profiles of carbon, oxygen, and nitrogen in a niobium matrix. Particle accelerators use niobium superconducting cavities to propel charged particles to high energies. The superconductive properties of niobium allow efficient operation of the accelerator. Oxygen and nitrogen can be alloyed with niobium at the surface in ppm-ppt levels to improve the efficiency of these cavities, while carbon is often a contaminant which can be detrimental to cavity performance. The enhancement is strongly dependent on the concentration of oxygen and nitrogen, making the need for accurate and reliable SIMS a necessity.

SIMS is extensively used by the semi-conductor industry to determine ppm concentrations of impurities. Most commonly, semiconductors are comprised of high purity single crystal silicon which has been doped with an impurity (such as arsenic) to improve the conductive properties of the wafer. The concentration of the impurity can have a profound effect on the electrical properties of the semiconductor. As a result, much research related to improving SIMS is geared toward single crystal silicon matrices. SIMS performed on polycrystalline materials adds complexity to SIMS quantification as differences in sputter rates and ion yields must be considered.

This thesis will act as a comprehensive investigation into the sources of uncertainty which cause inaccuracies in data output and instrument calibration for polycrystalline materials. Although niobium was chosen as the principal material for observation, the findings are intended to guide other materials scientists and SIMS users on the mitigation

steps to reduce the sources of error which propagate into attained concentration quantification for polycrystalline materials, particularly metals.

1.1 Research Hypotheses

Trace level addition of impurities for material alloying is becoming progressively significant for modern science and technology. As impurity concentrations reach ppm levels, accurate and precise quantification of these values becomes increasingly difficult. This proposal intends to provide a fundamental understanding to the causes of SIMS uncertainty. We suggest the analysis of nitrogen and oxygen in niobium. Our hypotheses are:

Hypothesis 1: Uncertainties have been deterministic in nature. It is hypothesized that the cause of uncertainty is a result of grain orientation effects, sample topography and instrumental artifacts. It is also hypothesized that these factors which add error to analyses can be controlled to reduce the uncertainty.

Hypothesis 2: Oxygen and nitrogen in niobium are suitable for such a study. It is hypothesized that once mitigation measures have been developed, SIMS can be used to determine the concentrations of various conditions which affects the diffusion of oxygen and nitrogen within the niobium lattice.

Hypothesis 3: Mitigation measures which increase the quantitative precision of ppm detection of impurities can be used for real world applications. It is hypothesized that this technique can be used to study the furnace environment to identify and quantify contaminants during the nitrogen doping and oxygen alloying process.

Chapter 2 Background

2.1 Intro to Particle Accelerators

Particle accelerators are an important class of instruments in which an electric field is used to propel charged particles. These instruments find uses from radiotherapy and the production of unstable isotopes for cancer treatments to real-time imaging of proteins. Most of these instruments operate as normal conducting instruments as the desired purpose of the equipment does not necessitate exceedingly high-power operation. However, the high energy accelerators used for cutting edge physics research, such as the Large Hadron Collider (LHC), the Continuous Electron Beam Accelerator Facility (CEBAF), the European X-Ray Free Electron Laser (X-FEL), and Linac Coherent Light Source (LCLS II) require operation as superconducting machines which employ the use of superconducting radiofrequency (SRF) technology.

2.2 Evolution of Modern Particle Accelerators

In 1911, Earnest Rutherford's "gold foil experiment" was performed which used the emission of alpha particles to pass through a gold foil[1]. The experiment for the first time showed that the atom was not one solid particle but existed as a very small positively charged nucleus surrounded by much larger region in which negatively charged subatomic particles (electrons) move. George Gamow's 1928 discovery of nuclear decay via alpha particle emission led Rutherford to believe that 500 MeV energy could be sufficient energy to split a lithium atom, allowing further studies of the nucleus. Rutherford pursued this by collaborating with Crockcroft and Walton to create a generator capable of 700 MeV, and

thus the birth of the first high energy particle accelerator[2-5]. This accelerator consisted of metal biased tubes housed in a larger evacuated glass tube. The metal tubes were discontinuous to allow for subsequent metal tubes to add to the accelerating power. In 1932, this invention was used to split the lithium atom using a 400 MeV accelerated proton beam and Crockroft and Walton were awarded the Nobel Prize in 1951[5].

In 1924 G. Ising proposed that a radio frequency generator could also achieve particle acceleration by using a resonant radio wave to create an oscillating electric field to propel particles[6]. Later in 1927 Rolf Wideröe showed proof of concept and designed the first rf particle accelerator but achieved only 50 keV accelerating gradient[7, 8]. The design showed that sequential baffles in a hollow cavity would cause an additive effect to the accelerating gradient. The scale needed to create a linear accelerator (linac) at this time was difficult to achieve. Therefore, a cyclic version, called the cyclotron, was created by Ernest Lawrence in 1931 to solve this dilemma[9, 10]. The design was improved to where 5 MeV was achieved by 1935[5].

As the designs improved over the next several decades, it was realized that the current technology had a limit. Further increasing the power of the accelerators led to power losses and heat dissipation into the cavity walls, making higher gradient usage cost prohibitive. In the 1960's Stanford University experimented with using superconducting radio frequency (SRF) cavities to replace copper RF cavities[11]. By 1977 Stanford developed the first superconducting accelerator. The accelerator consisted of a 27 meter linac using a series of seven-celled niobium SRF cavities. Since then, a worldwide effort to improve niobium SRF technology was enacted to where now Nb SRF cavities are approaching their physics limits.

2.3 Niobium SRF Cavities

Modern particle accelerators are comprised of a chain of SRF cavities which are responsible for propelling the charged particles to high energies[11]. The cavities use an injected radio wave at a resonant frequency to build up high electromagnetic field within the cavity. Accelerator structures are typically designed such that the rf phase change during the particle transit time through one cell corresponds to 180 degrees, so that negatively charged particles always encounter positive electric fields, and thus gain energy. An ionization source injects charged particles into the cavity in pulses corresponding to arbitrary submultiples of the resonant frequency. Each cavity in the series provides an additive increase in energy when all drive phases are tightly synchronized. Such linear accelerators can be arbitrarily long as needed to suit the need, or folded on itself to recirculated the beam several times through the same linac, as is done in CEBAF.

The performance of these cavities is described by the quality factor (Q_0), which is defined as the ratio of stored energy to energy lost in 1 RF period. The energy loss is usually a result of power dissipated due to surface resistance of the cavities. Typical quality factors for normal conducting copper cavities are $\approx 10^4$ [11]. Switching to niobium SRF cavities, the quality factor can be improved to $\approx 10^{10}$ but requires operation at liquid helium temperatures, (typically 2.0 - 4.2K). Even with the additional and substantial cryogenic cost of operating at 2 K, niobium SRF cavities are more efficient and can operate at much higher accelerating gradients than copper RF cavities. New models of linacs require continuous wave (CW) operation, in which the cavities are always powered on as opposed to the XFEL which uses high powered pulsed rf sources for higher gradient operation [12]. Economic viability to run in CW increasingly requires the cavities have low loss, meaning less heat loss into the cavity walls.

2.4 Superconductivity and Cryogenics of Nb SRF Cavities

Superconductors are a class of materials which are able to pass exceptionally high electrical currents at the surface of the material when below some critical temperature (T_c) and magnetic field (B_c). For niobium the T_c is 9.3 K[13]. However, the performance efficiency of the niobium SRF cavities is improved with even colder temperatures. The target operational temperature for most Nb SRF cavities is 2 K[14, 15].

To maintain a temperature of 2 K, the niobium SRF cavities are housed in cryomodules, in which the cavities are bathed in liquid helium. The liquid helium is continually produced and cooled by a cryo-plant in which any helium boiled off in the process is cooled back to its liquid state in a closed loop process. Production of liquid helium is expensive and substantial cost is required to maintain the cryo-plants[16]. Therefore, scientists around the globe are collaborating on methods to reduce cost and to increase the efficiency of particle accelerator operation.

2.5 Nitrogen Doping

By the 2000's extensive progress to improve the performance of Nb SRF cavities had been achieved. Methods to develop higher performing cavities with higher purity niobium, with cleaner processes and with smoother surface finishes were all essential in developing niobium SRF cavities which could operate at accelerating gradients of more than 40 MV/m. However, operation at higher accelerating gradients causes the cavities to operate less efficiently (Q-Slope), meaning a decrease in the quality factor (Figure 1). As a result, the cavity wall heats up non-linearly leading to increased refrigeration costs. The result is increased capital and operating costs for the required cryogenic system for such an accelerator [16]. To further reduce operational costs a new material or other surface

modifications was needed, which led to the investigation of nitrogen doping of Nb SRF cavities.

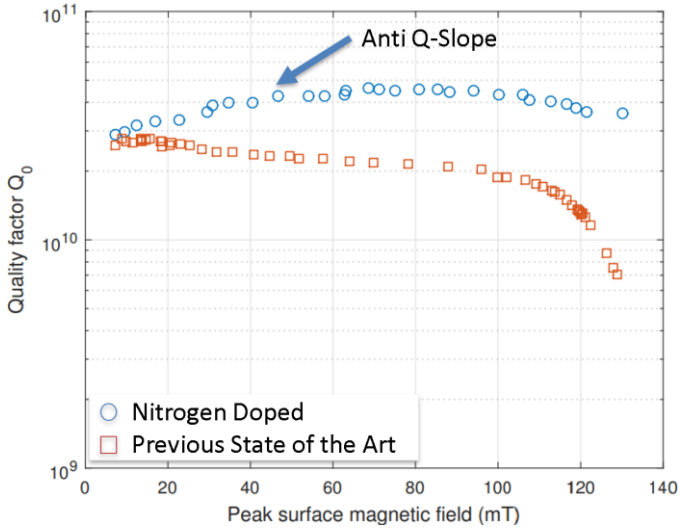

Figure 1. Cavity performance plots for a state-of-the-art 1.3 GHz niobium cavity (red) and a similar cavity having received nitrogen doping treatment cavity (blue). The nitrogen doped cavity is capable of operating more efficiently (Q_o) at higher accelerating gradients. (~66% lower losses at 120 mT, for example) (Reproduced with permission from Maniscalco et. al 2017) [17]

Nitrogen doping is a process which was serendipitously discovered in 2013 at Fermi National Accelerator Laboratory (Fermilab)[18-20]. Their researchers were investigating the potential of using NbN as a surface treatment to improve cavity performance. The nitride coating was found to be detrimental to cavity performance and the nitrides were removed to repurpose the cavity. Following the nitride removal by shallow electropolish, the performance properties of the cavity was reevaluated and found that the quality factor improved by a factor of four[18]. This effect was then confirmed at Jefferson Lab (JLab) and Cornell. By 2015 the Linac Coherent Light Source II (LCLS II) project was proposed

to construct a linear accelerator as SLAC which would utilize nitrogen doped cavities[12, 15, 21]. Construction of this accelerator is nearing completion.

Nitrogen doping consists of heating the cavities to a high temperature, typically 800C,in vacuum[20]. After several hours annealing time, a low pressure stream of nitrogen gas is supplied while at 800C for a few additional minutes. Nitrogen reacts with the surface niobium forming niobium nitrides and also diffuses a few microns into the surface. After cooldown, the nitrides are subsequently removed via electropolishing, leaving behind nitrogen which has diffused into the interstitial sites of the niobium lattice forming an alloy. The depth to which it diffuses and with what concentration profile is dependent on the doping recipe chosen and local conditions. This gradient in nitrogen concentration is inversely proportional to the electron mean free path which is the distance an electron can travel before it interacts with an impurity (Figure 2)[17]. The mean free path has another relationship which states as you decrease the mean free path from the clean limit (no impurities) the surface resistance of typical superconductors also decreases (Figure 3)[16]. This also agrees with the BCS theory prediction. However, increasing the impurity content too much causes the resistance to increase after some critical concentration is reached. Reducing the mean free path yields an anti-Q slope, which suggests that with increased nitrogen content, cavities are more efficient when operating at higher accelerating gradients (Figure 4)[17]. Therefore, these parameters are controlled by the nitrogen concentration which can be tuned by removing the surface layer until the desired nitrogen concentration is met.

The high temperature furnace environment provides an opportunity for other unwanted contaminants to also adhere to the surface which can prevent nitride growth[22].

Other interstitials such as carbon are almost always present as contaminants in some form and cause nitrogen to compete for interstitial spaces which makes tuning the overall interstitial content difficult. Because the extent of contamination is unknown, performance tests can yield poor results that appear mysterious to cavity production facilities. Over the last decade the process has been continually refined to produce more and more cavities with fewer failing specifications. However, the cause and the extent of contamination has not been fully studied.

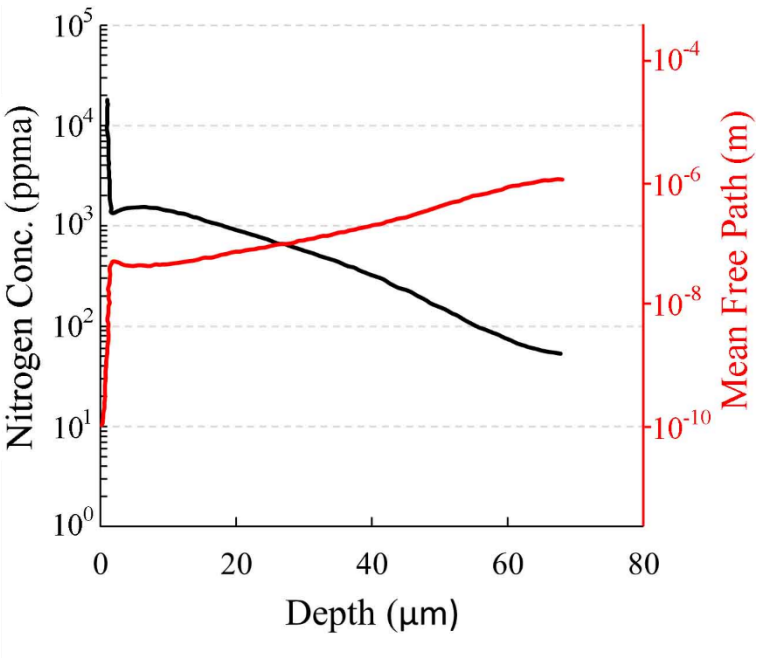

Figure 2. Plot showing the inverse correlation of nitrogen concentration to the mean free path. The addition of nitrogen into the niobium lattice reduces the distance an electron can travel before it interacts with an impurity. [16]

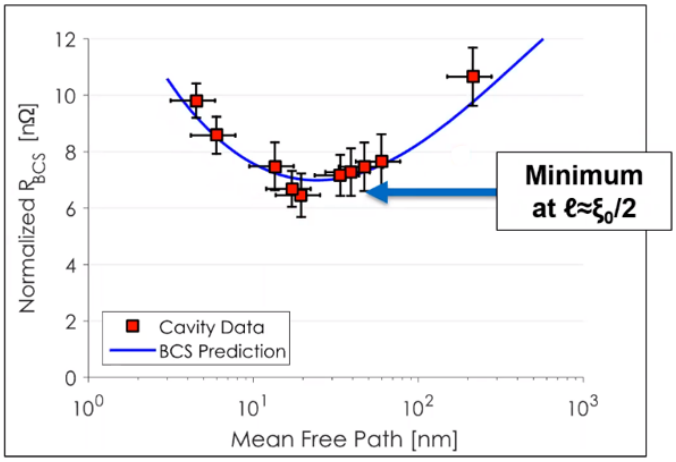

Figure 3. Dependency of the BCS surface resistance to the mean free path. The data suggests that a critical nitrogen concentration exists which will minimize the surface resistance of niobium. (Reproduced with permission from Maniscalco et. al 2017) [17]

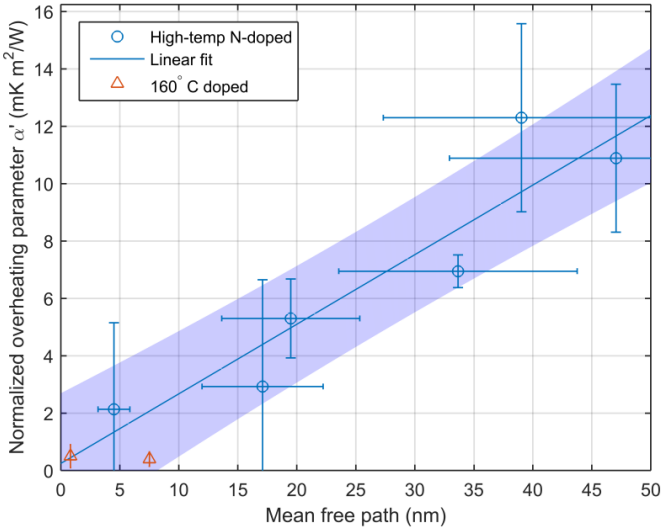

Figure 4. Plot correlating the overheating parameter to the mean free path. The data suggests that increasing the nitrogen content will increase the anti Q slope, meaning the cavities will operate more efficiently with increased accelerating gradients as a result of nitrogen content. (Reproduced with permission from Maniscalco et. al 2017) [17]

2.6 Oxygen Alloying

Oxygen alloying is emerging as a promising technique which could replace nitrogen doping as the new state of the art. Posen et. al. 2020 [23] reported that at lower temperature baking oxygen could diffuse into the interstitial sites fed by an external source of oxygen. The results showed an enhancement in the quality factor. However, the authors were unsure of oxygen's involvement in the increase in cavity performance. In Ito et. al. 2021 [24] KEK determined cavity performances by varying the furnace baking of niobium up to 800^{o}C. It reported that lower temperature baking at 300^{o} C resulted in higher quality factors in which the authors hypothesized that oxygen diffusion was responsible. The quality factor enhancement via oxygen diffusion was confirmed in Lechner et. al 2021 [25] where it was shown that diffusion profiles could be simulated based on the furnace temperature and baking time. We showed that oxygen migration at these low temperatures could be predicted and modeled. SIMS depth profiles showed that the predictions could be replicated experimentally.

Oxygen alloying is an attractive alternative to nitrogen doping because the technique uses the dissolution of the oxide layer at temperatures from 120^{o} C - 300^{o} C to diffuse oxygen into the interstitial sites of the niobium lattice. Oxygen (28 kcal/mol) has a lower activation energy than carbon (34 kcal/mol) and nitrogen (39 kcal/mol). Therefore, by keeping the temperature lower, the diffusibility of carbon and nitrogen is negligible which selectively makes oxygen the primary diffusant (Figure 5). A major challenge with nitrogen doping was the lack of control to selectively diffuse nitrogen into the bulk which makes predictive modeling challenging. Fortunately, a model for oxygen dissolution and diffusion was previously established.

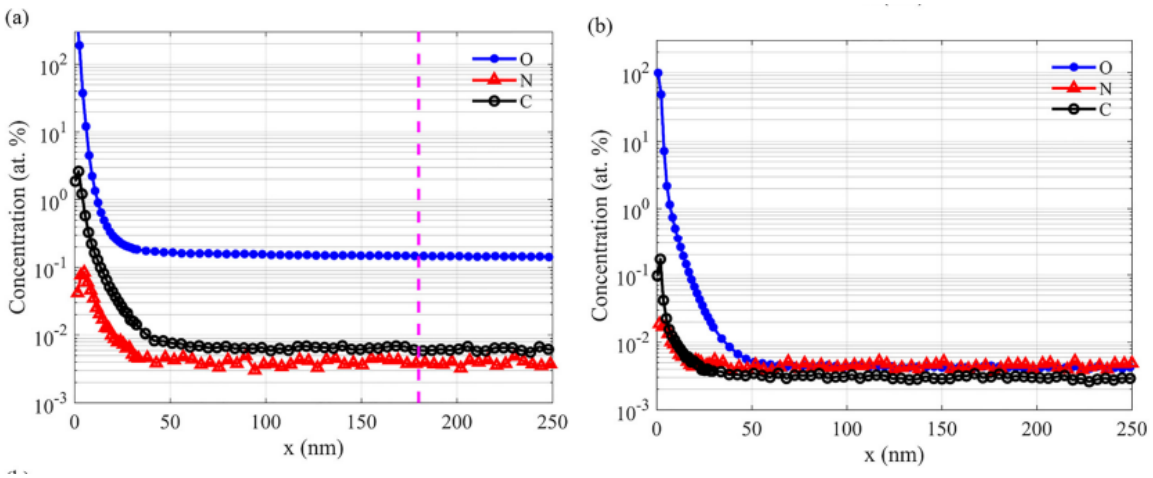

Figure 5 SIMS depth profiles of carbon, oxygen, and nitrogen for (a) an oxygen alloyed sample processed at 300°C for 2.6 hrs and (b) an electropolished niobium sample without additional heat treatments. The data shows the oxygen content can be selectively diffused using the oxygen alloying process. (Reproduced with permission from Lechner et. al 2017) [25]

Ciovati developed an oxygen diffusion model that included the effects of finite source near surface interstitial oxygen as well as the niobium pentoxide diffusion and dissolution[26]. The focus of this study was to investigate oxygen diffusion behavior at temperatures between 90°C and 200°C. Lechner et. al. 2021 further refined the model to include processing temperatures up to 350°C as well as to study the source term as it was previously unexplored. The validity of theoretical modeling was verified by using SIMS to experimentally observe the diffusion of oxygen at various baking conditions (Figure 6). Well quantified SIMS depth profiles from different conditions could all be fit with a single diffusion model with parameters substantiated by other works.

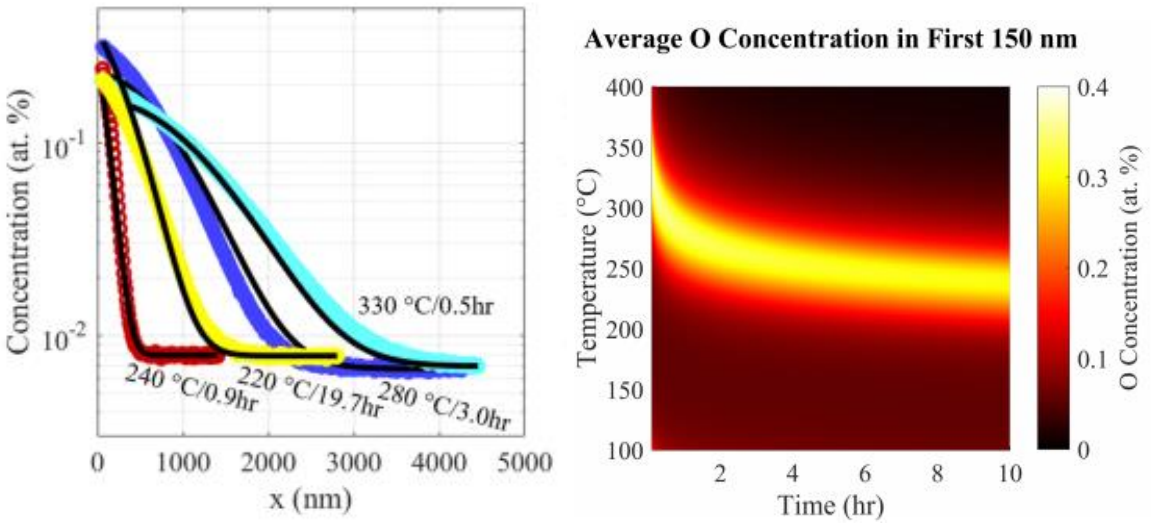

Figure 6. SIMS depth profiles of oxygen alloyed as compared with the theoretical modelling for the oxide layer dissolution and diffusion (black lines). (b) A series of experimental baking procedures, with varied baking temperatures and times, were tested resulting in a predictive model which allows for the concentration of oxygen to be tuned. (Reproduced with permission from Lechner et. al 2017)[25]

2.7 Characterization of SRF Materials.

As mentioned in previous sections, the concentration of near surface impurities can have profound effects on the performance of SRF cavities. Some impurities, such as nitrogen and oxygen, are intentionally added in very low concentrations to improve SRF cavity performance. Other impurities, such as carbon and metallic contaminants, can prevent surface nitrides from forming, cause nitrogen and oxygen to compete for interstitial space, form normal conducting pockets on the cavity (quenching), and other effects which have not yet been fully studied. Thus, it is imperative to examine the surface concentration of impurities and monitor the diffusional behavior as a function of depth. SIMS is perhaps the most effective tool to monitor the impurity concentrations as the technique can easily achieve ppm detection limits. Also, the depth profiling function allows for the concentration

to be monitored as a function of depth with nanometer depth resolution for dynamic SIMS and sub-angstrom depth resolution possible for Time-of-Flight SIMS. These techniques are covered in the next chapter in greater detail.

Chapter 3 Secondary Ion Mass Spectrometry (SIMS)

3.1 Motivation for SIMS

Secondary Ion Mass Spectrometry (SIMS) is a technique which uses the bombardment of a primary ion source to erode the surface of a solid sample in a process called sputtering[27, 28]. Much of the eroded material is ionized and extracted into a secondary ion beam the contents of which are sorted by mass/charge ratio and then detected using a mass spectrometer (Figure 7). The range of detection varies but for the instrumentation used in this study runs from 1 amu to ~1000 amu, thereby making the detection of all elemental species possible[29]. Additionally, SIMS instruments have some of the best detection limits available with parts per billion (ppb) reported[29]. Due to the very low detection limits, coupled with excellent depth resolution, the microelectronics and semiconductor industries are the fields which most commonly utilize SIMS[27, 30, 31].

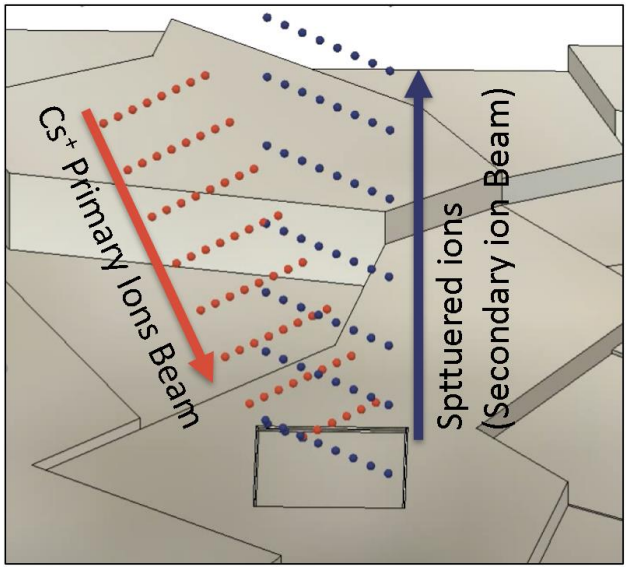

Figure 7. Diagram showing the sputtering mechanism during SIMS analysis. The impact of the Cs^+ primary ions generates a collision cascade which causes some of the atoms at the surface of the material to be ejected as secondary ions. The secondary ions are extracted into a beam and detected by the mass analyzer.

The sputtered material is ejected in the form of neutral atoms as well as negative and positive ions. Biasing the extraction lens allows for the selection of the desired ionic species[32]. This is an important fact as the probability of ion formation is not constant for all species, depending on several factors including the chemical environment of the species as well as the type of primary ion used for bombardment. For example, the probability of ionization is increased, particularly for metals, when sputtering occurs from an oxide as opposed to its metallic form. Therefore, metals are often best detected when using O_2^+ as the primary ion source[29]. Some elements, such as nitrogen, have inherently poor ionization potentials as a monatomic ion. However, polyatomic ions such as CN^- have very good ionization potentials and must be monitored to determine the nitrogen content.

SIMS instruments are often equipped with multiple ion sources, most commonly Cs^+, O_2^+, and O^- to ensure sufficient secondary ion yield for a desired impurity species. Choosing the proper source is crucial for guaranteeing adequate detection and quantification impurities of SIMS. Figure 8 shows the sensitivities, denoted by the relative sensitivity factor (RSF)[30], of various elements for Cs^+ and O_2^+ ion sources. Note that the plots in Figure 8 are for impurities in a silicon matrix. Elemental sensitivity is affected by the bulk sample matrix, commonly referred to as a matrix effect[33]. Therefore, a reference material of a similar matrix must be used to determine the relative sensitivity factor (RSF) used for subsequent quantification of an experimental sample. This topic is discussed in Section 3.3 in greater detail.

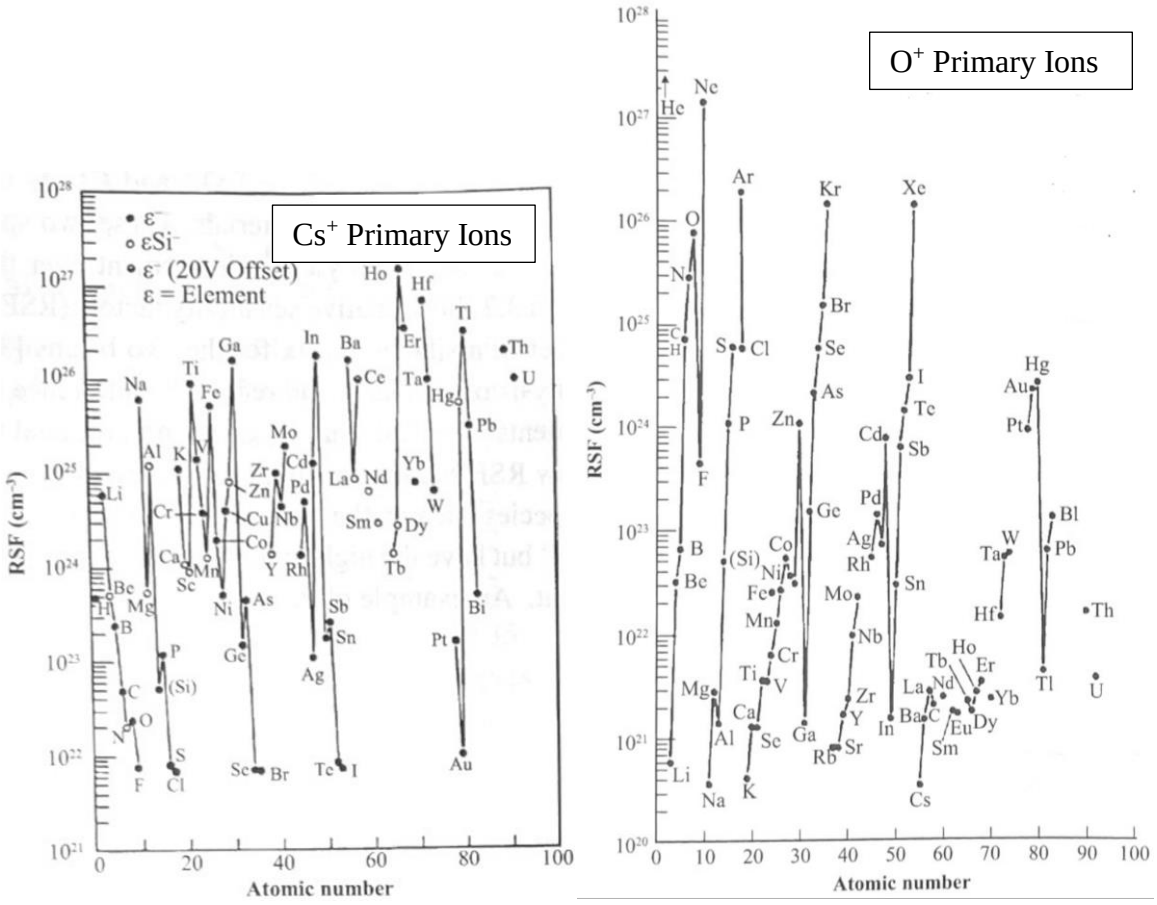

Figure 8. Plots show the relative sensitivity factors as a result of using a (a) Cs^+ primary ion beam and an (b) O_2^+ primary ion beam. Note carbon, nitrogen and oxygen are better detected using a Cs^+ beam while most metallic species are better detected using an O_2^+ beam. Reproduced with permission from Stevie 2016 [29]

3.2 SIMS Sources

Although many types of ionization sources exist, O_2^+ and Cs^+ ion sources are the most commonly used. This is largely because each of the chemical interactions which take place during ion bombardment which can enhance the positive and negative secondary ion yields respectively [29]. Another commonly used ion source is the liquid metal ion source

which usually consists of gallium. These sources typically have a smaller interaction volume via ion bombardment and provide lower secondary ion yield, making them much more useful for imaging rather than the production of secondary ions. As such these sources are more commonly found on focused ion beams (FIB) and ToF-SIMS for imaging and mapping. The experiments presented in this dissertation were largely performed using the CAMECA 7f geo, which is equipped with O_2^+ and Cs^+ ion sources and these will be described in greater detail.

3.2.1. Cesium Microbeam Source

The cesium microbeam source is commonly used in SIMS applications in which the analysis of electronegative impurities is desired. The cesium is housed in a cylindrical reservoir in the form of cesium carbonate (Cs_2CO_3). Current is applied to a tungsten filament to heat the Cs_2CO_3 to form Cs. The ionized portion of the frit consists of a high work function tungsten frit which is heated to ~1000˚C where the Cs vapor is ionized with near 100% efficiency. Immediately following the ionizer, a potential is applied to an extraction plate to collect the Cs ions into the primary ion beam. The primary ion beam is then focused by a series of lenses and apertures which determine the beam current, beam concentricity, and raster size prior to sample bombardment. An image of a Cesium microbeam source is provided in figure 9.

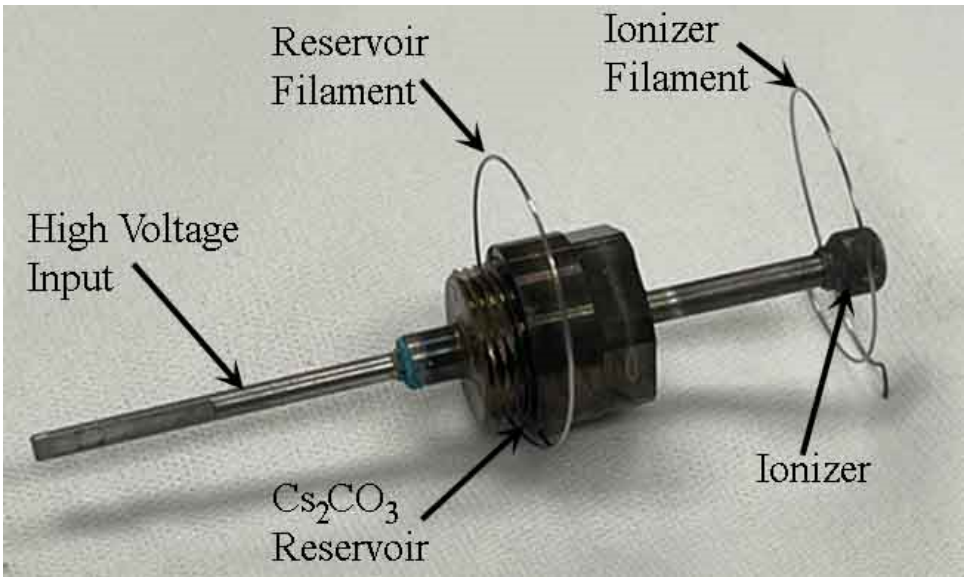

Figure 9. Cesium Microbeam Source.

3.2.2 Duoplasmatron Source

Plasmatrons are ion sources which convert gaseous atoms into an ion beam. In the case of the CAMECA 7f geo, oxygen gas (O_2) is leaked at a low pressure into the interior of a hollow cathode. A schematic is provided in Figure 10. The oxygen pressure is controlled with a regulator. The duoplasmatron source degrades over time[29]. This occurs because the nickel hollow cathode oxidizes and must periodically be cleaned to remove the oxide. A strong electric field is formed between the hollow cathode and the anode which causes a plasma to form[32]. The oxygen plasma is concentrated into a small beam by a magnetic field produced by the intermediate electrode and the coil which also the basis of the name "duoplasmatron"[29, 32]. Following the anode, a biased extraction plate collects the oxygen ions and forms a beam which is directed through the primary column similar to the Cs^+ ion beam. Both O^+ and O_2^+ ions are generated but O_2^+ is selected with a magnetic sector on the

primary column because O_2^+ has less equivalent impact energy and has significantly higher ion current.

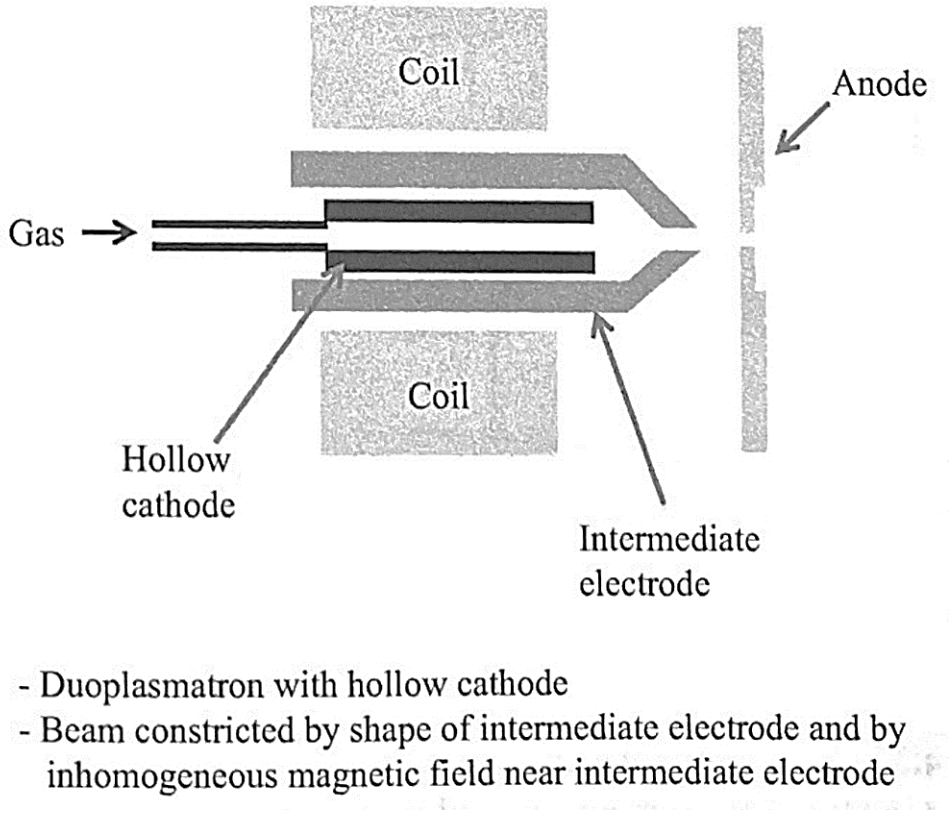

Figure 10. Duoplasmatron Source. Reproduced with permission from Stevie 2016[29].

3.3 Dynamic vs. Static SIMS

SIMS instrumentation can be classified into two categories, static and dynamic SIMS, in which the two most common mass analyzers for these are time of flight (ToF) and magnetic sector analyzers respectively[27]. This classification is based on the damage each of these techniques inflict on a surface during the analysis. Static SIMS uses a low ion bombardment dose with the intent that no ion strikes a location that has already been bombarded. The techniques were deemed capable of determining the "static" chemical state

of a surface. This technique yields fraction of a monolayer depth resolution and excellent lateral resolution making this system ideal for chemical mapping. It is estimated that between 10^{12} - 10^{13} ions/cm^2 is the dose for this analysis and is referred to as the static limit. This can be further understood mathematically, and the time to remove a monolayer can be calculated[27].

$$t_m = \frac{d}{I_p} \times \frac{Ae}{y}$$

Where: t_m is the lifetime of the monolayer, d is the dose of primary ions , I_p is the primary beam current, A is the surface area in terms of atomic density, e is the charge of an electron, and y is the sputter yield of the material. . Typically, static conditions can only be maintained for a short period[27]. The minimal sputtering of atoms however comes at a cost. The reduced number of ions sputtered limits the number of ions detected by the mass spectrometer. In other words, static SIMS does not provide good detection limits.

Dynamic SIMS utilizes a continuous ion beam to bombard a surface. This results in many more ions impacting the surface per analytical cycle, resulting in quicker erosion of a surface. As a result, more secondary ions are ejected, subsequently increasing the number of ions detected. Therefore, dynamic SIMS takes advantage of the destructive nature of the continuous primary beam to increase the detection limit, making dynamic SIMS one of the best analytical methods in terms of sensitivity[31, 34]. The faster sputtering rates allow for analyses to be monitored as a function of depth. This is especially useful for understanding diffusional behaviors of interstitial alloying elements. Although most analyses are a micrometer or less, analyses exceeding 50 μm have been reported making this technique useful for sub-surface analysis as well.

Time of Flight SIMS is the most common type of static SIMS and is named for the type of mass analyzer attached to the instrument. The secondary column consists of an extraction plate which is used to direct the secondary ions through a flight tube in which the ions eventually reach the detector[29]. The ions are separated based on the time it takes for the ions to reach the detector. The flight time can be mathematically expressed as:

$$t = d(m/2qV)^{1/2}$$

Where: *t* is the flight time, *d* is the length of the flight tube, *m* is the mass of the ion, *q* is the charge of the ion, and *V* is the extraction voltage. Uniquely, this allows for all masses to simultaneously be analyzed per each beam pulsation.

Magnetic sector analyzer SIMS are commonly used as dynamic SIMS instruments, but tend to be larger and much more complex schematically than the ToF (Figure 11). For this analyzer, the extraction plate directs the secondary ions through a series of apertures and lenses in which electrostatic and magnetic sectors are used to filter unwanted masses prior to the beam reaching the detector[27, 30, 35]. The beam passes through a flight tube within the magnetic sector in which the magnetic field changes the trajectory of the beam based on the mass to charge ratio of the ionic species. This is expressed mathematically as:

$$m/q = B^2r^2/2V$$

Where: *m* is the mass of the ion, *q* is the charge of the ion, *B* is the magnetic field, *r* is the radius of curvature of the magnetic sector and *V* is the accelerating voltage of the secondary beam. The desired mass is calibrated to allow the secondary beam to pass through the exit slit. The varying trajectories of unwanted masses are blocked and unable to pass through the exit slit. The exit slit is adjustable so that the width of the slit can be tuned to allow only a certain range of masses to be collected and is therefore responsible for the mass resolution

of the instrument. This makes the magnetic sector also very useful to differentiate between species which may have mass interferences. However, only one mass can be selected at a time which makes the collection of a mass spectrum more time consuming than ToF SIMS, thereby making the analysis of the near surface challenging.

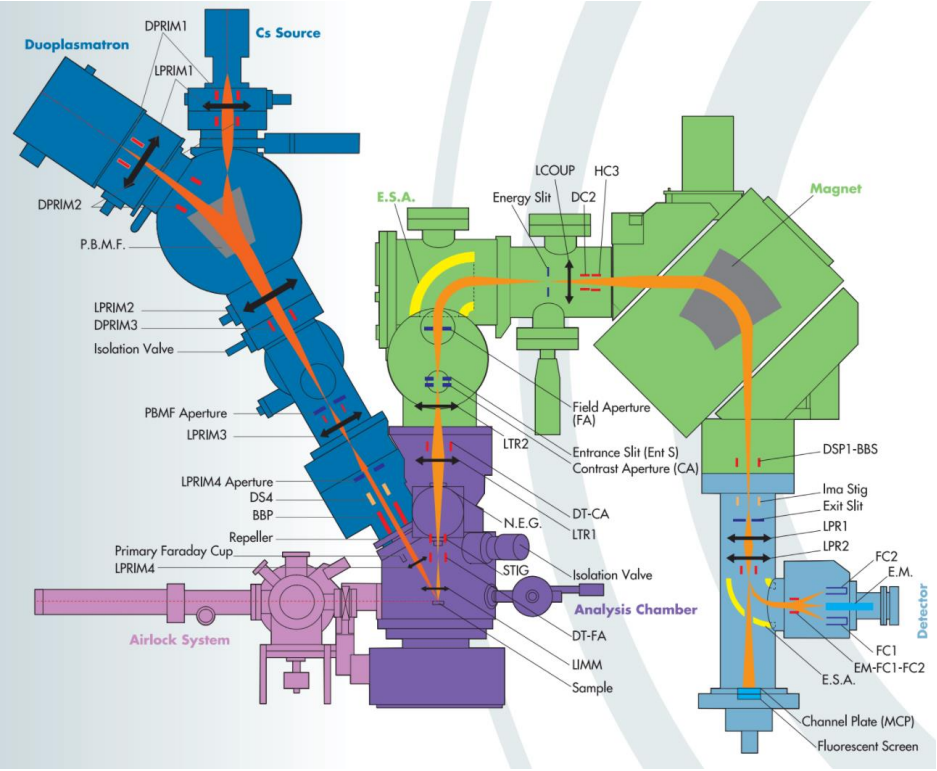

Figure 11 Schematic of the CAMECA 7f Geo. Image courtesy of CAMECA.

3.4 SIMS Quantitation

The detection of the secondary ions is usually done with either a faraday cup or an electron multiplier. Both detectors are necessary as they are responsible for detecting high and low count rates respectively[29]. Both detectors detect ions from the incoming secondary ion beam and display the signal in terms of counts or intensity. To convert from

counts to concentration, a reference standard must first be analyzed to determine a calibration factor called the relative sensitivity factor (RSF)[29].

$$RSF = (\Phi C I_m t)/(z I_s)$$

Where Φ is the implanted dose of the target species (here, *N*), *C* is the number of data collection cycles, I_m is the intensity of the matrix species, *t* time per cycle, *z* is the crater depth, and I_s is the summation of the intensities from the reference species. To convert to concentration, the ratio of impurity counts and matrix counts for an experimental sample is simply multiplied by the RSF. See equation below[29]:

$$Conc = \frac{I_s}{I_m} \times RSF$$

Currently only 5 traceable reference standards exist and 3 are for silicon matrices due to the semiconductor industries' widespread use of SIMS. Therefore, reference standards must be fabricated via ion implantation. This technique implants ions of a known dosage in a matrix matching that of the experimental sample. The energy of the implantation process controls the depth distribution at which the implanted ions will come to rest. The concentration of the dose can sometimes be verified by Rutherford backscattering spectrometry (RBS)[27]. However, the detection of light elements by RBS is poor.

Uncertainty of RSF determination is an issue that has been extensively studied for semiconductor materials. Wilson *et al*. 1991 [36] performed an eight-year study to determine a variety of RSF values in single matrices, but also included multiple analysts, multiple semiconductor type matrices, and varied instrument conditions. RSF variation up to 60% was reported. The uncertainty was hypothesized to have resulted from non-

uniformity of instrumental conditions (i.e. beam current, raster size, different analysts, sample mounting). More tightly controlled experimental conditions were reported to improve the RSF uncertainty between 20% - 30 %, though the exact mitigation measures were often not reported. Laufer *et al*. 2011[37] investigated the RSF values of various impurities for Cu_2O matrix. Most impurities exhibited RSF uncertainties ~25%. However, C, N and Si impurities exhibited uncertainties over 50%. It was suggested that impurities with high secondary ion yields would exhibit less RSF uncertainty. However, a comprehensive study in reduction of RSF uncertainty for polycrystalline materials has not yet been accomplished. Tuggle *et. al. 2017* [38] reported that uncertainty for RSF determination for niobium SRF materials was approximately 40%.

Round robin studies of semiconductor implant standards have reported it is possible to achieve RSF values around between 1-4% [39, 40]. These samples are implanted into single crystal implant standards. Single crystal implant standards are ideal as they minimize effects due to random grain orientations and sputter rate variations which can lead to variations in secondary ion sputter yield. It is generally expected that RSF values can vary between 20% - 60% for polycrystalline materials [36, 39, 41, 42]. However, a comprehensive study regarding the cause and mitigation measures for the high uncertainties has not yet been performed.

3.5 Applications for SIMS

SIMS instrumentation is not especially common when considering the availability of other characterization tools. This is particularly true with dynamic SIMS instruments as they tend to cost more than one million dollars. The semiconductor industry is the top user

of SIMS instruments[31]. As a result, many research topics related to improving SIMS methodology are geared toward semiconductor materials. Most commonly, semiconductors are comprised of high purity single crystal silicon which has been doped with an impurity (for example, arsenic) to improve the conductive properties of the wafer. The concentration of the impurity can have a profound effect on the electrical properties of the semiconductor. The world depends on semiconductors for electronic devices, particularly for chips used for computers, integrated circuits and a myriad of other uses. Thus, it is no surprise that the majority of topics related to SIMS research are related to the semiconductor industry. However other fields also depend on SIMS. The geological field relies on its ability to differentiate various isotope concentrations which can be used for dating purposes. Recently the SRF industry has been using SIMS to analyze the surface of niobium materials to correlate impurity concentrations to the performance SRF cavities for particle acceleration.

SIMS usage in the SRF field is rarely quantitative. In a survey at the Tesla Technology Collaboration meeting (TTC 2020)[43], the majority of SIMS users reported that they did not use implant standards in their study. Some users cited the difficulty to achieve reproducible results and at times the inability to detect implanted species as the reason why implant standards were not used (Figure 12). Therefore, results are mostly reported as a ratio of impurity/matrix counts. Recent discoveries, such as oxygen alloying, depend on accurate reporting of concentration to test the validity of predictive modeling. As such the industry has expressed a desire to reduce RSF uncertainty as much as possible, ideally 10% RSD or below.

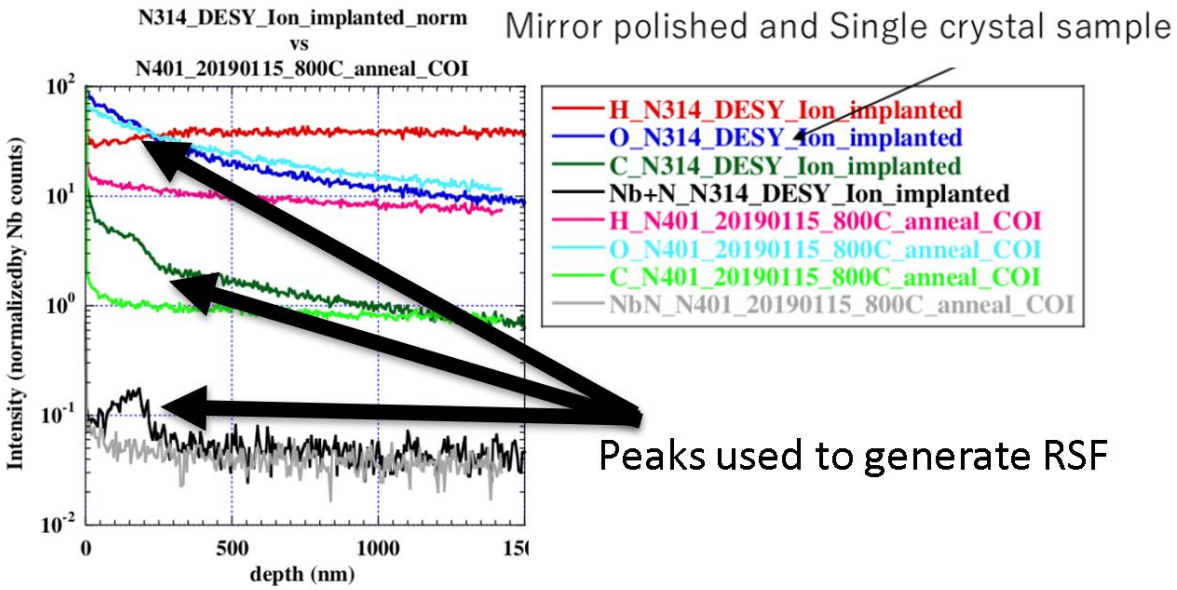

Figure 12. Analysis of an implant standard via ToF SIMS. Note the difficulty in detecting C, N, and O peaks from ion implantation. Data courtesy of Taro Konomi, KEK and Marc Wenskat, DESY.

Chapter 4: Research Topics

SIMS is currently used within the SRF community as a tool to be used to compare data sets, which does not take full advantage of its use as an instrument for quantitative analysis. This is mostly a result of the sources of RSF uncertainty being generally misunderstood. Many of the improvements made for reducing RSF uncertainty are for single crystal specimens due to the heavy usage of SIMS in the semiconductor field. As a result, the effects of sputter rate variation and other grain orientation effects have not yet been evaluated. This thesis aims to identify sources of uncertainty and provide solutions to improve RSF uncertainty to make SIMS a viable tool for the identification and quantitation of ppm level impurities and contaminants.

The topics considered for this study are:

1. Determine implant standard quality and its impact on RSF variation.
2. Determine the effects of surface topography and its influence on RSF deviation. Additionally suggest instrumental parameters which may mitigate topography as a source of RSF deviation.
3. Investigate RSF variation as a function of working distance variation, resulting from sample loading and its source of RSF deviation.
4. Determine if certain grain orientations generate differing RSF values.
5. Determine if SIMS can be used to Identify near surface contamination and to evaluate the effectiveness of furnace caps for niobium SRF cavities.
6. Via use of SIMS determine if oxygen alloying is less susceptible to surface contamination compared with nitrogen alloying (nitrogen doping).

Chapter 5: Advances in Secondary Ion Mass Spectrometry for N-Doped Niobium

Published in Journal of Vacuum Science and Technology B (2021)[30]

Accurate SIMS measurement of nitrogen in niobium relies on the use of closely equivalent standards, made by ion implantation, to convert nitrogen signal intensity to nitrogen content by determination of relative sensitivity factors (RSF). Accurate RSF values for ppm-range nitrogen contents are increasingly critical, as more precision is sought in processes for next-generation superconducting radio-frequency (SRF) accelerator cavities. Factors influencing RSF value measurements were investigated with the aim of reliably attaining better than 10% accuracy in nitrogen concentrations at various depths into the bulk. This has been accomplished for materials typical of SRF cavities at the cost of increased attention to all aspects.

5.1 INTRODUCTION

Particle accelerators are an important family of research instruments which use a microwave electric field in a resonant cavity to propel charged particles to GeV-range energies. The leading machines rely on superconducting radiofrequency (SRF) technology operating at 2 K to achieve optimal performance [11]. X-ray free electron lasers are a current example. The first-generation machines European X-ray Free Electron Laser (E-XFEL) and the Linac Coherent Light Source (LCLS) showed the potential to reveal significant new information about bio-active proteins *in situ*. The prospective science that

could be accomplished motivated a decision to build a next generation machine (LCLS-II) currently under construction at SLAC National Accelerator Laboratory [12].

Fortunately, the discovery of nitrogen doping at Fermi National Accelerator Laboratory (FNAL) occurred during the design phase of the LCLS-II [22]. It allows for cavities to operate at a higher efficiency (increased Q_0) resulting in reduced initial and operating costs [19]. This led to the adoption of nitrogen doping technology for LCLS- II and a scale-up program was initiated. Despite favorable results in single cell cavities, reproducing them in functional nine-cell cavities encountered difficulty [12]. An early area of concern was the possibility of varying nitrogen levels in vendor-supplied materials. An analytical method was needed that could quantitatively determine nitrogen contents to well below 100 ppm. The semiconductor industry faces similar problems with doping and has shown that dynamic SIMS could be developed for this purpose.

SIMS quantitation can be achieved by comparing the dopant signal intensities of both an experimental and a known reference material. The reference material matches the experimental matrix with a dopant concentration near that of the experimental. The relationship of the measured signal intensity to the known dopant content (relative sensitivity factor – RSF) affords a path to quantitation when the content is unknown. Using this method, SIMS performed by JLab and Virginia Tech allowed for investigation of vendor supplied LCLS-II material. A major finding was that the as-received nitrogen content of all the vendor- supplied material was within specification [38].

While the design of LCLS-II was underway, additional studies indicated that shorter x-ray wavelengths would enable further unique experiments. Such x-ray wavelengths could be obtained from a higher energy electron beam from the accelerator, obtained in turn from

higher performance from the SRF cavities. Accordingly, an upgrade program was launched – LCLS-II HE [21]. An experiment-based method for modeling cavity performance was needed, requiring a more precise SIMS method. Previous quantitation found that the RSF measurements could vary by as much as 50%; a value far more than the <10% target [38, 44]. Our objective in this study is to improve SIMS quantitation of nitrogen in niobium. The issue is error in RSF values calculated from reference materials. Here we report investigation of the factors which cause such RSF uncertainty and demonstrate a mitigation strategy.

5.2 SIMS

The concentration of dopants, typically in the ppm range, affects the electrical properties of a semiconductor. Accurately knowing their concentrations is important to achieving the desired properties. For decades SIMS has been an invaluable semiconductor industry tool to accurately quantify ppm levels of dopants [40]. Niobium SRF materials offer several complications. The specimens are typically polycrystalline and may have notable surface topography due to (e.g.) preferential etching of the grains during surface treatments. Grain sizes range from ~ 50 μm typical of vendor-supplied sheet stock to more than 200 μm after high temperature annealing. The relationship of feature size to primary beam raster size must be considered. Furthermore, commercial and traceable reference materials do not exist for niobium materials and must be fabricated by ion implantation. In contrast to implanted silicon materials, implanted niobium standards cannot be cross-checked by RBS due to poor RBS detection limits for light elements in heavy element matrices. These are among the challenges that need to be addressed to achieve accurate and precise measurement of nitrogen content in niobium matrices.

To properly quantify the concentrations of dopants, the instrument must first be calibrated with standards prepared by implanting known doses of nitrogen in a niobium matrix. Analysis of the implant standards enables determination of the relative sensitivity factor used to convert detected nitrogen signal intensity to nitrogen concentration [29]. The formula is shown below, where Φ is the implanted dose of the target species (here, N), C the number of data collection cycles, I_m is the intensity of the matrix species, t time per cycle, z is the crater depth, and I_s is the summation of the intensities from the reference species.

$$RSF = (\Phi C I_m t)/(z I_s)$$

The crater is idealized as a constant depth with a flat bottom in a flat specimen surface.

A critical component of the RSF calculation is the crater depth measurement. The quality of the instrument tune can affect the crater shape and is a property well understood by SIMS analysts. Flat crater bottoms are required to precisely measure sputter rate. Uncertainty in the sputter crater depth increases the uncertainty of the calculated RSF value. Another factor which can affect the crater depth determination is the surface roughness of the implant standard. Further, different Nb grain orientations may have significantly different sputter rates, which motivates quantitative profiling of single grains.

A further topographical effect on the apparent secondary ion yield has been studied in the context of the observed concentration of oxygen isotopes in geological samples [45-48]. The difference in sample topography causes changes in the surface electrostatic field which alters the trajectory of the secondary ions as they enter the column. Mitigation is possible by adjusting the dynamic transfer contrast optics prior to data collection to center secondary ions as they approach the entrance slit [49, 50]. Our previously reported SIMS

experiments, which yielded 50% uncertainty of the RSF values, were performed without the dynamic transfer optics correction. Here we report the effectiveness of use of this secondary beam tuning correction for SRF materials.

5.3 EXPERIMENTAL

The SIMS measurements were performed on a CAMECA 7f Geo magnetic sector SIMS instrument. A Cs^+ primary ion beam with an accelerating voltage of 5 kV was rastered over the surface with a current initially starting at 100 nA. The beam current was later lowered to 25 nA to increase the quality of the beam tune by reducing its spot size. The beam was set to raster over a 150 µm × 150 µm area and data were collected from a 63 µm × 63 µm area in the center of the raster. $^{12}C^-$, $^{16}O^-$, $^{93}NbN^-$ secondary ions were detected in conjunction with a $^{93}Nb^-$ reference signal. NbN^- was monitored as the indicator for N, since the secondary ion yield for N^- is negligible. Experiments performed included the analysis of polycrystalline, single crystal and bicrystal samples, and an investigation of the sample holder geometry's effect on RSF. Beam centering by alignment of the dynamic transfer contrast optics (DTCA-X and DTCA-Y) was used only during experiments where mentioned.

Following the SIMS data collection, a KLA-Tencor Alpha Step 500 stylus profilometer was used to determine crater depths. The stylus was scanned in both axes of the SIMS crater. The stylus was scanned at a rate of 50 µm/s to acquire a 500 µm profile. Results from both axes were averaged to yield a net value. CAMECA WinCurve data analysis software was used to determine the RSF and subsequently convert the depth profile data from signal intensity to concentration.

Crystal orientation was determined by electron backscatter diffraction (EBSD). An FEI NanoLab SEM/FIB outfitted with an EDAX model TSL EBSD camera was used to acquire the orientation image maps (OIM). The samples were mounted with a specimen pre-tilt of 70^{o}, at which the OIM maps were acquired with an electron beam voltage of 30 kV and beam current of 21 nA.

5.4 Samples

To ensure samples fit the CAMECA 7f sample holder with maximum efficiency, 10 x 6 mm coupons were cut by electrical discharge machining (EDM). Both polycrystalline and large bicrystal or single crystal specimens were prepared. The specimens were polished by a series of steps including buffered chemical polishing (BCP), nanopolishing (NP), and electropolishing (EP) [51-53]. Experimental samples were nitrogen doped at the Thomas Jefferson National Accelerator Facility (JLab) using recipes in Table 1. Following the doping process, an additional 5 µm EP was performed to remove the surface nitrides. The samples designated as implantation standards were sent to Leonard Kroko, Inc. where they were implanted with carbon, oxygen, and nitrogen. Early implant standards such as NL 133 were implanted with all three target species. However, to avoid possible mass interferences between NbN^{-} and $NbCH_2^{-}$ the implantation of carbon was dropped for L78, L79, and U52. Shown in Figure 13 is a representative depth profile for the implantation standards.

Table 1. Process history of implant standards and experimental samples.

Sample	Type of Sample
NL 133	Implant Standard – 30 µm EP, pre-annealed at 900C before cutting $2x10^{15}$ atoms/cm^2 of carbon at 135 keV $2x10^{15}$ atoms/cm^2 of oxygen, at 180 keV $2x10^{15}$ atoms/cm^2 of nitrogen, at 160 keV
NL 134	Implant Standard – 30 µm EP, pre-annealed at 900C before cutting $2x10^{15}$ atoms/cm^2 of carbon at 135 keV $2x10^{15}$ atoms/cm^2 of oxygen, at 180 keV $2x10^{15}$ atoms/cm^2 of nitrogen, at 160 keV
NL 136	Implant Standard – 30 µm EP, pre-annealed at 900C before cutting $2x10^{15}$ atoms/cm^2 of carbon at 135 keV $2x10^{15}$ atoms/cm^2 of oxygen, at 180 keV $2x10^{15}$ atoms/cm^2 of nitrogen, at 160 keV
NL 115	N-Doped 3N60 inside the beam tube of EZ SSC-05 – 30 µm EP, pre-annealed at 900C before cutting, after doping hydrofluoric acid (HF) soak for 9 hours total, 5 µm EP
NL 140	N-Doped 2N0 inside KEK04, pre-annealed at 900C before cutting,
NL 147	N-Doped 3N60 inside HE-353, no pre-annealing performed. No EP following doping
L 78	Niobium Implant Standard – 30 µm BCP $2x10^{15}$ atoms/cm^2 of oxygen, at 180 keV $2x10^{15}$ atoms/cm^2 of nitrogen, at 160 keV
L 79	Niobium Implant Standard – 30 µm BCP $2x10^{15}$ atoms/cm^2 of oxygen, at 180 keV $2x10^{15}$ atoms/cm^2 of nitrogen, at 160 keV
U 52	Niobium Implant Standard – 50 µm EP nanopolish $2x10^{15}$ atoms/cm^2 of oxygen, at 180 keV $2x10^{15}$ atoms/cm^2 of nitrogen, at 160 keV
Si# 2293	Silicon Implant Standard

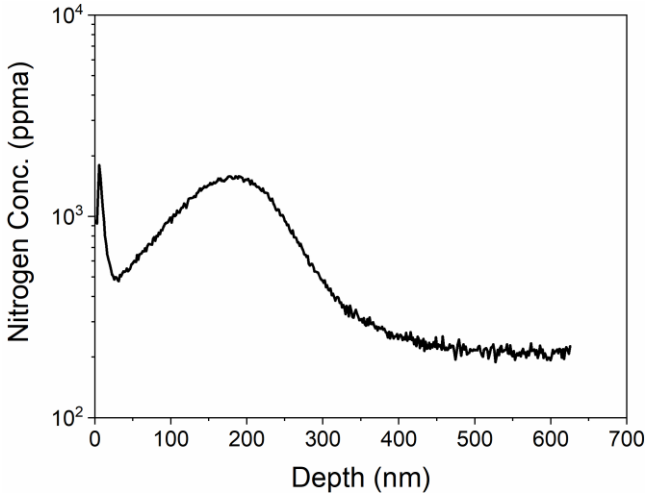

Figure 13. Representative NbN^- depth profile of an implantation standard. Depicted above is implant standard U52 which contains $2x10^{15}$ atoms/cm^2 of nitrogen dosed at 160 keV into a niobium matrix.

5.5 RESULTS AND DISCUSSION

5.5.1 Polycrystalline Materials

Our previous SIMS measurements of polycrystalline N-doped specimens reported an apparent concentration difference between grains of different crystallographic orientation [38]. Specifically, a large difference in atomic parts per million (ppma) concentration was observed between [001] and [111] orientations on the same sample [54]. In addition, the sputter rates varied from grain to grain. Therefore, investigation to understand the cause became necessary. To determine the effect of grain orientation on the instrument calibration or nitrogen uptake, EBSD was performed on the specimens to identify the surface normal grain orientations.

As a first step, orientation image maps (OIM) were acquired from locations covering more than several square millimeters on the surface of a nitrogen-implanted polycrystalline specimen (NL 133) and combined to obtain a single OIM of the sample surface (Figure 14 a.) SIMS data were collected at the locations indicated by the squares.

An RSF was calculated for each (Figure 14 b.) However, no correlation between grain orientation and RSF was observed. Further, the RSF was observed to vary substantially, yielding a 40% RSD (relative standard deviation). Replicate implant standards were analyzed and found to vary 16% and 14% for NL 134 and 136 respectively (Figure 15).

Though samples NL 133, NL 134 and NL 136 were electropolished as a final preparation step, grain height variation was noted. Electropolishing when performed under optimal conditions will yield a sub-100 nm finish [51, 55, 56]. Differential surface removal has been observed in previous studies and achieving an ideal surface is non-trivial [57]. Continual improvement is the subject of further investigation.

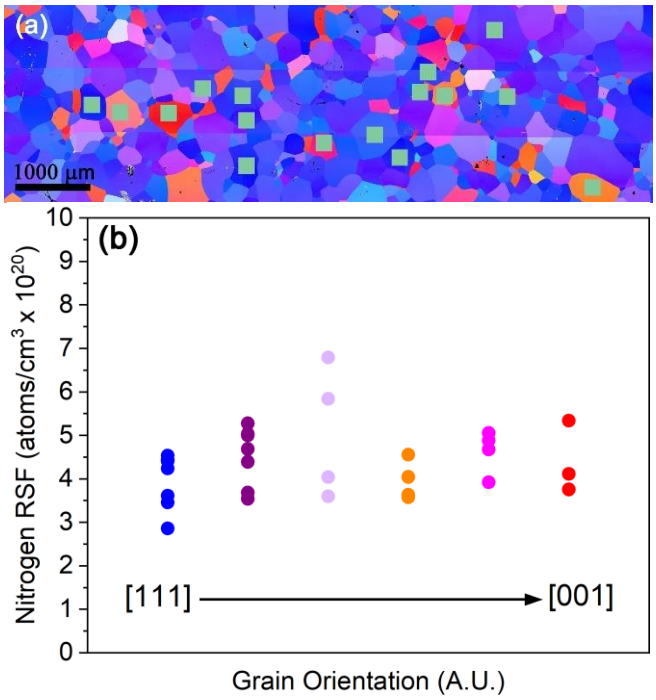

Figure 14. a) EBSD OIM map of the NL 133 Implant Standard. Locations where SIMS analyses were performed are noted. b) NbN^- RSF was calculated for each data point and plotted as a function of grain orientation. No discernible correlation was found.

5.5.2 Single/Bicrystal Implant Standards

To gain further insight into the effect of grain orientation on RSF, single and bicrystal samples were analyzed. Due to the pristine and flat nature of the single crystals, reproducible and consistent RSF values could be established when compared to polycrystalline samples (Figure 15). To better understand the effect of sample positioning on the RSF, single crystal implant standard U52 was rotated in 90^{o} increments in the sample holder. It was observed that the sputter rate changed as a result of sample rotation, but the RSF was unaffected. Though the analysis time and sputter depth are variables which affect the RSF calculation, this suggests the nitrogen and niobium intensities adjusted to normalize the change in sputter rate.

Implant standard U52 was found to have the most reproducible RSF values compared to the L78 and L79 large grain implant standards, as a result of U52 having a superior surface finish (Figure 16). Accurate crater depth determination is reliant on the crater bottom being flat and parallel to the sample's external surface. Poor instrument tuning or rough standard finishes introduce error into the crater depth determination which propagates to the RSF determination. Figure 17 shows a comparison of profilometry scans between L79 and U52.

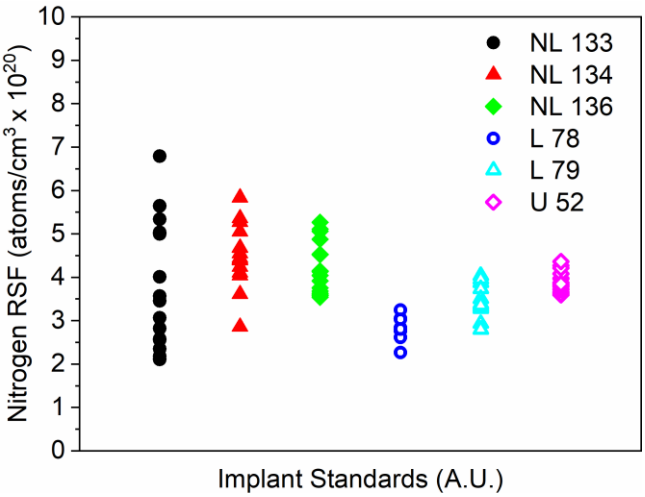

Figure 15. Plot depicting RSF values per analysis. Each column shows analyses run for a specified sample. Changing from polycrystalline standards to single crystals yielded more precise RSF values. Further increasing the surface quality to the smoothest finish (U52) increased the precision.

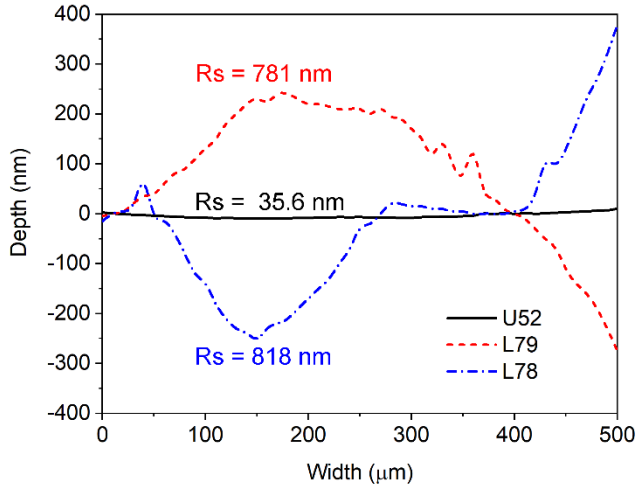

Figure 16. Representative profilometry scans of the single and bicrystal implant standards.

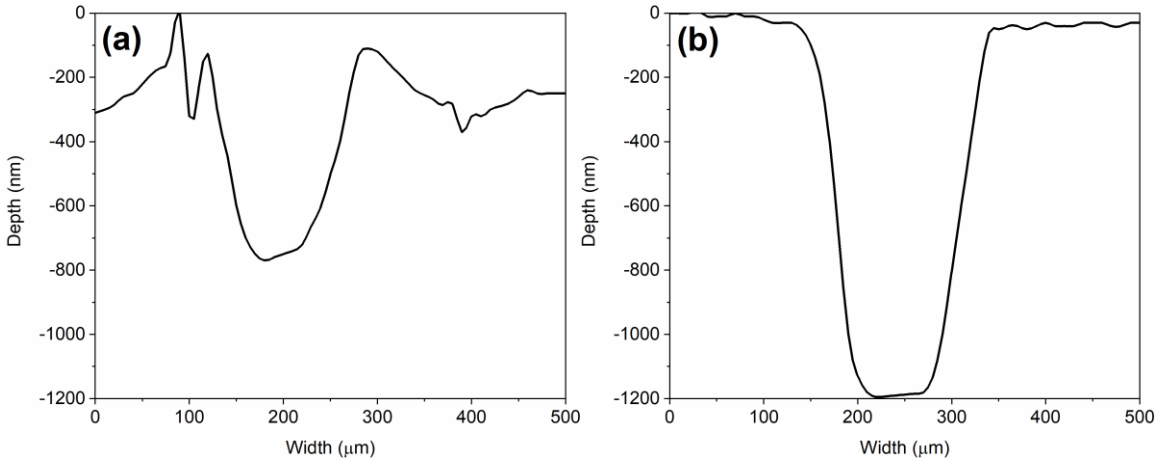

Figure 17. Comparison of profilometry scans for single crystal implant standards. The surface finish for U52 was observed to be much smoother which yields accurate crater depths and minimizes the propagation of error for RSF determination.

5.5.3 CAMECA Sample Holder- DTCA Effectiveness

It was observed that the U52 implant standard yielded consistent RSF values. However, in the experiment, the specimen was loaded into the sample holder in the same location and analyses were taken given the same sample loading conditions. Peres et al. (2011) observed that the topography effect on the reproducibility of SIMS analyses is not limited to the sample but includes the sample holder [58]. As a result, the CAMECA 7f Geo specimen holder was investigated to uncover effects which may change the RSF. This holder is capable of loading 1-4 specimens approximately 5 mm x 5 mm loaded individually or to full capacity (Figure 18a). The specimens are held in place by springs that apply a flexural load to the thin faceplate of the sample holder (Figure 18a). To determine if the loading force variation may result in a change in RSF, SIMS analysis was performed on implant standard U52 in which the sample holder contained 2 specimens and repeated with 4 specimens. The results showed a clear change in RSF because of the loading force change

(Figure 18 b,c). The impact of changing the loading force was observed by monitoring the niobium matrix signal. The results showed a signal change as a function of loading force (Figure 18 b). These findings suggest that the loading force can change the working distance of specimens, which can in turn cause a trajectory change of the secondary ion beam as it approaches the secondary column, resulting in signal change and alteration of the system calibration.

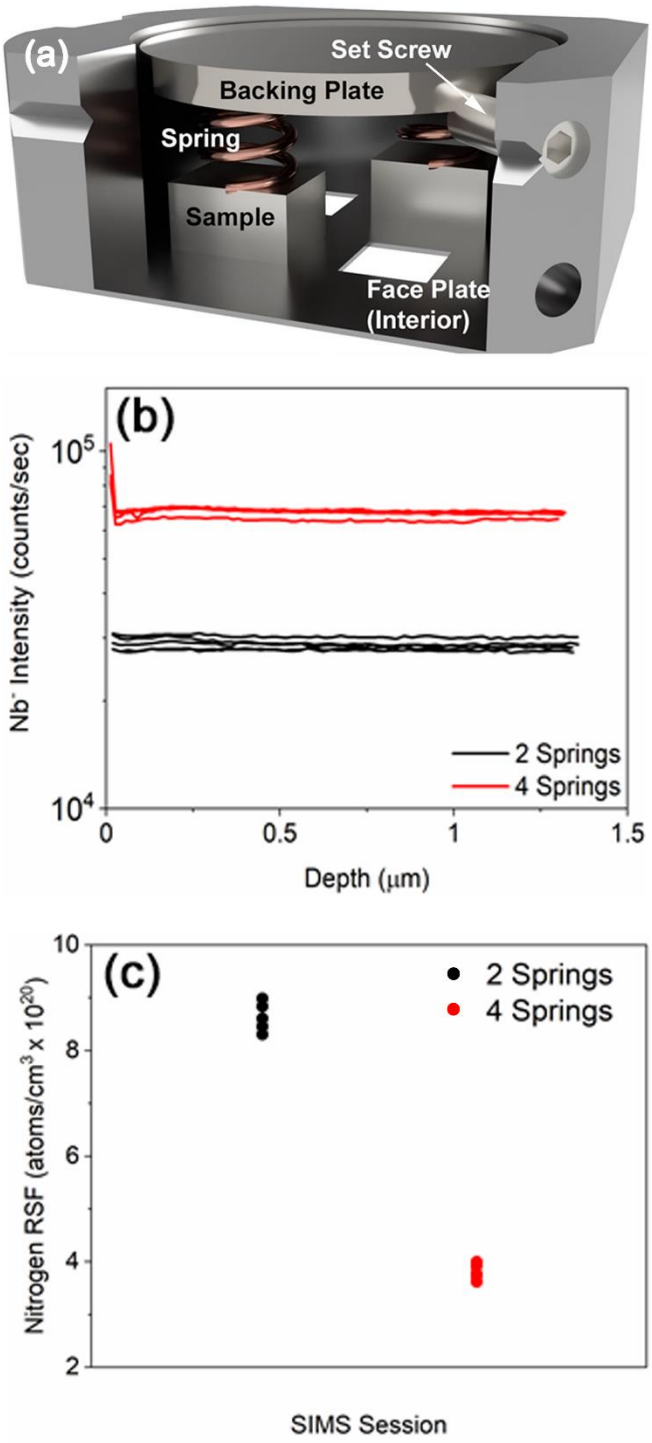

Figure 18. Depiction of a loaded CAMECA 7f Geo sample holder. Samples are placed into position and held in place by compressing copper springs between the sample and the backing plate. The force applied can cause deflection of the face plate resulting in an observable change in b) the niobium matrix signal and the c) RSF.

Topographical variations of the sample itself are expected in addition to working distance changes caused by sample loading. Therefore, to better understand how the RSF may change as a function of position on a sample holder, a silicon implant standard denoted as Si-N 2293 was fractured and loaded into three of the four slots of the sample holder. The remaining spot was loaded with a different Si-N implant standard with the same dose but different implantation energy to determine reproducibility between implant standards. Figure 19 shows the SIMS analysis locations. A proposed method for mitigating these topographical effects is to center the beam by using the dynamic transfer contrast apertures (DTCA).

The DTCA consists of two sets of deflection plates located in the transfer optics region of the secondary column and is purposed with centering the secondary ion beam in the contrast aperture. Height variations in SIMS samples can cause the secondary ion beam trajectory to become off centered causing the contrast aperture to filter essential beam signal, thereby, tampering with the ratio of matrix and impurity signals and thus leading to uncertainty in the RSF calibration. The DTCA can be adjusted in two dimensions in which the aperture is scanned in both the X and Y axis. The beam centering function scans on both lateral dimensions of the beam to correct the trajectory of the secondary beam as it enters the column, which maximizes the signal intensity. Although automation of the beam centering function is possible, it was observed that the automation was inconsistent in finding the signal maximum if the matrix intensity was relatively low. For niobium, the matrix intensity consistently yielded values below where this feature could be automated. Therefore, manual adjustment was made prior to each analysis.

To compare the effectiveness of using this method, the experiment was performed with and without use of the DTCA. The results (Table 2) show that without the beam centering correction, the RSF varied 47% by only varying the analysis location. By using the beam centering parameter and adjusting the DTCA prior to each analysis the RSD was reduced to 1.5%. Points A and B were dosed the same as D through H but were from a different parent sample. Use of the DTCA revealed that the derived RSF was inherently different. This suggests that although implant standards may be nominally dosed the same, some variation may arise that translates into calibration error. Unlike many of the standards used in the semiconductor field, RBS cannot be used as a quality control for nitrogen implanted into niobium. This issue is noted, and the mitigation will be discussed in a future report. Without a secondary method, such as RBS, to check the dose, we are relying on the number provided by the implanter and that can be affected by mass interferences and by effects such as sample charging. One solution is to implant a piece of silicon at the same time and compare the result with prior implanted samples.

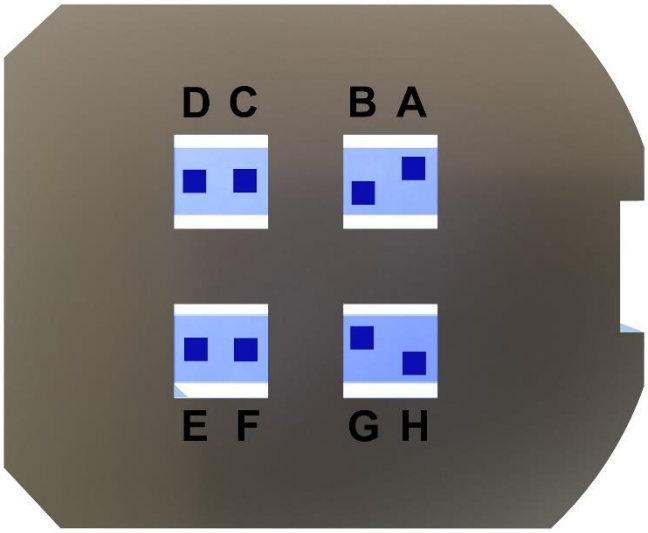

Figure 19. A map of the SIMS analysis showing location of RSF values as a function of sample position. Corresponding data are located in Table 2.

Table 2. Data from the RSF location mapping. Locations correspond with Figure 19. The analysis was performed with and without the DTCA beam centering function. The results clearly show an improvement in RSF reproducibility as well as matrix intensity, which are noted by the bolded values. Note: as the beam centering function increased the overall counts of the analysis, the matrix signal was changed from $^{28}Si_3$ to $^{28}Si_4$ to prevent damage to the electron multiplier.

	Without Beam Centering			With Beam Centering		
SiN 2293	Depth AVG (nm)	$^{28}Si_3$ Intensity x10^4	RSF (atoms/cm^3) x10^{20}	Depth AVG (nm)	$^{28}Si_4$ Intensity x10^4	RSF (atoms/cm^3) x10^{20}
A	879	47.6	8.11	801	37.8	0.75
B	875	56.6	8.70	770	32.2	0.75
Average	877	52.1	8.41	738	35.0	0.75
StDEV	2.8	6.36	0.4	84	3.96	0.01
%RSD	**0.3%**	**12.2%**	**5.0%**	**11.4%**	**11.3%**	**1.8%**
C	876	98.4	17.9	772	33.5	1.34
D	875	4.12	5.75	748	33.2	1.33
E	870	4.76	6.42	753	34.4	1.38
F	863	21.6	11.8	762	34.9	1.38
G	865	9.27	8.66	752	33.1	1.36
H	859	82.3	16.6	739	34.7	1.37
Average	868	36.7	11.2	754	34.0	1.36
StDEV	6.8	42.3	5.2	11	0.79	0.02
%RSD	**0.8%**	**115.1%**	**46.2%**	**1.5%**	**2.3%**	**1.5%**

5.5.4 Practical Applications- DTCA

The implant standards previously tested were reanalyzed with the beam centering function. NL133, for which an RSF variation of 40% had been measured, yielded the most notable change in precision as the uncertainty was reduced to 9.7%. Reduction in uncertainties was observed for all other implants with the values noted in Figure 20. As was the case in the previous experiments, the RSF precision was superior for the single crystal and bicrystal standards.

Previous SIMS analysis of N-doped samples appeared to show variation in nitrogen content as a function of grain orientation. However, at the time of analysis, effects of surface topography were not accounted for. A profilometry scan of a SIMS analyzed [111] grain adjacent to [001] grains showed that the grain height could vary as much as 1.5 μm (Figure 21), which is sufficient to alter the trajectory of the secondary ion beam. Additional SEM analysis performed on sample NL 115 showed the presence of surface features on [111] grains that were absent from [001] grains (Figure 22), If these are nano-nitrides as some have suggested, then the nitrogen content of the [111] grains surface may be higher than the [001] grains, not the opposite. Therefore, sample NL 115 was re-analyzed with DTCA beam centering to determine the effectiveness of this method on such a sample. All scans showed an increase in nitrogen content versus previously reported, which is apparently a result of correcting the secondary beam trajectory. Additionally, the [111] grains now reported nitrogen content higher than that of the [001] grains, which is consistent with the notion that the observed features are indeed nano-nitrides (Figure 23). “Nano-nitrides” were also observed on sample NL 140, therefore the experiment was repeated to determine if the observation could be reproduced. This sample was also

observed to have higher nitrogen content in grains with a [111] normal surface orientation (Figure 24).

Reduction of method uncertainty was deemed essential to providing reliable and reproducible data to correlate SIMS data and cavity performance. The cavity co-doped with Sample NL 147 was found to perform outstandingly well in rf testing (Figure 25). SIMS was performed on the sample without removal of the surface nitrides by EP. The data showed a sharp decline in nitrogen content over 1.5 micron from approximately 50% to ~ 1000 ppma (Figure 26). A further modest reduction in the nitrogen content was also observed after this nitride layer was removed followed by a return to ~1300 ppma. Understanding in detail how this nitrogen content and its variation by doping process conditions contributes to the corresponding SRF cavity performance is a matter of great interest and ongoing analysis. These process conditions are not yet optimized.

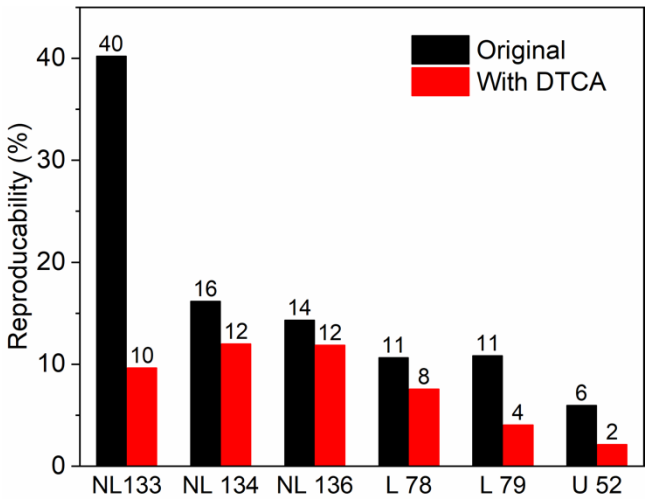

Figure 20. Comparison of RSF variation of implant standards. The plot shows that precision of RSF values improved for all tested implant standards when DTCA was used.

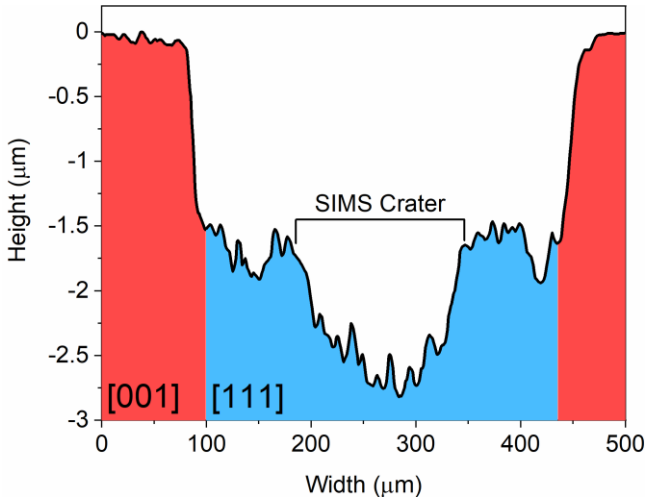

Figure 21. Profilometry scan of N-doped sample NL 115 in a region where a [111] grain is adjacent to [001] grains. The scan shows a height difference of roughly 1.5 μm between [111] and [001] grains. The [111] grains were observed to be especially rough due to the presence of "nano-nitrides" in the grain. SIMS was performed on this specific grain and the crater is noted.

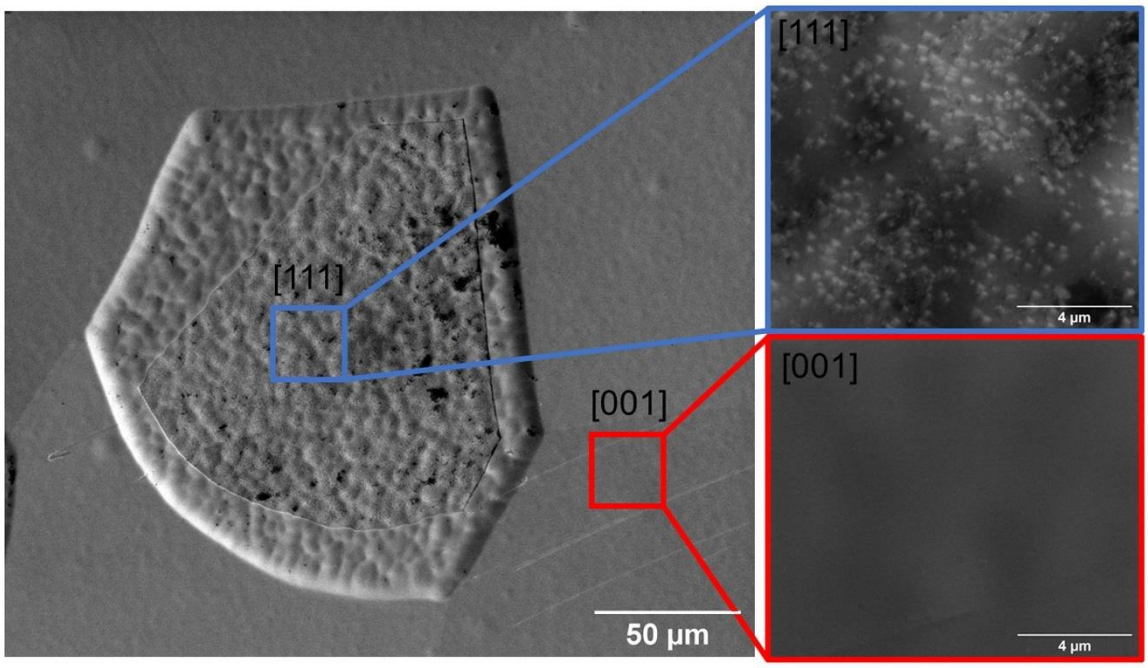

Figure 22. SEM image of N-Doped sample NL 115. The image shows particles hypothesized to be “nano-nitrides” present on near [111] grains but absent from [001] grains.

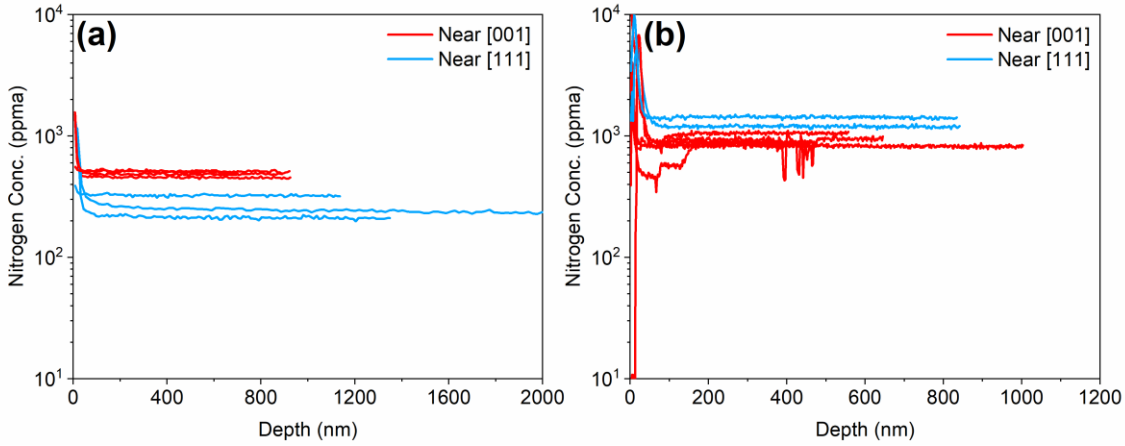

Figure 23. Comparison of SIMS data with and without beam centering. a.) previously reported results showed that the nitrogen content was unexpectedly lower in the [111] grains. b.) By centering the secondary beam with the DTCA aperture prior to the analysis the signal intensity increased resulting in an apparent increase of nitrogen content. [111] grains now show a higher nitrogen content, consistent with the roughness observed on the [111] grains being nano- nitrides.

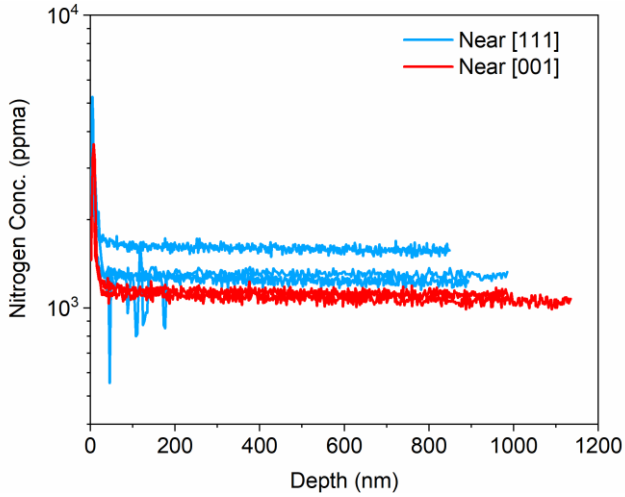

Figure 24. SIMS data for sample NL 140, an N-Doped sample with small particles observed on the surface. As was the case for sample NL 115, the NbN- concentration was higher for near [111] grains.

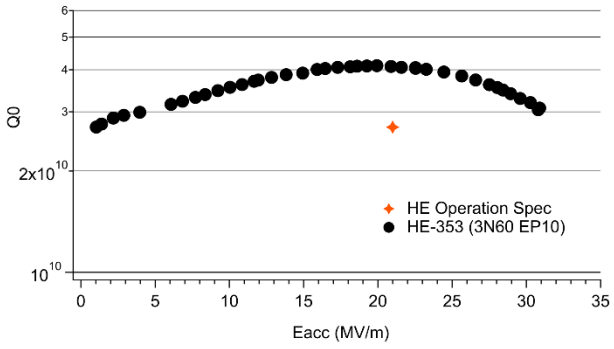

Figure 25. Resonance quality factor (Q0) vs. effective accelerating gradient for cavity HE-353, co-processed with sample NL 147. The performance requirement of the LCLS-II HE accelerator project is noted.

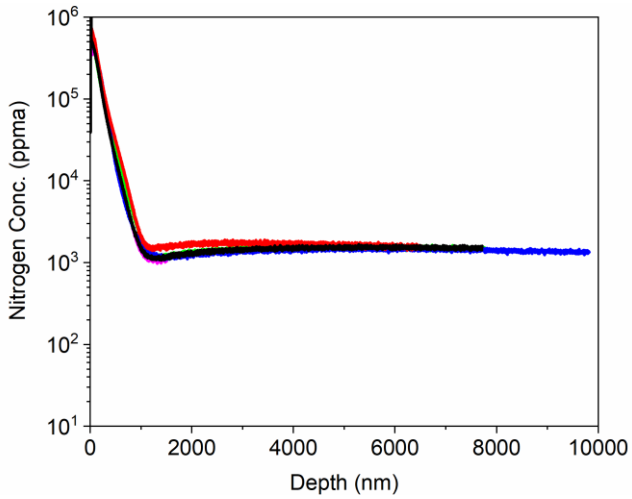

Figure 26. SIMS depth profiles for sample NL 147. The data show a sharp decline in NbN- concentration which reaches a local minimum at the interface between the nitride layer and the bulk niobium. The concentration of the N increases in the bulk before beginning diffusion-limited decay into the bulk.

5.6 SUMMARY AND CONCLUSIONS

Accurate and precise quantification of nitrogen of N-doped niobium has previously proven challenging. Our previous work reported that the RSF value may deviate up to 50% by changing implant standards or simply changing the grain. This level of uncertainty is unacceptable for SRF applications and method improvement is critical.

Previous reports of nitrogen content deviation as a function of grain orientation should be examined carefully to be sure that topographic effects are adequately accounted for. Analysis of polycrystalline materials may yield different concentrations for different grains or grain combinations. This may be a result of different grain height with respect to the mass spectrometer, effectively changing the working distance. As a result, the beam may become off-centered as it passes through the secondary column, altering the baseline

signal and instrument calibration. The instrument calibration obtained with use of the polycrystalline implant standard NL 133 yielded RSF values that varied drastically from grain to grain. Furthermore, the sample holders themselves were observed to cause the working distance to deviate as a function of holder position. Additionally, the loading force to hold the samples in place was observed to cause a change in the working distance which resulted in a deviation in RSF values. All these geometrical challenges to the precise location of the sampled surface can be mitigated by centering the beam with the DTCA-x and DTCA-y apertures.

The influence of the DTCA apertures is immediately seen in the RSF variability. The RSF reproducibility was observed to have been improved from 40% to 9.6% RSD for the polycrystalline implant standard NL 133. Using a single grain implant standard, such as U52, further reduces the uncertainty to 2%. All other implant standards showed an improvement in precision when beam centering was performed. The impact of this change was further observed by analyzing the N-doped NL 115 cavity sample. Previous results were affected by surface topography and incorrectly showed a reduction of nitrogen content within the [111] grains of these samples. SEM analysis showed that the [111] grains uniquely contain a higher nitrogen content than is expected, consistent with nano-nitrides. The phenomenon was reproduced and observed by analyzing NL 140 in which the presence of ‘nano nitrides” were also noted. An observable difference in the average nitrogen content was noted when comparing the previous data set to the current. The lack of DTCA adjustment prior to each scan can account for some deviation. However, two separate implant standards were used for each analysis. As an absolute and traceable implant does

not currently exist for nitrogen in niobium, further work is needed to refine analysis to establish excellent quantization results regardless of the implant standard used.

Improvement of the SIMS analytical methods was a critical step to performing routine analysis of SRF materials. Due to superior cavity performance associated with sample NL 147, understanding the pathway from doping to performance became a high priority. SIMS was found to be a critical step for understanding the material science of the cavity surface preparation. The nitride layer was determined to be 1 μm followed by a minimum in nitrogen concentration at the interface. The concentration of nitrogen was observed to then increase before presumably decaying within the diffusion layer to typical bulk concentrations of ~60 ppma.

Considering all factors, we conclude that if care as described above is taken, an uncertainty of < 10 % in local nitrogen concentration with depth is reliably attainable using dynamic SIMS, for niobium materials in SRF applications.

Chapter 6: Improved quantitation of SIMS depth profile measurements of niobium via sample holder design improvements and characterization of grain orientation effects

Published in Journal of Vacuum Science and Technology B (2022)[59]

The importance of SIMS analyses for "N-doped" impurity alloyed niobium and other surface-alloyed materials continues to increase. A major hurdle is the uncertainty of instrument calibration due to changes in sample height either from sample surface topography or from the sample holder itself. The CAMECA sample holder design allows for many types of samples to be analyzed. However, a drawback is that the holder faceplate can bend, contributing to relative sensitivity factor (RSF) uncertainty into the SIMS results. Here we describe an improved sample holder having a reinforced faceplate to prevent deflection, reducing uncertainty. Simulations show that the new design significantly reduces deflection from 10 μm to 5 nm. Sample measurements show a reduction of RSF uncertainty from this source from 4.1% to 0.95%.

Grain orientation has long been suspected to affect RSF determination as well. A bicrystal implant standard, consisting of a randomly oriented and [001] grains, was successively rotated 15° between analyses. It was observed that 20% of the analyses performed on the randomly oriented grain exhibited anomalously high RSF values as well as slow sputter rates. These features were associated with the changing of the grain normal orientation with respect to the primary Cs^+ beam. The grain orientation associated with the rise in RSF was simulated and determined to be the [101] crystallographic plane, thus

indicating that ion channeling was responsible for the significantly increased RSF. FIB analysis confirmed slower sputter rates for the cardinal crystallographic orientations, indicating that ion channeling would be evident for each.

6.1 INTRODUCTION

Progress in related materials science and engineering is an important chapter in the history of progress in accelerator science and technology. Milestones such as the switch from copper to niobium that enabled superconductive radiofrequency (SRF) and, improved processing including buffered chemical polishing (BCP), electropolishing (EP), and vacuum baking have incrementally improved performance, now approaching niobium's physics limits [11]. In the last decade, Nb surface modification has come forward as a deployable technology. Incorporation of trace quantities of interstitials into the RF active layer enables increased energy efficiency (Q_o) [15, 18-20, 60-62] several-fold higher than the incumbent technology, an advantage so compelling that "nitrogen doping" was chosen for the newest major continuous wave accelerators (LCLS-II and LCLS-II HE) [12, 21, 63, 64]. Opportunities are aplenty in tuning interstitials for SRF applications to optimize Q and E_{acc} [17, 65-69] for the desired application and simplifying processing steps [23-25].

It is not an overstatement to say that progress is not only rapid, but is accelerating. A significant share of the responsibility for this is the introduction of materials science and engineering from the microelectronics community in processing and characterization, especially the latter [30, 56, 70-72]. As a near-surface phenomenon, SRF performance is greatly sensitive to near surface composition and its variation with depth in the RF-active layer [19].

Following its success in microelectronics, the SRF community has turned to secondary ion mass spectrometry (SIMS) [38].A discussion of issues encountered in reliably obtaining results in the uncertainty range needed for doping/alloying process development with practical SRF cavity materials has just appeared [54]. A discussion of the unresolved issues reported there, and others that are newly emerged, appears below. Producing cavities to accurately achieve a desired surface alloy state is costly and time-consuming [20]. Diffusion modeling may help in shaping an impurity profile to optimize Q_0 and accelerating gradient for a tailored application [25]. Accurate determination of the interstitial content via SIMS has proven to be vital for predictive modeling [73, 74]. Method uncertainty for quantitative SIMS analysis has been improved to roughly 10% uncertainty for polycrystalline niobium samples. However, inexplicably inconsistent data points continue to plague occasional SIMS analyses. These data points are suspected to be a result of grain orientation effects. Seemingly random crystallite orientations have been found to exhibit RSF values which deviate up to a factor of five compared to a baseline RSF value for a polycrystalline niobium material. The same phenomenon can cause seemingly random grains to appear to exhibit misleadingly low impurity concentrations for experimental samples. It is important to identify the conditions which cause these variations to prevent the misrepresentation of impurity concentrations for niobium SRF materials.

The varying surface topography of polycrystalline grains can affect the RSF determination and subsequently the quantitation of SIMS data [46, 47]. This effect can be mitigated by adjusting an aperture (the CAMECA dynamic contrast aperture) between analyses to correct the beam trajectory error resulting from the varying surface topography [50]. Changes in the working distance can also result from flaws in the sample holder

design [58]. The design and construction of existing standard SIMS sample holders permits more deformation than the dynamic transfer contrast apertures (DTCA) can in some circumstances correct. In this work we describe a rigid sample holder that mitigates working distance variations.

6.2 EXPERIMENTAL

The manufacturer-provided holder for the CAMECA IMS 7f Geo, shown in FIG 25, is constructed of stainless steel and contains a 25 mm cavity with a 0.1 mm tantalum faceplate. The tantalum acts as a high strength foil to limit deflection when pressure is applied to hold the sample. However, the faceplate is only supported around the circumference, thus, deflection is inevitable. Additionally, the force applied to the faceplate can vary depending on the number of samples in the holder thereby making the working distance inconsistent between loads. A new sample holder (Figure 28) was designed to maximize the number of [our standard] samples that can be analyzed, while supporting the faceplate to resist deflection.

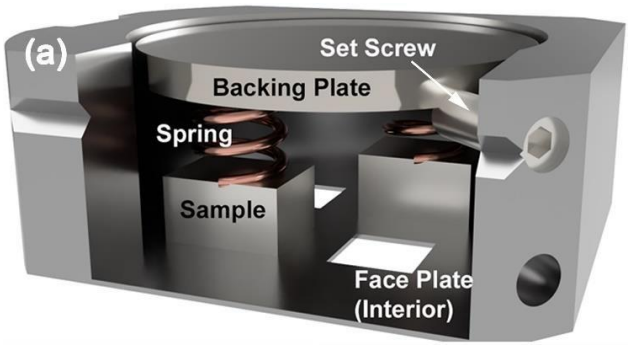

Figure 27. Loaded CAMECA 7f Geo sample holder. Samples are placed into position shown and held in place by compressing copper springs between the sample and the backing plate. The force applied can cause deflection of the faceplate resulting in an

observable change in the niobium matrix signal and the RSF. (Reproduced from J. Angle et. al. 2021) [30].

Our typical Nb samples provided for analysis are 6 mm × 10 mm and 3 mm thick. The 7f Geo has a maximum stage travel of ~ 23 mm × ~23 mm. Using these constraints, we designed a new holder in with 2 mm support ribs to stiffen the holder. The support ribs are offset into the holder to allow the backing plate to rest and compress the springs with constant force. A tantalum faceplate with a thickness of 0.1mm was spot welded to the holder face to contain the samples within the holder.

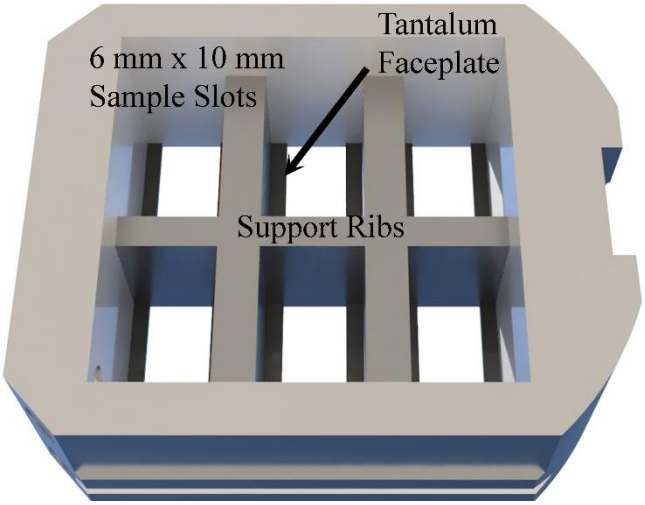

Figure 28. Depiction of the newly fabricated SIMS sample holder for our standard niobium samples. Each sample is individually supported by structural ribbing to prevent the faceplate from deflection due to sample loading. The individual ribbing also ensures that constant force is applied independent of the number of samples loaded.

The holder was designed using the computer aided design (CAD) software Autodesk Fusion 360. A major advantage here is that static loading of component parts can be simulated. Therefore, to determine the significance of using a new sample holder, the standard CAMECA design was modelled in parallel with the new one. The materials

database did not include tantalum, so the properties of 404 stainless steel, which has a similar elastic modulus [75, 76], were substituted. To determine the loading force, an MTS 30 kN load frame was used in compression to measure the force applied to the faceplate using the CAMCECA copper loading springs depressed to 12.5 mm. It was found that the four springs combined would apply no greater than 2 N of force to the faceplate. This value was used as a maximum value to simulate the force exerted onto the faceplate of each holder. The static stress simulator of Autodesk Fusion 360 was used to calculate the displacement of the faceplate of each holder using 2 N of total applied force. The results indicated a maximum deflection of 10 µm for the standard CAMECA design, with the new design deflecting only 5 nm (Figure 29).

6.3 RESULTS AND DISCUSSION

6.3.1 Effect of Increased Rigidity

The new holder was tested to determine RSF variance as a function of position on the holder. A silicon wafer ion implanted with 2×10^{15} atoms/cm^2 nitrogen at 160 keV was fractured into six segments which were then loaded into the sample holder. To remove any debris from the fracturing process, the surface was rinsed with ethanol and blown dry with nitrogen. The sample holder was then loaded in to the CAMECA 7f Geo and allowed to evacuate overnight. SIMS was performed using a Cs^+ primary ion beam with an accelerating voltage of 5kV and an impact energy of 8 keV utilizing a beam current of 25 nA. The beam was rastered over an area of 150 µm × 150 µm area and data were collected from a 63 µm × 63 µm area in the center of the raster. $^{28}Si^{14}N^-$ secondary ions were detected in conjunction with a $^{28}Si_4^-$ reference signal.

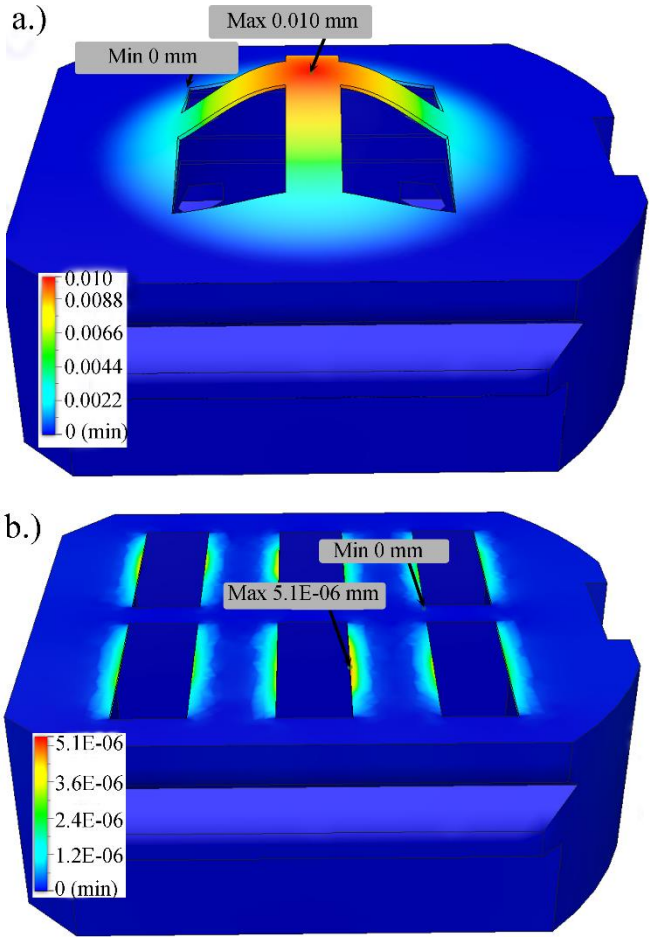

Figure 29. Static stress simulations of the a.) standard CAMECA 4 slot sample holder vs. the b.) newly designed 6 slot Nb SRF cavity sample holder. Simulations of the new design showed that sample deflection could be reduced from 10 µm to 5 nm.

Table 3. SIMS results for N-Doped Si Implant Standard.

	CAMECA Holder		New Holder	
Spot	**$^{28}Si_4$ Counts $\times 10^5$**	**RSF $\times 10^{20}$**	**$^{28}Si_4$ Counts $\times 10^5$**	**RSF $\times 10^{20}$**
A	2.17	1.332	3.37	1.024
B	1.86	1.347	3.45	1.002
C	1.78	1.455	3.50	1.007
D	2.06	1.328	3.32	1.017
E	1.94	1.386	3.82	1.001
F	1.95	1.295	3.26	1.002
Avg.	**1.96**	**1.35**	**3.45**	**1.008**
StDev	**0.14**	**0.06**	**0.20**	**0.01**
%RSD	**7.1**	**4.1%**	**5.7**	**0.95%**

SiN^- was monitored as the indicator for N, since the secondary ion yield for N^- is negligible. As the objective of this experiment is to evaluate the effect of the holder, the DTCA was not adjusted between runs. The results, summarized in Table 3, show that the new sample holder design presents a significantly reduced %RSD in agreement with reduced simulated deflection. It was further observed that matrix signal counts increased and RSF values decreased for the new holder. The RSF for the new six-sample holder was found to exhibit an uncertainty 0.95% RSD for single crystals installed with common orientation.

6.3.2 Effect of Grain Orientation

SIMS analyses are performed on experimental samples with grain sizes ranging from 200 µm - 500 µm. They tend to be preferentially oriented near the [111] or [001] crystal orientations with respect to normal. An extensive study in Angle et al. 2021[30], showed that higher RSF uncertainty existed for polycrystalline niobium versus single crystals, exhibiting 12%, and 2% variability respectively. While the increase in variability

when using polycrystalline niobium is expected, the cause is still unknown. SIMS analyses of cavity witness samples have shown that certain grains may exhibit uncharacteristically higher matrix signals, which appear to cause a reduction in the values obtained for nitrogen concentration (Figure 30) if common RSF values are assumed. Additionally, these grains typically are associated with low sputter rates. The effect appears to occur randomly and appears to occur in grain orientations away from major crystallographic planes. Additionally, the effect can be uniquely observed in a single grain through analyses performed on grains of matching orientations. Therefore, it was hypothesized that rotating the sample about normal causes certain grains to yield higher count rates (orientation dependent secondary ion yield), causing the RSF to change.

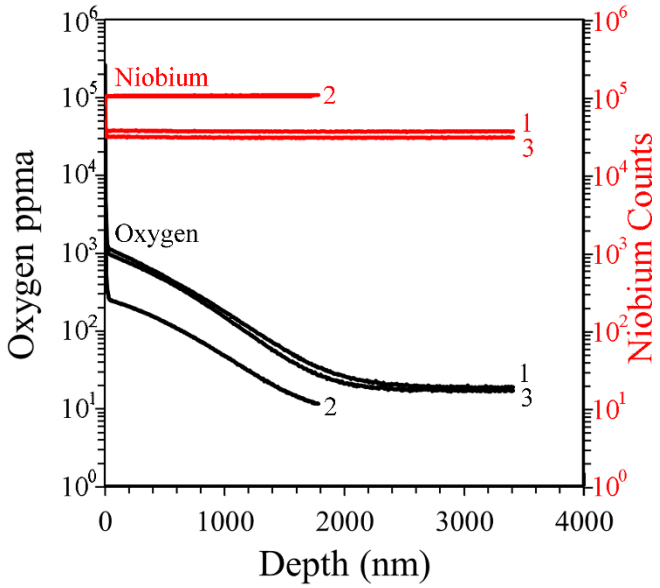

Figure 30. SIMS Depth profile of an oxygen alloyed specimen which was tested in triplicate. Analyses were performed on differing grains. Note that replicate 2, as indicated in plot above, exhibited a higher matrix signal and a slower sputter rate which resulted in an apparent oxygen concentration. It is thought that the RSF used is incorrect for this specific grain orientation.

To explore the grain orientation effect, an experiment was created in which grain orientation is varied in 15° increments around the normal. It also makes possible the ability to probe the impact of specimen holder deformation. To rotate the sample in the SIMS, a further new holder was created from a standard CAMECA holder with a 16 mm sample window (Figure 31). A custom disc insert was cut to allow for a 16 mm circular portion to rest in the sample window. A 6 mm × 12 mm rectangular chamber with 0.75 mm lips was machined to allow the sample to be loaded at the proper working distance. Markings were scribed every 15° to define specific rotations (Figure 31a). The sample insert was rotated with a pair of tweezers and locked into place with a setscrew. The sample was held into place with a copper spring and a backing plate with approximately 2 N of force applied. Though made of stainless steel, the faceplate material for this holder was much thicker (0.35 mm) and more rigid than the 4-hole style holder. To ensure that holder deflection would not factor into the RSF determination, a static stress simulation was also performed for this holder. The simulation suggested the holder would deflect 0.47 nm; therefore, holder effects are assumed to be negligible (Figure 31b).

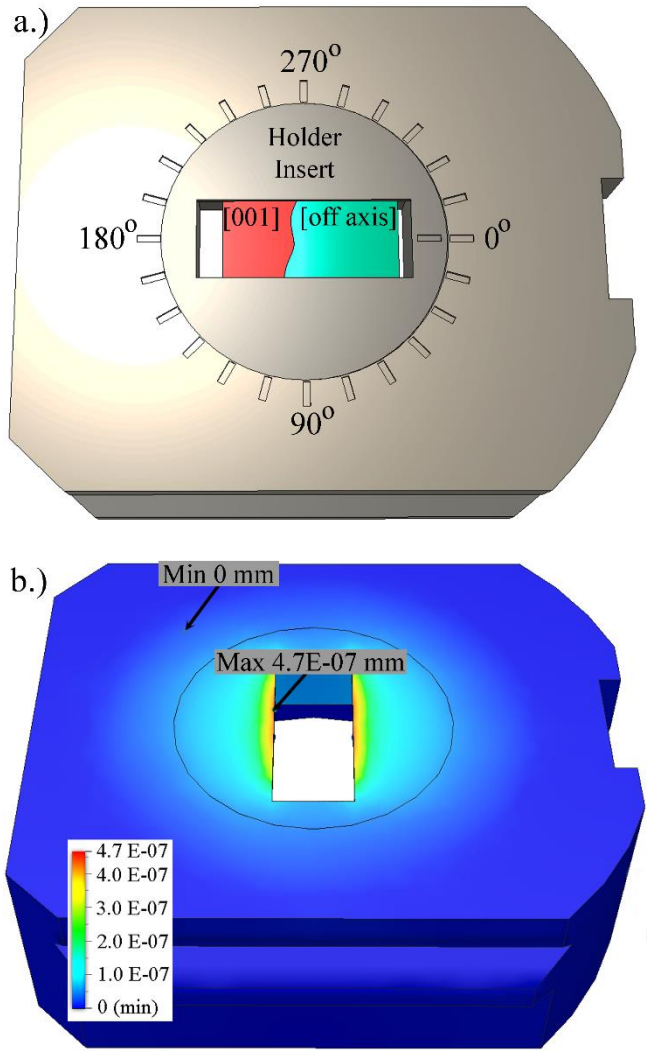

Figure 31. A.) Diagram showing the rotational sample holder with the bicrystal implant standard. The holder insert is rotated and locked in place by a set screw. B.) Color plot of deflection from the static stress simulations of the rotational holder presenting negligible deflection.

6.3.3 SIMS Performance

A bicrystal implant standard denoted as HL 24 with one random and one [001] normal grain orientation was chosen for this experiment. The implant standard was dosed with 2×10^{15} atoms/cm^2 of oxygen and nitrogen at 180 keV and 160 keV by Leonard Kroko

Inc. respectively. SIMS was performed using the same analysis conditions as earlier: a Cs+ primary ion with an 8 keV impact energy and 25 nA of beam current. Following each analysis, the sample holder was removed, and the crater depth was determined with a Tencor AlphaStep 500 stylus profilometer. The insert containing the implant standard was then rotated 15° and the holder was then returned to the SIMS. Prior to the next analysis, the sample holder was held in the intro chamber for 1 hr with gentle heat from a heat lamp (no greater than 60° C) to remove adsorbed water This cycle was repeated until one full revolution was complete. The RSF was calculated at each rotation with results shown in Figure 32. The results show that sample rotation had no effect for the [001] crystal. The random crystal orientation was found to have a 75° window in which the nitrogen RSF value was observed to increase. This indicates that ~20% of arbitrary rotational scenarios would risk a deviation in nitrogen concentration quantification. Excluding the 75° window, the nitrogen RSF was determined to remain generally constant with a value of $5.2 \pm 0.8 \times 10^{20}$. The maximum value for the 75° window was found to be 20×10^{20}.

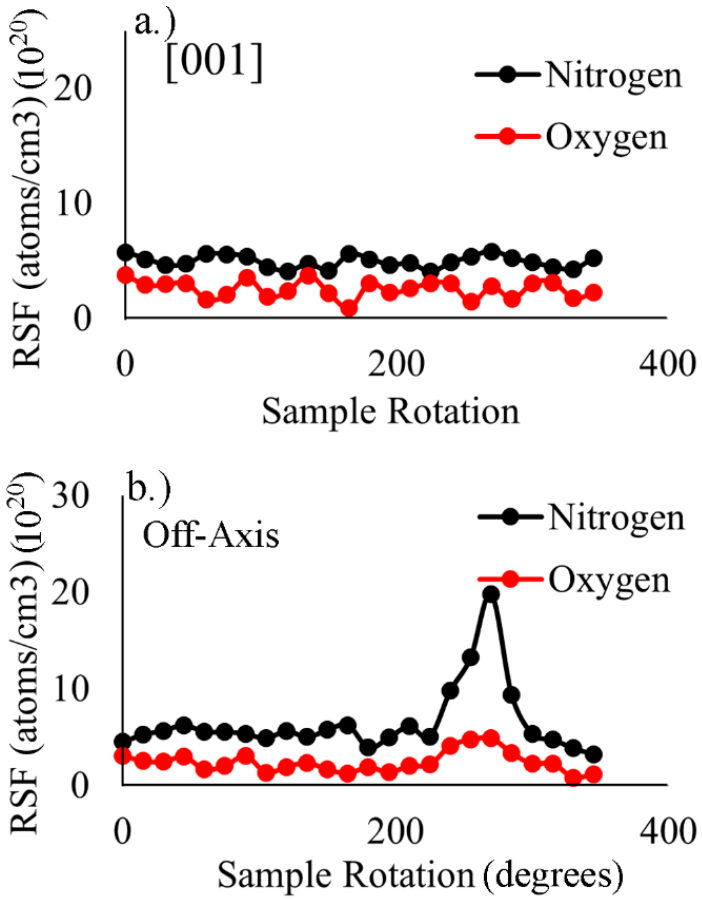

Figure 32. Plots showing the rotational analysis of the bicrystal implant standard for the a.) [001] and b.) a randomly oriented grain. The plots show the nitrogen (black) and oxygen (red) RSF measured for each arbitrary rotation.

Oxygen was found to exhibit an increase around the same ~75° window and the RSF value was similarly affected. Excluding the 75° window, the RSF average was found to be $2.4 \pm 0.6 \times 10^{19}$ with a maximum increased value of 4.9×10^{19}. The relative RSF variation with rotation outside of the 75° window for oxygen was observed to vary more than nitrogen, exhibiting values of 30% and 13% respectively.

6.3.4 Determination of orientation effects

The rise in RSF was found to correlate to a particular sample orientation with respect to the primary ion beam. Specifically, the rise was observed when the primary beam was tilted 23.9° along the equatorial axis of the sample. Therefore, it was hypothesized that the crystal orientation normal to the primary beam was likely the cause of the increased RSF and reduced sputter rate.

An FEI NanoLab 600 SEM/FIB equipped with an EDAX TSL EBSD detector was used to determine the crystallographic orientations of all the faces of the bicrystal implant standard. Since the specimen was electropolished, no further sample preparation was needed. Data acquisition was performed using beam conditions of 30 kV/ 21 nA, which yielded an average confidence interval of 0.93. The EDAX OIM software was used to generate inverse pole figures as well as show the lattice orientation for each crystal orientation (Figure 33). The orientation responsible for increasing the RSF was determined to lie 23.9° offset between the normal and axial face of the implant standard. Using this information, the orientation was simulated in Autodesk Fusion 360. The lattice orientation as defined by the EBSD software was used as endpoints to elucidate the 90° transformational path from the normal face to the axial face. Once the transformation direction was determined, the lattice orientation was rotated 23.9° to determine the orientation with respect to the primary beam, which was found to be the [101] plane (Figure 34). From the grain orientation simulation as well as the low sputter rates associated from the phenomenon, it was determined that the higher RSF values are a result of ion beam channeling.

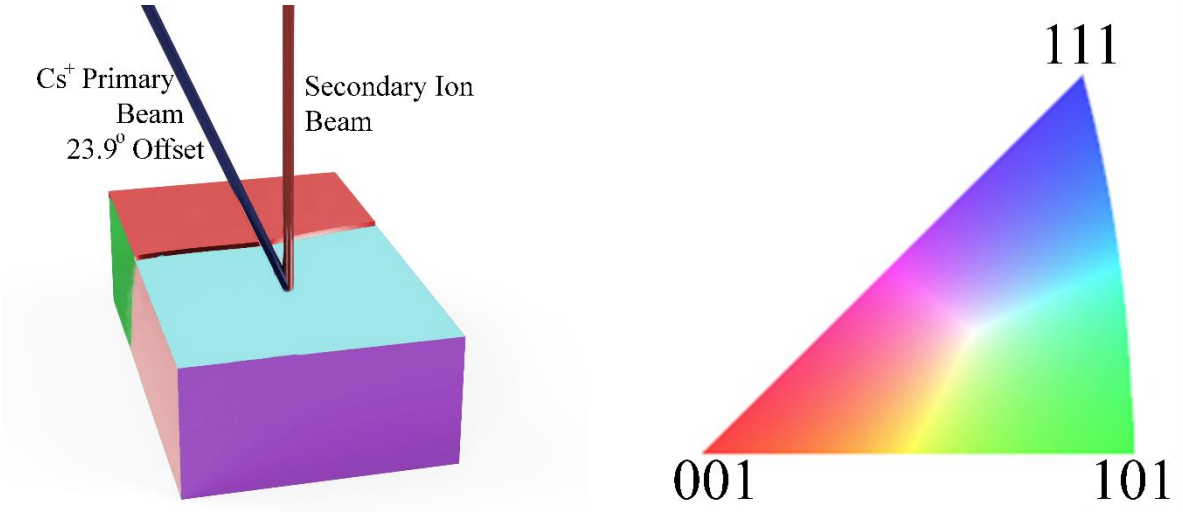

Figure 33. A diagram showing the crystal orientations of the bicrystal implant standard HL 24. The colors found on the sample faces correspond to a grain orientation indicated by the colorized IPF triangle. The low indexing blue grain illustrated above is the grain which was found to have a higher-than-expected RSF value when the sample was loaded so the Cs+ primary beam was rotated 23.9° along the equatorial axis of the sample.

Ion beam channeling is a well-known phenomenon in which ions traveling perpendicular to a major crystallographic plane will penetrate much deeper into a material compared to a generic orientation [77]. The alignment of atoms along a major crystallographic plane creates 'channels' of interstitial space which allows the ions to penetrate more deeply before collisions happen. As the collisions are occurring deeper into the material, less material is removed in the sputtering process, resulting in slower sputter rates [78]. The change in sputtering mechanics also changes the fractionalization of secondary ions. Since both RSF and concentration of impurity atom determinations are dependent on the ratio of matrix to impurity secondary intensities, this deviation causes these values to be inaccurately measured when ion channeling conditions are inconsistently present.

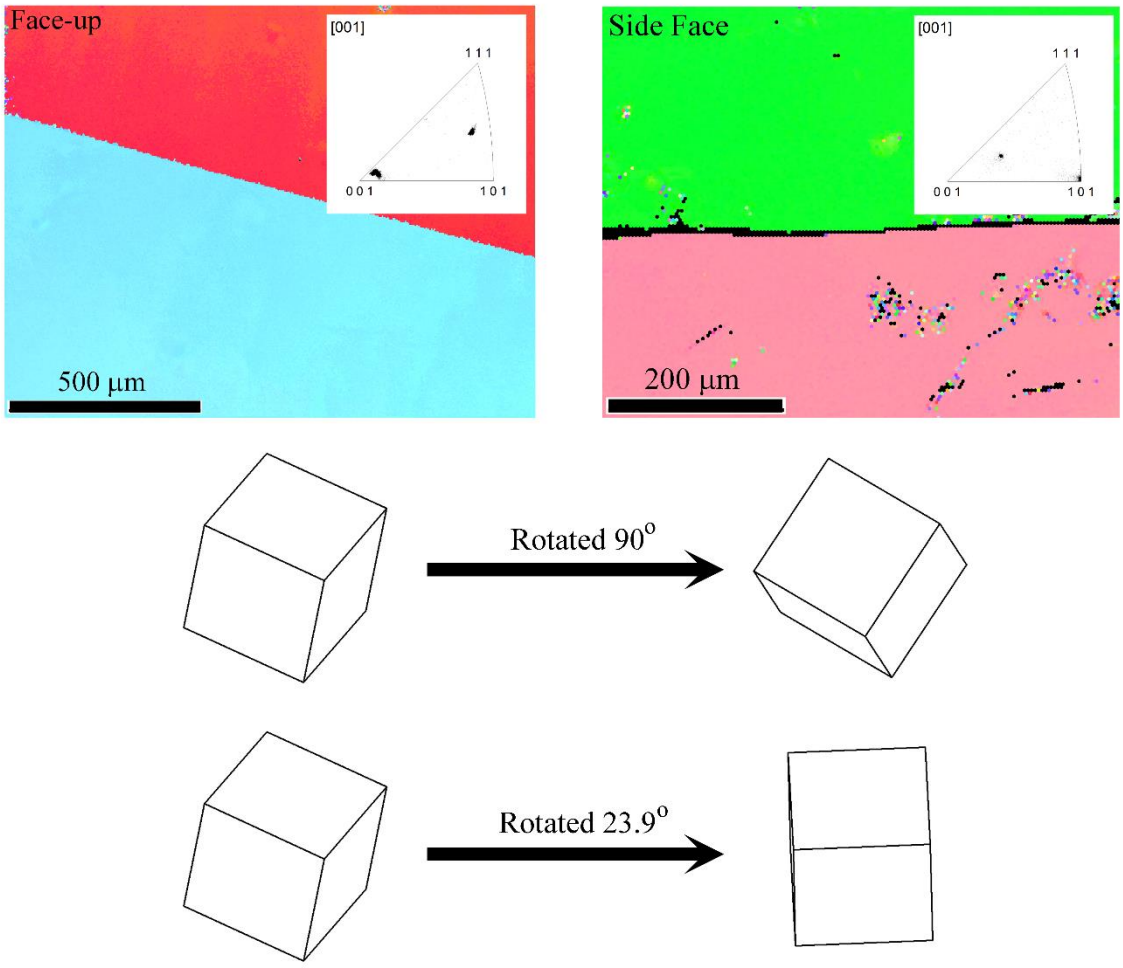

Figure 34. Shows the EBSD orientation image maps of the analysis surface (face-up) and the side face of the grain yielding high RSF values. The two faces represent the defined endpoints of a transformation that can be simulated to determine the crystal orientation at 23.9° offset from the analysis surface. The orientation which was offset 23.9° was found to be the [101] plane.

To verify this phenomenon in niobium and to evaluate the overall sputter rates for niobium, the FEI NanoLab 600 focused ion beam (FIB) was used to sputter craters on selected niobium grains. Prior to sputtering, EBSD orientation image maps were acquired on the niobium substrates to select varying grain orientations for analysis (Figure 35). The substrates were then tilted so that the Ga^+ ion beam was normal to the substrates. Sputtering

was performed using an accelerating voltage and beam current of 30 kV and 21 nA respectively. The Ga^+ ion beam was rastered over a 75 µm × 75 µm area for 15 minutes. Crater depth measurement via stylus profilometry was used to determine the sputter rates for the various niobium grains. The sputter rate data was then imported in Origin 2021b to generate a contour plot for the sputter rates.

It was observed that all three major crystallographic planes exhibited slower sputter rates than those with a random intermediate orientation, albeit the effect was less evident for the [101] plane. This suggests the ion channeling might also increase the RSF for the [111] and [001] planes as was evident for the [101] plane rotating sample SIMS study.

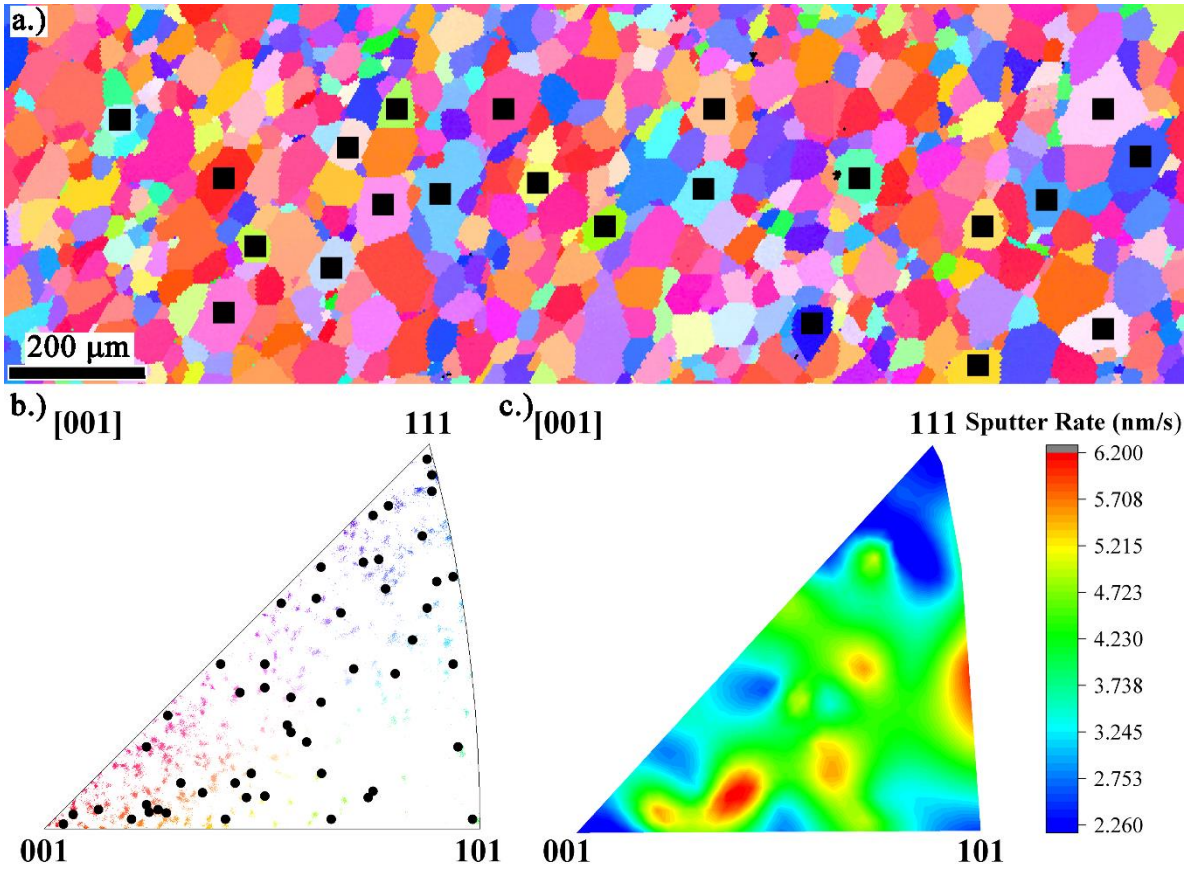

Figure 35. A.) EBSD orientation image map (OIM) of a niobium substrate. A Ga+ ion beam was rastered over a 75 µm × 75 µm area to generate craters in select grains to determine the

sputter rates of a wide array of orientations. B.) The inverse pole figure with the FIB locations annotated. C.) The sputter rates for each orientation were used to generate a sputter rate contour plot. The sputter rates nearing the major crystal planes were observed to be much slower than intermediate oriented grains due to ion channelling[38].

6.4 SUMMARY AND CONCLUSIONS

Ongoing SIMS studies showed that working distance variation, if substantial, cannot be resolved by adjusting the DTCA between sample analyses. The changes in the working distance are caused by the deflection of the faceplate on the sample holder which ultimately adversely affects the calibration of the instrument and quantitation of the SIMS results. To mitigate this effect, JLab and Virginia Tech designed a new sample holder, specific to hold 6 mm × 10 mm × 3 mm niobium Nb samples. Support ribs were added to prevent faceplate deflection. Static stress simulations suggest this addition substantially reduced deflection of the faceplate from 10 μm to 5 nm. Single crystal N-doped silicon wafers were analyzed to determine RSF variation due to the sample holder. It was determined that switching from the CAMECA standard SIMS holder to the improved sample holder could reduce RSF uncertainty from 4.1% to 0.95%.

Grain orientation effects were investigated by rotating a bicrystal implant standard in 15° increments and recording the nitrogen RSF. It was observed that the [001] grain, with respect to normal, results remained unaffected by sample rotation, while the randomly oriented grain saw a five-fold increase when rotated to a particular critical configuration. This is attributed to the primary Cs^+ beam interacting 23.9° offset from the normal vector of the sample surface. Using EBSD to determine the orientation of the analysis surface and

side surface of the specimen, the grain orientation offset 23.9° was simulated and found to be the [101] grain orientation.

Since the ion beam is interacting with a major crystallographic plane, ion channeling was determined to be the cause of the anomalous increase in RSF. Convincing evidence that ion channeling was occurring was the drastic reduction in sputter rate and significantly increased secondary ion to matix yield. This change in the secondary ion fractionization changes the RSF for impurity species. To experimentally verify ion channeling and a reduction of sputter rate for the [111], [001], and [101] crystallographic planes, FIB was performed on a variety of grain orientations to compare sputter rates. As expected, the three cardinal orientations exhibited a reduction in sputter rates. This suggests there might be significant RSF variations for all three cardinal directions with respect to the SIMS primary ion beam.

Associating ion channeling with an increase of RSF for niobium matrices suggests that the researcher should conduct experiments to avoid ion channeling. It is difficult to predict which off-axis grain orientation would experience ion channeling prior to the analysis. It is more practical to perform EBSD prior to the SIMS analysis to select grains with normals very near the major crystallographic planes, since rotating these grains 23.9° degrees will not approach an alternative major crystallographic plane, thus avoiding ion channeling. This method would generate the most accurate and consistent results and avoids inaccurate instrument calibration.

It was observed that the oxygen RSF also increased at the same critical channeling rotational configuration, but not as drastically as the nitrogen RSF. For other rotational

configurations the relative oxygen RSF was found to vary more than nitrogen, yielding RSF variations of 30% and 13% respectively.

Chapter 7: A SIMS Approach for the Analysis of Furnace Contamination

Detection of surface contamination for SRF material is difficult due to the miniscule quantities and near atomic depth resolution needed. Inspection of samples known to have experienced surface contamination were found to have inconsistent nitride coverage after nitrogen doping, with EBSD analysis suggesting that nitride suppression tends to be most prevalent when deviating from the [111] and [001] normal grain orientations. XPS was first chosen to survey contaminated samples to see if identification was possible. Peaks indicating contamination were observed in the spectra, however the intensity was marginally above the baseline suggesting an alternative technique with greater sensitivity was needed, pointing to SIMS.

Typically, furnace caps are used to prevent contamination from reaching the interior surface of the cavities during the high temperature vacuum bake that leads into exposure to nitrogen gas. Although to date little is known about the effectiveness of these caps, SIMS analysis was performed on samples exposed to the furnace environment and protected using furnace caps. The results showed that furnace caps were very effective in limiting contamination from the furnace environment. However, especially “dirty” furnaces could still allow contaminants to reach the interior of the cavities. These furnaces were cleaned with the results showing minimal contamination for samples exposed to the furnace environment.

SIMS analysis was also performed to compare the cleanliness of samples fully prepared by nitrogen doping with those prepared by oxygen alloying. Carbon contamination

was found to be nearly 10x higher for protected nitrogen doped and electropolished samples. However, both preparation techniques mostly showed sub part per million (ppm) levels of metallic contamination with the oxygen alloyed still exhibiting in most cases less metallic contamination.

7.1 INTRODUCTION

Superconducting radiofrequency (SRF) cavities are at the heart of advanced particle accelerators, where they propel charged particles to relativistic energies essential to probe the most fundamental properties of matter[11]. Currently, niobium cavities cooled to 2 K are used for these applications. Next generation machines, like SLAC's LCLS-II HE, demand increased performance[12, 21, 74]. Researchers at Fermilab have reported a process to obtain a new level of energy efficiency with (Q_0 = 3.5 × 10^{10} at 16 MV/m) "nitrogen doping" [18]. It is achieved by heating niobium SRF cavities in vacuum to roughly 800˚C, and then flowing a low pressure stream of nitrogen gas inside the cavities for a brief period. The surface becomes decorated with lossy nitrides which subsequently must be removed by electropolishing[52, 60, 70, 79]. The final result is a low concentration of nitrogen which has thermally diffused into interstitial sites of the niobium cavities' crystalline surface (properly termed "surface alloying").

These "N-doped" niobium cavities are processed with meticulous attention to detail to avoid a premature reduction in efficiency with increasing power ("quenching")[17]. Avoiding contamination throughout the fabrication process is critical. To guard against this, cavities are capped during heating(see Figure 36) to prevent contaminants from reaching the interior cavity surface since these may limit the performance of the cavities[22].

However, mitigation of furnace contamination by capping the cavities solves the contamination issue prophylactically, rather than seeks to understand it.

Furnace caps are now widely used by SRF cavity manufacturers. Surprisingly, little mention of their use is made in the literature. Even less is known about the effectiveness of using furnace caps as a preventative measure for contamination. To the best of our knowledge, the first mention of using a protective shield was mentioned by A.V. Eliutin et. al. (1991) [80]. The authors made use of a titanium shield to act as a barrier and to purify niobium as a getter. Since then, baking with titanium has been avoided as the titanium itself can act as a source of contamination[22]. Fermilab used niobium end caps and niobium foil to limit the transfer of unwanted gasses as well as to prevent line-of-sight contamination in the furnace[22, 81]. RF tests showed that using the furnace caps improved cavity performance, although the sources of contamination were never identified.

Cavity contamination is difficult to prevent for the nitrogen doping process due to the high temperature requirement of the process. Oxygen alloying is a new alternative to "nitrogen doping" and has the potential to be a cleaner and more cost-effective process. This process bakes the SRF cavities at a much cooler 300˚C and does not require an external source of oxygen[24]. Rather, the native oxide layer is dissolved and diffused into the surface's interstitial sites, which achieves the same increase in cryogenic load efficiency[25, 82]. As a result, an electropolishing step is not required to remove any unwanted surface material. The 300˚C temperature is sufficiently high to allow for oxygen diffusion, yet low enough to prevent diffusion of carbon and nitrogen. It is also hypothesized to be less likely to allow for deposition of metallic contaminants, which is investigated in this article.

Characterization of the contaminated cavities may lead to further understanding of the doping process and act as a quality assurance check to prevent costly loss of materials. An ultra-sensitive means of surface composition measurement is required. This is accomplished by SIMS, a surface characterization method which uses a primary ion beam to impact the surface of a sample in which the surface is sputtered at a very controlled rate[31, 34, 38]. The sputtered material is then ionized, and a secondary ion beam is formed. The secondary ion beam is directed through a magnetic sector which separates the ions according to their mass-to-charge ratio (*m/q*) before being monitored by either a Faraday cup or an electron multiplier. Predetermined *m/q* ratios can be detected as a function of time and depth, ("depth profiling") to monitor specific elemental concentration profiles. Alternatively, the magnetic sector can scan over a range of *m/q* ratios to acquire a mass spectrum, which is better suited for identifying unknown species. Both of these SIMS techniques are capable of monitoring elemental concentrations in the part-per-million (ppm) to part-per-billion (ppb) range. Although SIMS is most commonly used for semi-conductors and microelectronics, it has become increasingly important to the SRF field[35]. Method improvements in quantification of polycrystalline materials have enabled impurity content analysis of niobium to be reported in the ppm range with less than 10% uncertainty[30, 83]. In this study, we take advantage of the versatility and sensitivity of SIMS to identify contaminants arising from processing niobium SRF cavities at high temperatures in vacuum, investigate the protective measures of using furnace caps, and compare the contamination potential of nitrogen doped and oxygen alloyed samples.

7.2 EXPERIMENTAL

7.2.1 Furnace Cap Design and Procedure

Furnace caps are designed to not be gas tight, as the inside cavity surface must be allowed to absorb significant gas (~160 std. cc of N_2 in the case of an LCLS-II HE 9-cell cavity) quantity during the few-minute doping process. RRR grade niobium was machined to include thru-holes to allow for gas transfer conductance but to block line-of-sight contamination from hot furnace surfaces from which there might be metal evaporation. The holes are designed to be small in diameter with respect to their depth which results in multiple wall collisions to prevent contaminants from reaching the interior cavity surface. Two holes on the edge of the caps are also included to attach the caps to the cavities with molybdenum bolts. Prior to assembly, all hardware associated with the caps is precleaned by buffered chemical polishing (BCP).

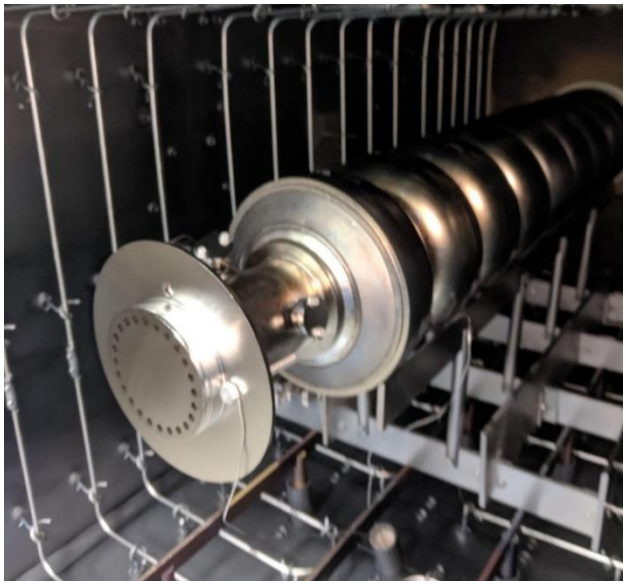

Figure 36. Depiction of a 9-cell cavity with furnace caps attached, loaded in N-doping furnace.

7.2.2 Witness Sample Preparation

Rather than sacrifice entire cavities to obtain process specimens, witness samples are used to perform representative cost-effective characterization of the cavities. Cavity grade niobium sheets 2.8 mm thick were heated to 900 °C for 3 hours in a vacuum oven. This was done to ensure adequately large grains so that each SIMS sputter profile is fully within a single grain. 6 mm × 10 mm specimens were electro-discharge machined (EDM) from this sheet stock for XPS, SEM and SIMS investigation. A 50 μm chemical removal was performed via buffered chemical polishing. Samples were subsequently "nano-polished" to yield a surface finish smoother than 200 nm R_a. The final preparation step is a few micron electropolish, presenting a surface quite analogous to that of a prepared Nb cavity.

One specimen is placed inside of the cavity protected by the furnace cap (Figure 37) with another specimen placed outside the cavity exposed to the furnace environment. The cavities, as well as the witness samples, were subjected to various duration nitrogen doping protocols. The witness samples are then placed in concave diaphragm boxes where only the corners of the specimens touch any other surface prior to characterization.

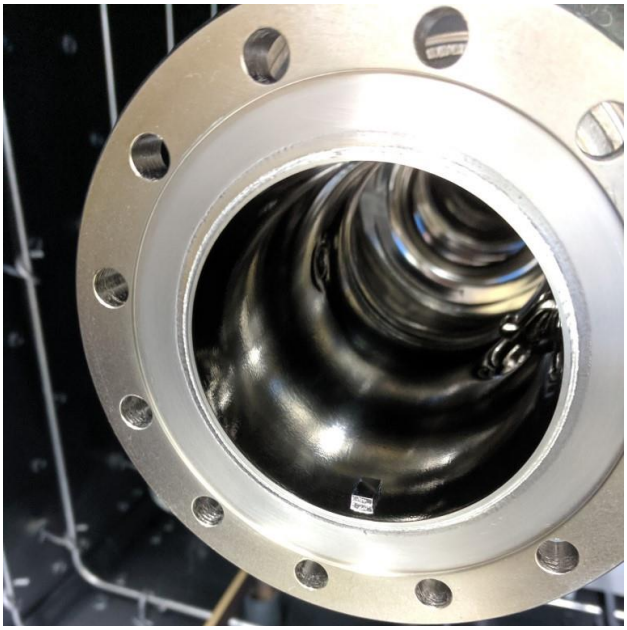

Figure 37. Shows a witness sample placed just inside of a cavity prior to nitrogen doping.

7.2.3 Cavity Preparation

High purity RRR grade niobium sheets are placed into dome shaped dies to press and form half cells by deep drawing. Several sets of these half cells are electron beam (EB) welded to generate the 9-cell cavity shape used for many current cavity designs. Potential defects and contaminants generated during fabrication are removed by buffered chemical polishing (BCP). Prior to cavity insertion into the doping furnace, the witness samples are placed just inside the cavity and furnace caps were applied. Detailed studies of cavity preparation are available[20].

Nitrogen doping was performed in three different furnaces to determine the extent of contamination. Each furnace followed the 3N60 doping procedure detailed below, among others. The materials (the cavities and witness samples) were loaded into a vacuum furnace and heated to 800 °C for 3 hours in 10^{-7} torr vacuum conditions. Nitrogen gas was bled into

the furnace to sustain 25 mTorr for 3 min, re-evacuated, and held for 60 min. Then all heat was turned off and the furnace was cooled to ambient. Following the heat treatment, the materials were removed from the furnace. Where noted, electropolishing was performed to remove the surface layer containing nitrides. The cavities were then cleaned of particulates with a high-pressure rinse (HPR) of ultrapure water, evacuated, and the low temperature rf properties were tested. SEM-EDS and EBSD were performed at JLab, with XPS and SIMS performed at Virginia Tech.

Table 4. Process history of experimental samples.

Sample	Furnace	Location in Furnace	Type of Sample
NL 108	Vendor 3	Protected	N-doped, 2N0, 5μm EP to remove Nitrides
NL 109	Vendor 3	Exposed	N-doped, 2N0, 5μm EP to remove Nitrides
NL 147	Vendor 1	Protected	N-doped, 3N60, Nitride Layer Intact
NL 148	Vendor 1	Exposed	N-doped, 3N60, Nitride Layer Intact
NL 149	Vendor 1	Protected	N-doped, 3N60, 5μm EP to remove Nitrides
NL 150	Vendor 1	Exposed	N-doped, 3N60, 5μm EP to remove Nitrides
NL 159	Vendor 2	Protected	N-doped, 3N60, Nitride Layer Intact
NL 160	Vendor 2	Exposed	N-doped, 3N60, Nitride Layer Intact
NL 166	Vendor 2	Exposed	N-doped, 3N60, Nitride Layer Intact
NL 479	Vendor 1	Protected	O-alloyed, 280˚C/ 0hr hold, furnace cooled
NL 486	Vendor 1	N/A	Unbaked Niobium

7.3 RESULTS AND DISCUSSION

7.4 Initial Characterization: SEM, XPS

Previous researchers reported[52, 84] irregular decoration of the niobium surface with nitrides following N-doping. Therefore, SEM was performed using a TESCAN SEM at JLab. The 6 mm × 10 mm coupons were mounted onto aluminum SEM pin stubs using carbon conductive tape. Imaging was performed at 5 kV accelerating voltage and 6 nA beam current at a working distance of 10 mm. Examination of the surfaces showed differences between witness samples doped inside the cavity vs. samples exposed to the furnace atmosphere. The exposed samples showed a decrease of niobium nitrides formed on the surface (Figure 38a). The extent of this "nitride suppression" varies from sample to sample. Electron backscatter diffraction (EBSD) was also performed on samples where nitride suppression was observed (Figure 38b). Nitride suppressed grains from the SEM images were cross-referenced to determine if nitride suppression correlated with specific grain orientations. The grains oriented nearest to the [111] or the [001] cardinal axes appeared to be the most free from nitride suppression. More statistics in a latter study are needed.

To understand the nitride suppression in more detail and to identify potential contaminants of the surface of these samples, XPS was performed at Virginia Tech on a Physical Electronics Quantera SXM. The XPS was chosen as a screening tool since it is non-destructive and has near atomic depth resolution, providing chemical information of approximately the top 10 nm of a surface. Spectra were acquired using an aluminum x-ray source with data collection at 280 eV pass energy and a 45° take-off angle. The scan range

was swept from 0–1100 eV with a 0.5 eV step size. To enhance the signal-to-noise ratio to detect low concentration contaminants, 100 sweeps were summed on each sample.

The survey scans showed differences between samples. The samples protected by the furnace caps appeared to be free of metallic contamination, whereas the samples exposed to the furnace environment were observed to have Sn present. However, the Sn observed in these scans was found to be in very low quantities with the concentration nearing the limit of detection (0.1 at.%) for XPS (Figure 39). For this reason, XPS can be used strictly as a qualitative screening technique for such contamination. Once it was discovered that contamination could be detected, a more sensitive technique was needed to confirm the presence of Sn as well as to search for any additional contaminants.

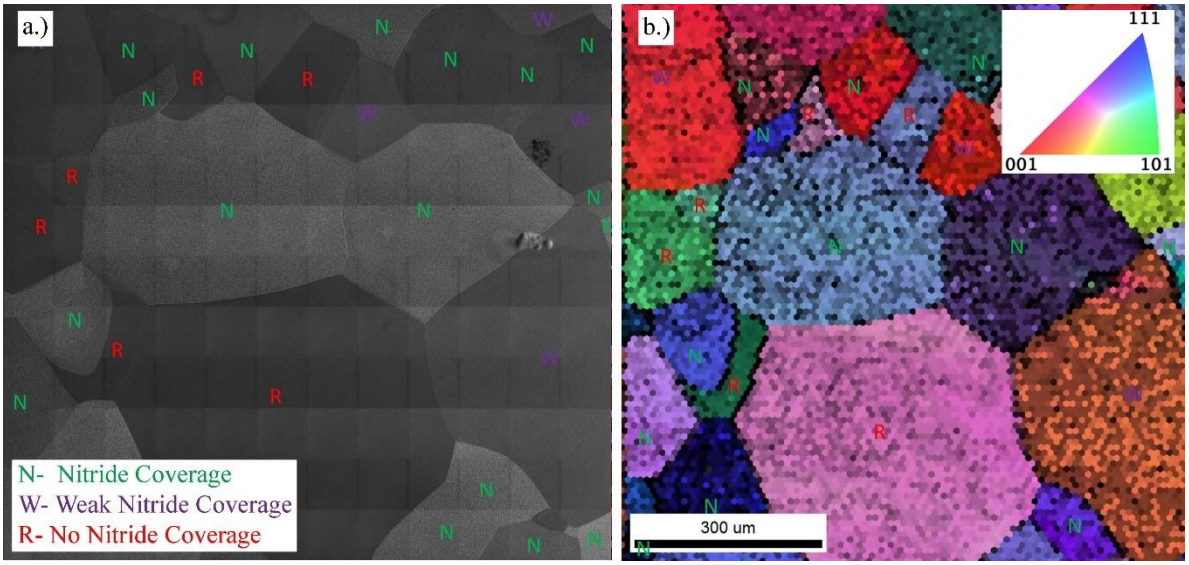

Figure 38. Image shows a composite SEM image of a contaminated sample with varying degrees of nitride coverage. B.) EBSD was performed. It was found that nitride suppression tends to be most prevalent when deviating from the [111] and [001] zone axes.

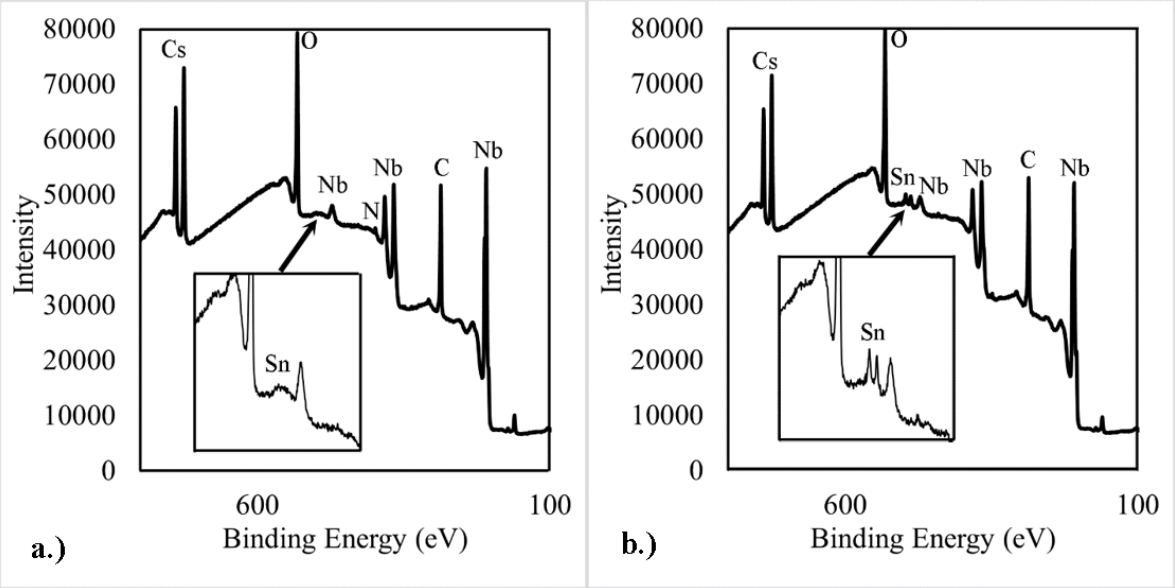

Figure 39. XPS survey scans for niobium witness samples which were a.) protected by furnace caps and b.) exposed to the furnace environment. The main observation for these scans was the presence of Sn found for the exposed sample. This signal was nearing the limit of detection (0.1 at. %) for this technique.

7.5 SIMS Mass Spectra: Furnace Cap Effectiveness

7.5.1 Nitrogen doped (nitrided surface)

Secondary ion mass spectrometry (SIMS) was performed at Virginia Tech using a CAMECA 7f Geo in mass spectral mode to further investigate the furnace contamination. While detection of all elements is possible by SIMS, the probability of ionization varies for all elements and depends heavily on the type of primary ion chosen for bombardment. Metallic elements are best detected in the presence of oxygen, thus an O_2^+ primary beam yields the best results (Figure 40 a,b). Conversely, electronegative elements, such as carbon, nitrogen, and oxygen, are best detected with a Cs^+ primary ion beam (Figure 40 c,d).

Therefore, a comprehensive investigation must include both beam conditions to identify all possible sources of contamination.

To determine the concentrations of impurities, the ratio of impurity to matrix counts is multiplied by the relative sensitivity factor (RSF) and is describe in the equation below.

$$Conc = \frac{I_s}{I_m} \times RSF$$

Ideally, an implant standard would be tested prior to the experimental samples to determine the RSF most accurately for each impurity. However, at the time of this study, the identity of the contaminants was unknown and an implant standard with these impurity species did not yet exist. Therefore, a semiquantitative analysis was performed using RSF values listed in Stevie (2016)[29]. Though the actual concentrations are likely to differ from the reported values, each set were quantified the same, making the data in this study useful for comparative purposes.

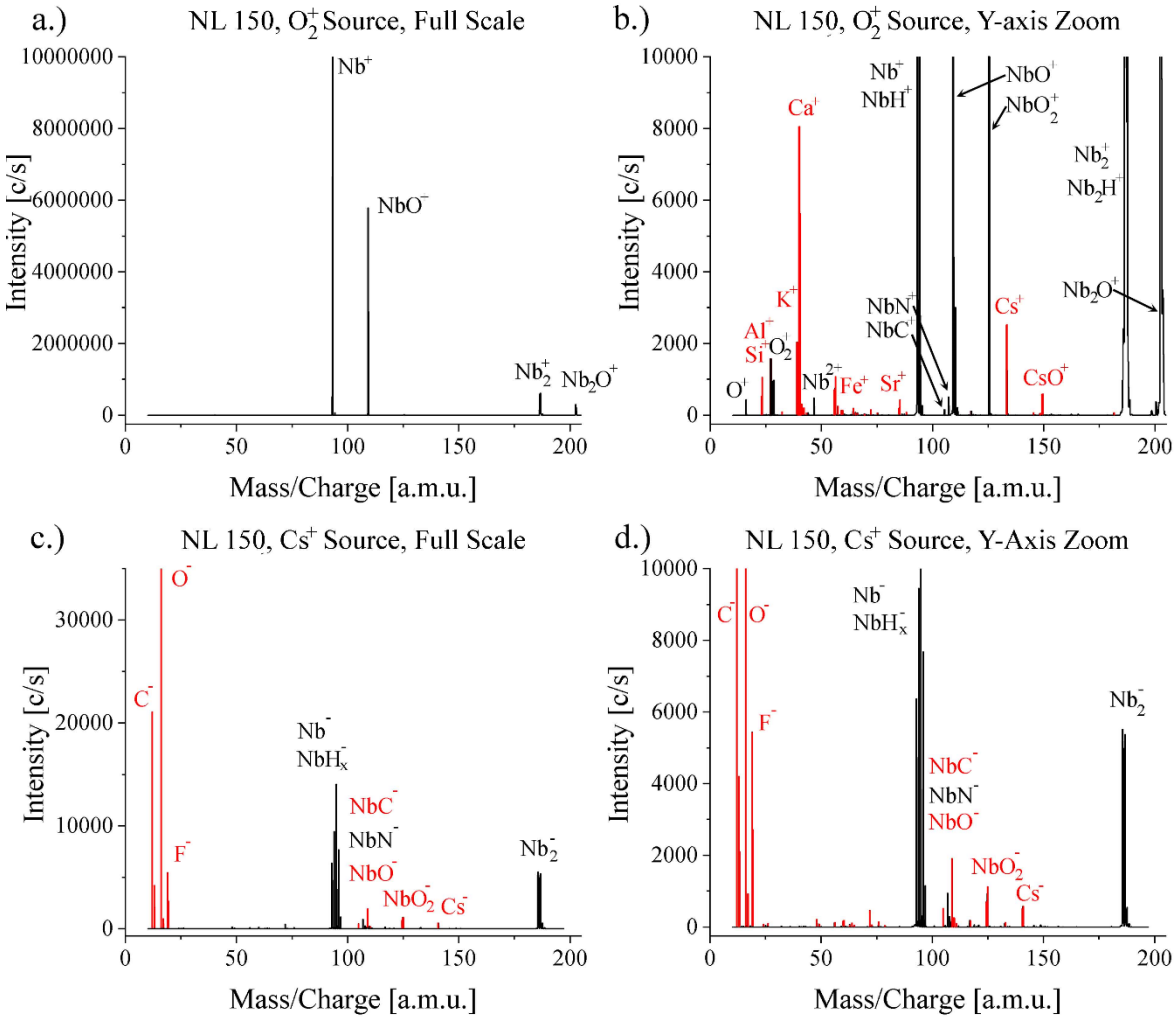

Figure 40. Example SIMS mass spectral analyses from a nitrogen doped sample exposed to the furnace environment (NL 150). Plots a) and b) show spectra at two different scales acquired with an oxygen source, with metallic species exhibiting stronger signals, where c) and d) show spectra acquired with a cesium source with the light elements being more present.

The protected and the exposed samples were analyzed using Cs^+ or an O_2^+ primary ion beams with an impact energy of 8 keV (5 kV source/ -3 kV sample) and a beam current of 25 nA. The beam was rastered over an area of 150 µm × 150 µm with an analysis window of 63 µm × 63 µm. The mass/charge was varied from 10 amu to 205 amu, which

ranges from carbon to Nb_2O^-, using a step size of 0.2 amu with each step analyzed for 1 second. The average sputter rate for niobium samples typically ranges from 0.5-0.8 nm/s at 25 nA of beam current. Therefore, to limit the analysis depth to <100nm, scan ranges were limited to 15 amu per analysis. The beam location was then moved 350 μm from the previous analysis and a new 15 amu scan was performed. This was repeated until the entire 10 amu to 205 amu window was surveyed which resulted in a 12 scan compilation ranging over 1400 μm × 1050 μm area of the sample surface. The total time for each scan was 78 seconds yielding a 40-60nm depth for each analysis. The first 5 seconds (top 1-5 nm) was found to show false high intensities for a given cycle. For example, scanning from 25-40 amu would yield a substantial peak at 25 amu regardless of whether the signal was real. To mitigate this, a sacrificial 1 amu scan was performed immediately prior to the 15 amu scan. Comparison mass spectra for Cs^+ and O_2^+ primary ion beam sources are shown in Figure 40.

Clear differences were observed by examining the spectra between the sample protected by the furnace caps and those exposed to the furnace environment. Representative mass spectra appear in Figures 41 and 42. Multiple data sets were acquired, and the results are summarized in Table 5. The results suggest that the furnace caps were effective in reducing carbon and oxygen as well as most metallic contamination on interior surface. However, calcium and potassium were found to be present on these samples regardless of the furnace caps used. It is hypothesized that this contamination may be a result of handling. Many laboratory gloves contain calcium stearate as well as other metallic stearates which act as a releasing agent during production. It is well known that this material may transfer when in use.

The overall effect on nitrogen uptake for NL 147 and NL 148 appears to have been minimal, yet NL 148 was noted to have higher light element content compared with the protected NL 147. The furnace used for NL 159 and NL 160 appears to have been more heavily contaminated, resulting in a strongly inhibiting effect on nitrogen uptake for the exposed NL 160. This is evidenced by monitoring the NbN^- peak located at 107 amu. The NbN^- peak was notable smaller than the other spectra, exhibiting less than 10% NbN^- signal compared to the other exposed sample. This suggests that usage of furnace caps is imperative if a furnace is suspected of being ‘dirty’.

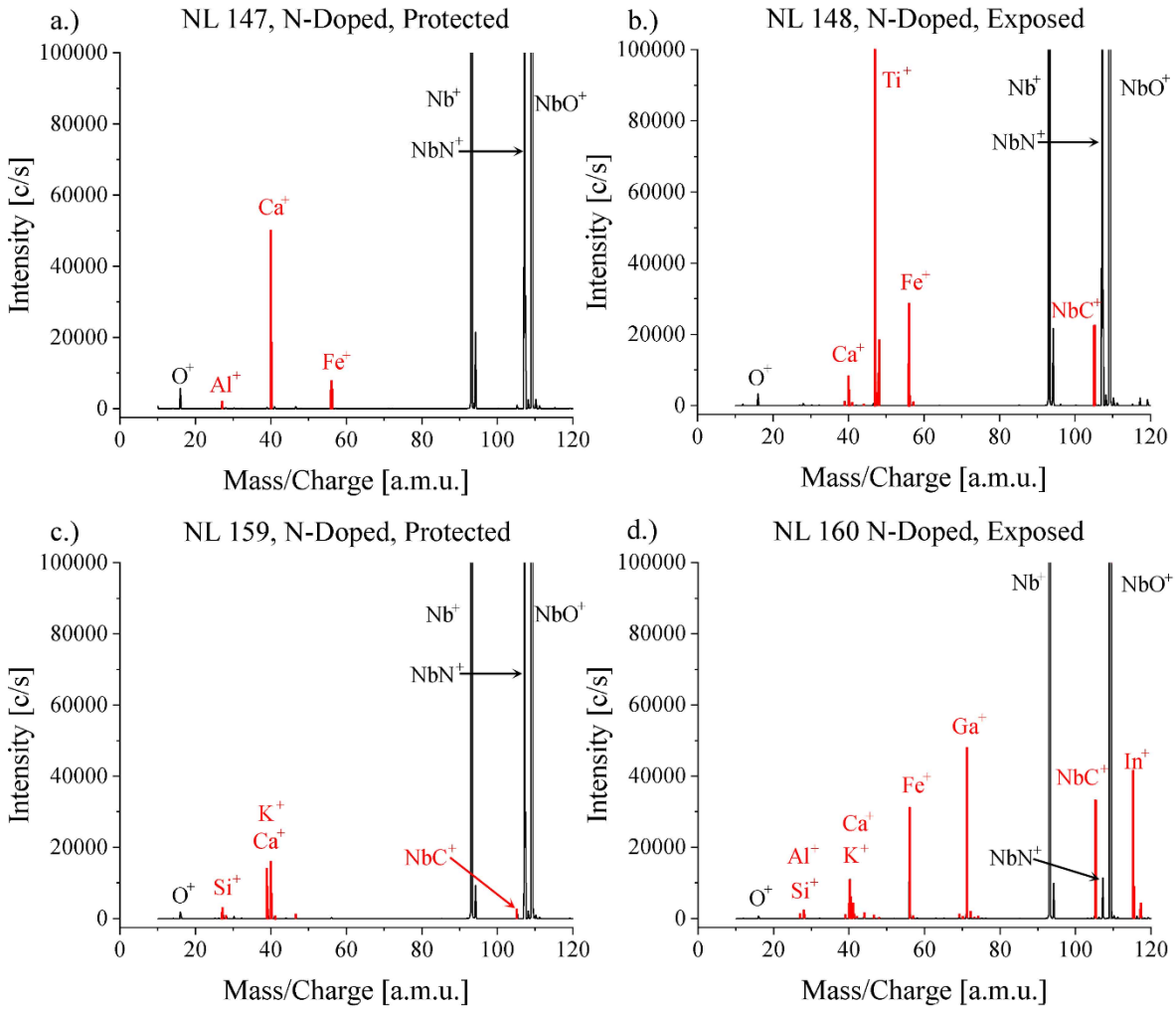

Figure 41. SIMS mass spectral analysis using O_2^+ primary beam for metallic content a.), c.) protected by furnace caps and b.), d.) exposed to the furnace environment. Note that several more peaks are observed for the sample exposed to the furnace environment, indicating that the furnace caps used blocked metallic contamination.

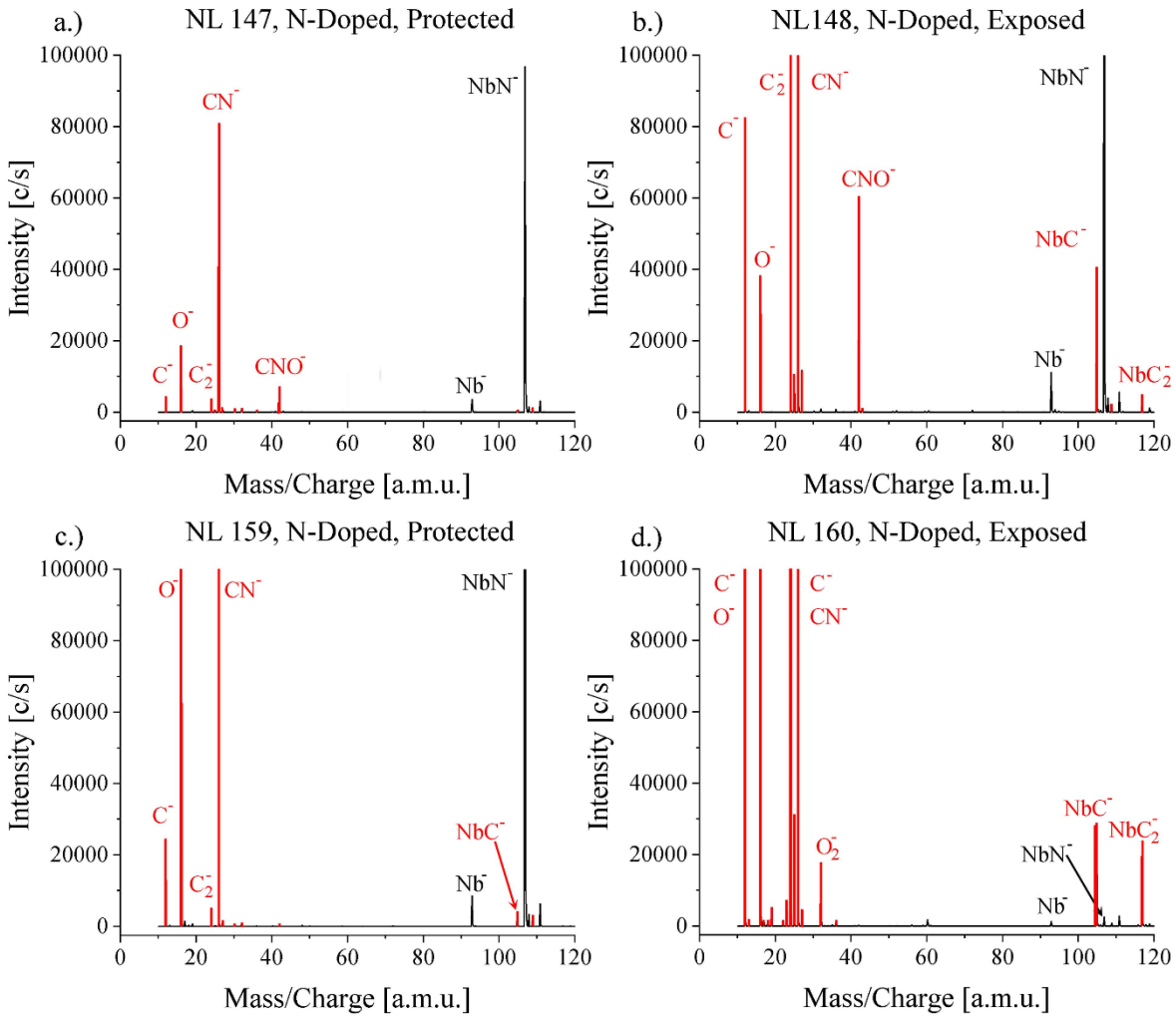

Figure 42. SIMS mass spectral analysis using Cs^+ primary beam for electronegative elements a.), c.) protected by furnace caps and b.), d.) exposed to the furnace environment. Note that several more peaks are observed for the sample exposed to the furnace environment, indicating the use of furnace caps blocks contamination.

Table 5. SIMS results for N-Doped sample with the nitride coating still present. Analyses performed prior to electropolishing.

	Semi-Quantitative Summary (Combined Cs^+ and O_2^+ data) Spectra at ~30 nm Depth Conc. (ppma)			
	NL 147 (N-Doped) Protected	NL 148 (N-Doped) Exposed	NL 159 (N-Doped) Protected	NL 160 (N-Doped) Exposed
C	1900	12000	4600	230000
N	240000	180000	340000	17000
O	1900	1200	7900	210000
Al	30	39	67	430
Si	1.4	86	5.0	350
K	11	750	544	700
Ca	713	2900	350	3900
Ti	2.2	6400	1.6	120
Fe	112	10000	8.5	11000
In	0.52	16	0.004	15000

In both cases, the concentrations of metallic contaminants were found to be much smaller for the protect samples (NL 147 and NL 159). The concentrations of titanium, iron, and indium were found to be several orders of magnitude higher than their protected counterparts. The furnace caps were found to also be effective at reducing light element contamination, especially carbon. However, the concentrations were still observed to be substantial, indicating that some gaseous contamination can still reach in the interior surface of the SRF cavities.

7.5.2 Post Electropolishing

The nitrogen doping process results in surface coverage of niobium nitride (NbN_2) which is highly detrimental to cavity performance. Therefore, the nitrides must be removed before the cavities can be placed into service[20, 55, 79]. To achieve a smooth removal of material, the Nb is electropolished. Electropolishing is a surface finishing technique that

relies on the dissolution a metal by eliminating microroughness and suppressing crystallographic etching. For niobium substrates, it is often performed with a 9:1 solution of sulfuric acid (96% H2SO4) and hydrofluoric acid (48% HF), while applying a ~10-20V potential between the anode (Nb cavity) and the cathode (high purity aluminum) producing a current density between 10-100 mA/cm^2[55, 85, 86]. The process is temperature controlled to maintain temperatures of ~6-20C.

Ideally, electropolishing would not only remove the surface nitrides but also facilitate the removal of surface contamination. To determine if the contaminants survive the electropolishing step, SIMS mass spectra were acquired using the same method as in Section B.1. Results indicate that the protected samples NL 108 and NL 149 showed less overall contamination (Figures 43 and 44) (Table 6). However, a substantial Ti peak at 48 amu was noted for NL 108 as observed in Figure 43a. The samples exposed (NL 109 and NL 150) were found to have more metallic elements present and in higher concentrations of metallic contamination indicating that the furnace caps reduce the impurity content of the final product.

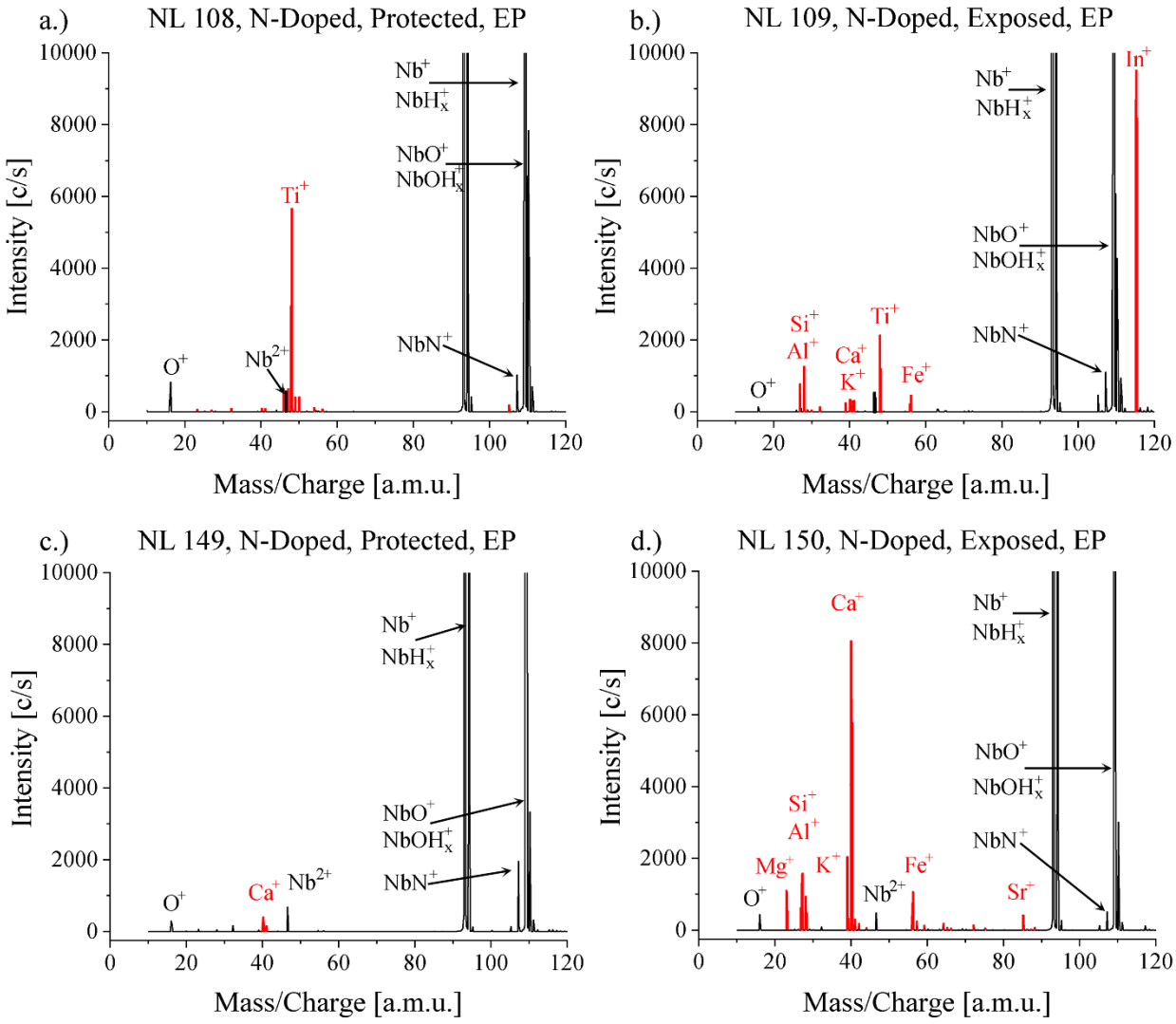

Figure 43. SIMS mass spectral analysis of electropolished witness samples using O_2^+ primary beam for metallic content a.), c.) protected by furnace caps and b.), d.) exposed to the furnace environment.

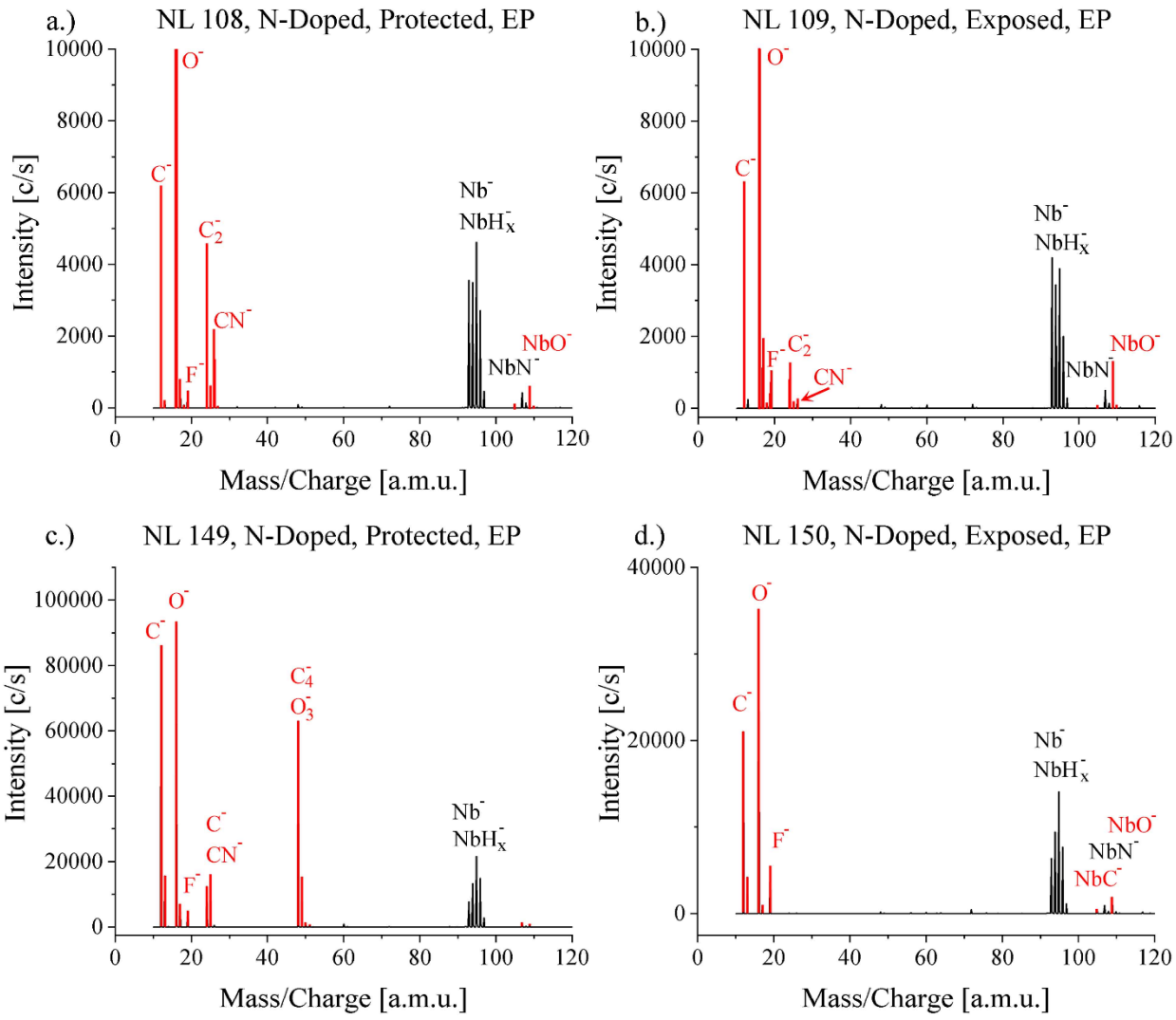

Figure 44. SIMS mass spectral analysis of electropolished witness samples using Cs^+ primary beam for electronegative elements a.), c.) protected by furnace caps and b.), d.) exposed to the furnace environment.

Table 6. SIMS results for N-Doped samples which have been electropolished to removed nitride coating.

	Semi-Quantitative Summary (Combined Cs^+ and O_2^+ data) Spectra at ~30 nm Depth Conc. (ppma)			
	108 protected (N-Doped, EP)	109 exposed (N-Doped, EP)	149 protected (N-Doped, EP)	150 exposed (N- Doped, EP)
C	2900	750	18000	5400
N	1100	3400	1100	1300
O	5400	30000	4300	2000
Al	0.38	4.0	0.019	220
Si	0.091	2.5	0.160	64
K	0.078	2.3	0.580	630
Ca	1.0	1.7	1.5	1400
Ti	61	47	0.006	0.003
Fe	0.76	1200	0.180	190
In	0	48	0.350	0.350

In general, the SIMS results for electropolished samples less contamination when compared to the contamination levels listed for samples with the nitride layer still intact. Both protected samples were observed to have notable concentrations of carbon with 2900 ppm and 18000ppm of carbon reported for NL 108 and 149 respectively. Oxygen content was similarly high with concentrations of 5400 and 4300 reported for NL 108 and 149 respectively. However, the electropolishing appeared to be effective at removing metallic contamination with the protected sample showing metallic content mostly below 1 ppm. Results from NL 108 showed 61 ppm of titanium present even though the sample was protected from the furnace environment, indicating that contamination may at times be present even after taking precautions to limit it.

7.5.3 Furnace Cleaning

Cavity production for the LCLS II-HE project is a collaborative effort of several different laboratories. The cavities produced must be capable of reaching accelerating gradients of 21 MV/m and have a Q_0 of at least 2.7×10^{10}. One reason cavities may exhibit high residual resistances are from furnace contamination[21]. One vender that experienced a trend of cavities failing specifications carried out an extensive cleaning process to remove sources of contamination by replacing multiple furnace components. While this effort led to successful production of cavities, it was unknown which contaminants were removed as a result of the cleaning process. Identification of troublesome contaminants may assist other producers in determining if their furnaces would also benefit from furnace cleaning. Therefore, exposed witness samples N-doped before and after the furnace cleaning (NL 160 and NL 166) were characterized with SIMS to evaluate the effectiveness of the furnace renovation as well as to identify contaminants which may have led to cavities that failed specification. The data are presented in Figure 45 and Table 7. The results show that cleaning the furnace had a profound effect on the contamination left on the samples. Figure 45c and d both show that light element contaminants, found between 12-32 amu, and metallic contaminants, located at 27- 92 amu, were nearly eliminated by furnace cleaning.

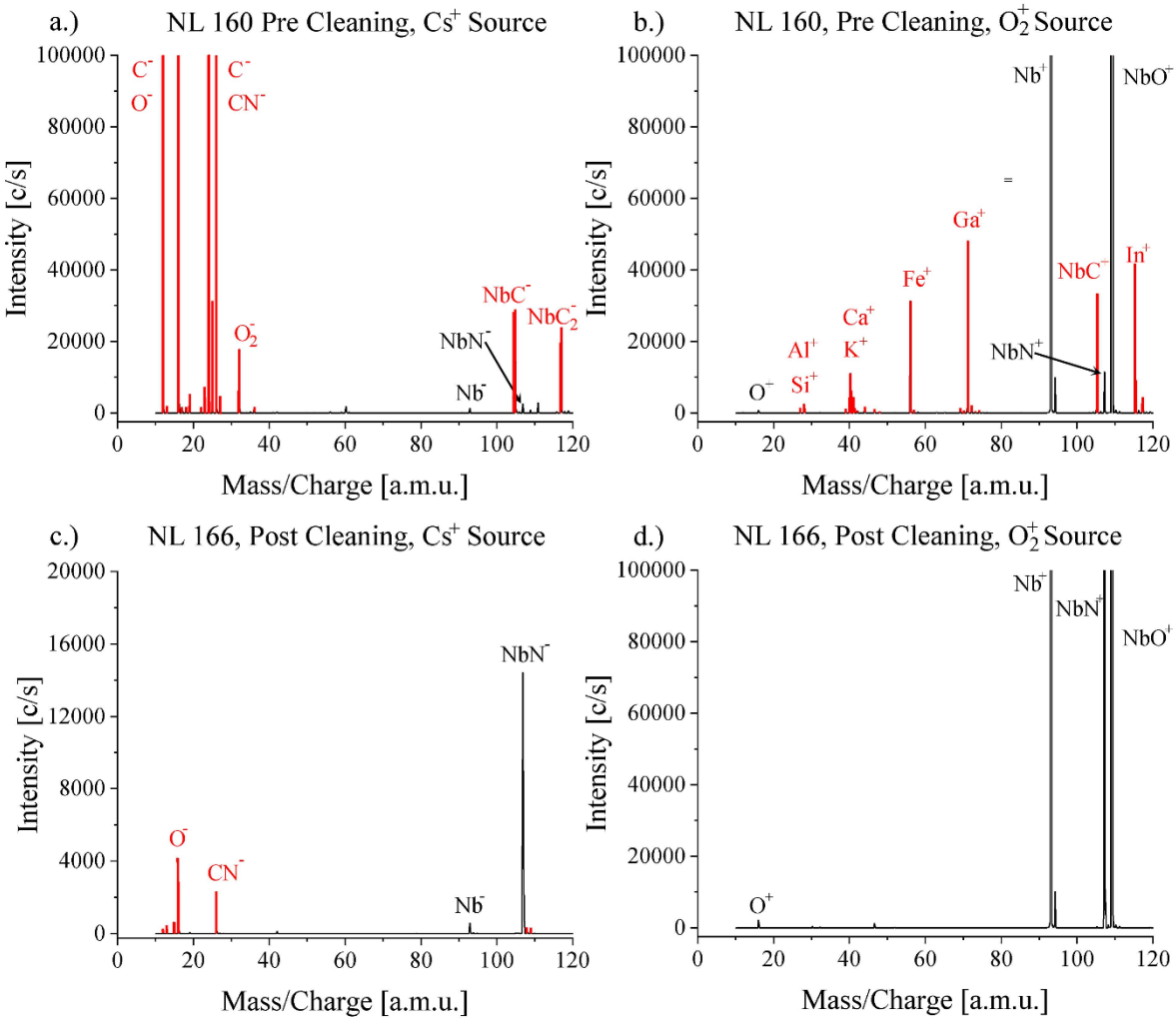

Figure 45. SIMS mass spectral analysis using both Cs^+ and O_2^+ identify all possible contaminants. A.) b.) showing a contaminated furnace environment prior to cleaning and c.) d.) showing the furnace nearly absent of contamination. Analysis of NL 166 showed the cleanest N-doped samples to date.

Table 7. SIMS results to detect contamination levels of N-doped samples before and after a doping furnace was cleaned.

Semi-Quantitative* Summary (Combined Cs^+ and O_2^+ data) Spectra at ~30 nm Depth Conc. (ppma)		
	NL 160 (doped, exposed) Prior to cleaning	NL 166 (doped, exposed) Post cleaning
C	230000	570
N	17000	230000
O	210000	2600
Al	430	<0.001
Si	350	0.008
K	700	0.59
Ca	3900	0.097
Ti	120	1.6
Fe	11000	8.5
In	15000	0.004

The two samples, which were doped in the same furnace, showed drastically different contamination levels prior to and after the furnace was refurbished. The sample doped after the furnace renovation clearly produced a surface with high nitride coverage as indicated by monitoring the NbN^- peak at 107 amu. Conversely the sample tested before the furnace refurbishment, was noted to have a weak NbN^- signal. Numerically, the nitrogen concentration was found to be nearly 15 times higher for sample tested after refurbishment. Metallic contamination was almost eliminated by the refurbishment reporting

concentrations approaching 10ppm or better, even when exposed to the furnace environment. Analysis of NL 166 showed the cleanest N-doped samples to date.

7.6 SIMS Depth Profiles: Influence of Contamination on Nitrogen Doping

SIMS depth profiles were obtained to determine if the contamination negatively influenced nitrogen diffusion. In theory, light elements, such as carbon and oxygen, may compete for interstitial space which prevents nitrogen diffusion, while metallic contaminants can inhibit the formation of nitrides. The instrument conditions were kept the same as the mass spectra work. However, specific masses were monitored as a function of depth. NL 159 and NL 160, N-doped and nitride coated sample were tested for this experiment with $^{12}C^-$, $^{93}Nb^-$ and $^{107}NbN^-$ secondary ions were monitored.

Previous works have indicated using the beam centering function available to the CAMECA 7F Geo can increase the accuracy and decrease the uncertainty between measurements [30]. As a result, the dynamic transfer contrast apertures were adjusted between analyses. The crater depth must be determined to convert the x axis of the depth profiles from time to depth. Crater depth determination was performed using a Tencor Alpha Step 500 stylus profilometer using a scan speed of 50 μm/s. Scans were performed on both axes of the crater and the average value was used. Conversion from counts to concentration is made possible by using an implantation standard prepared by Leonard Kroko, Inc. The niobium standard, first polished as the experimental samples, was dosed with 2×10^{15} atoms/cm^2 each of oxygen and nitrogen at 180 keV and 160 keV respectively.

The depth profiles revealed significant effect on both nitrogen and carbon diffusion associated with surface contamination. The sample protected by the furnace caps had a

baseline nitrogen content of 1320 ± 200 ppm whereas the content of the sample which was exposed was reduced to 200 ± 40 ppm of nitrogen (Figure 46 a). Conversely the carbon content was found to increase from 90 ± 80 ppm to 120 ± 20 ppm for the protected and the exposed samples, respectively. The carbon content was also found to diffuse more deeply for the exposed sample, reaching baseline at 870 ± 100 nm compared to 450 ± 120 nm for the protected sample (Figure 46 b).

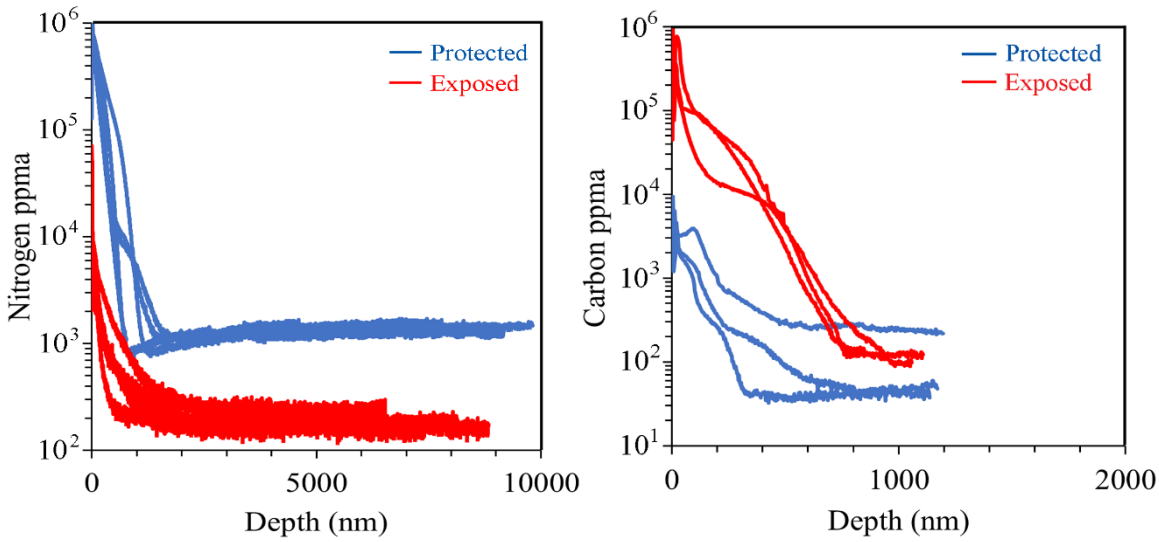

Figure 46. Depth profile of protected and exposed samples NL159 and NL 160. a.) shows a reduction in nitrogen uptake because of exposure to the furnace environment. Additionally, b.) shows that carbon had a higher concentration on the surface which diffused deeper into the bulk as a result of the exposure.

7.7 Nitrogen Doping compared with Oxygen Alloying

Oxygen alloying for optimum SRF properties is emerging as a promising technique which could replace nitrogen alloying (commonly referred to as “nitrogen doping”) as the new state of the art technique. A major advantage of oxygen alloying is that the process requires lower temperature baking. Ito et. al. determined that the quality factor improved for cavities baked around 300°C[24]. This was later confirmed in Lechner *et al*. to be a result of surface oxygen dissolution and diffusion into the niobium lattice[25, 82]. Additionally, it was shown that at 300˚C that the oxygen is the sole species which diffuses, indicating opportunity for greater control in achieving a desired oxygen concentration without having to compete with carbon and nitrogen for interstitial space. This suggests that the method is less susceptible to contamination than nitrogen doping. Therefore, SIMS mass spectra were acquired to compare witness samples (NL 149 and NL 150) from the nitrogen doping process to the oxygen alloying process (NL 479). Both sets of witness samples from the nitrogen doped and oxygen alloyed experiments were examined in a fully prepared state. Therefore, the nitrogen doped samples were electropolished to remove the top 5 μm of the surface. Electropolishing is considered unnecessary for oxygen alloying. An unbaked niobium sample (NL 486) was also tested to further explore contamination sources. The results are shown in Table 8.

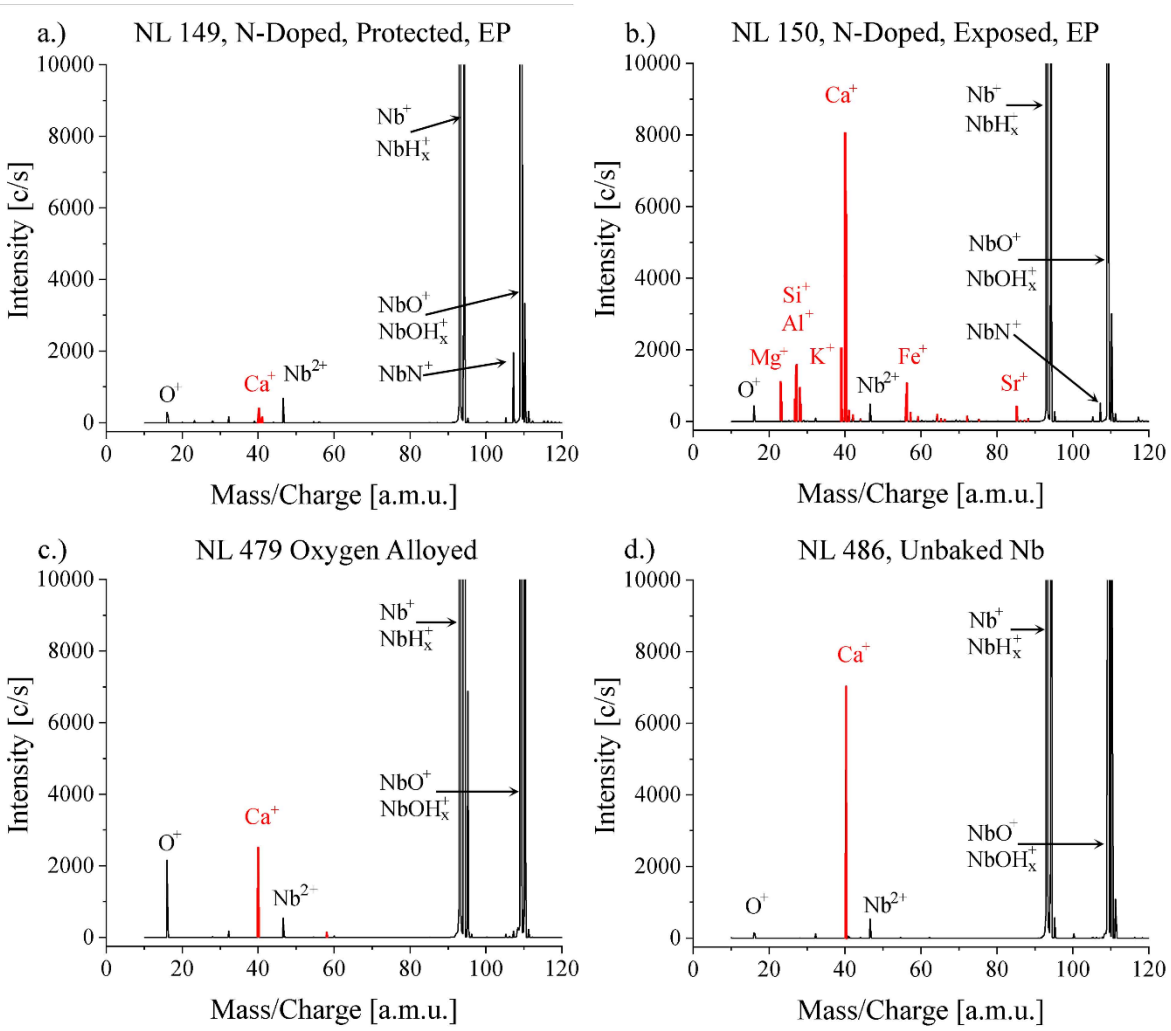

Figure 47. SIMS mass spectral analysis using an O_2^+ primary beam for metallic content: a) N-Doped protected by furnace caps with post electropolishing step b) N-Doped exposed by furnace caps with post electropolishing step c) O-alloyed sample and d) unbaked Nb specimen.

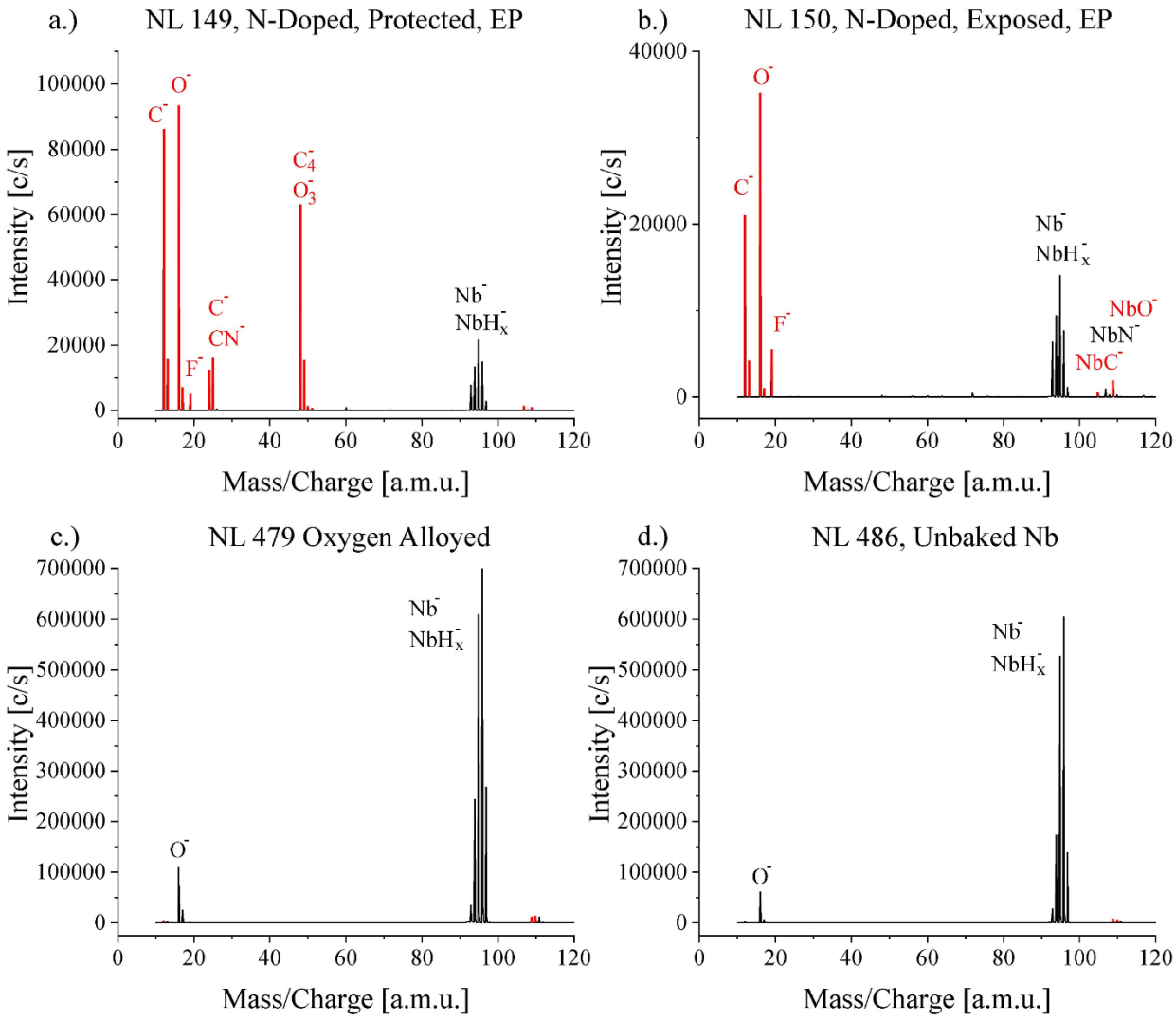

Figure 48. SIMS mass spectral analysis using an Cs^+ for C, N, and O content analysis: a) N-doped protected by furnace caps, with subsequent electropolishing step b) N-doped exposed to furnace , with subsequent electropolishing step c) O-alloyed sample and d) untreated Nb specimen.

Table 8. SIMS results comparing nitrogen doped, oxygen alloyed and unbaked niobium.

	Semi-Quantitative* Summary (Combined Cs^+ and O_2^+ data) Spectra at ~30 nm Depth Conc. (ppma)			
	149 (N-Doped, EP) Protected	150 (N- Doped, EP) Exposed	NL 479 (O Alloyed)	NL 486 (Nb, EP)
C	18000	5400	210	180
N	1100	1300	55	52
O	4300	2000	1100	780
Al	0.019	220	0.026	0.009
Si	0.160	64	0.045	0.012
K	0.580	630	0.067	0.028
Ca	1.5	1400	9.4	304
Ti	0.006	0.003	<0.001	<0.001
Fe	0.18	190	0.490	0.038
In	0.35	0.35	<0.001	<0.001

The light elements (C, N, O), which occupy interstitial locations, were found to have higher concentrations in nitrogen doped specimens than the oxygen alloyed sample analyzed. For both the protected N-doped sample and O-alloyed sample the concentration of metallic contaminants was found to be below 1 ppm with the exception of calcium. Though both samples had sub-ppm concentrations, the total metallic contamination levels were less for the oxygen alloyed sample. Calcium contamination was found to be also present on the unbaked EP niobium as well as the oxygen alloyed sample. This strongly supports the presumption that this contamination is a result of handling.

7.8 Summary

Contamination has been an ongoing problem for SRF cavity production and is aggravated since the advent of nitrogen doping due to the technique's high processing

temperatures. The impact of contamination on niobium surfaces is apparent by the absence of surface nitrides by SEM. In certain cases, nitride depletion appears to be grain specific. EBSD was performed in conjunction with the SEM analysis. Grains were tabulated and categorized by the extent of nitride suppression with the EBSD data superimposed. This revealed a correlation with the [111] and [001] grains closest to the zone axis being most resistant to nitride suppression. Limited statistics are available at the present time.

The identity of the surface contamination is difficult to determine due to the contamination layer being less than 100 nm thick. With its non-destructive nature and surface sensitivity, XPS was performed to screen for possible contaminants. Sn was observed to be qualitatively present on samples which were exposed to the furnace environment. However, when detected, the signal was marginally above the limit of detection. Later SIMS analysis did not agree with the detection of Sn. Though it was possible that the XPS results indicated some form of contamination, the low signal made accurate identification difficult.

SIMS was performed on N-doped witness samples protected or exposed to the furnace environment. A substantial increase in contamination was observed on the samples exposed to the furnace environment. The additional carbon and oxygen diffused into the exposed sample and generally led to a decrease in the nitrogen content. This also affected the nitrogen diffusion, as the samples heavily contaminated with carbon were found to have carbon diffusing more deeply and decreasing the baseline nitrogen content.

The furnace caps were also effective in preventing metallic contaminants from reaching the interior of the cavities. This appeared to be crucial as heavily contaminated specimens appeared to have increased metallic content even after 5 μm electro polished

surface removal. The protected specimens, which showed some contamination, had most of the metallic contaminants removed by the electropolishing step. The light elements (C, N, O) mostly survived the electropolishing indicating that cavities heavily contaminated with these elements would need further removal of the surface to repurpose a cavity. Recovery of a very "dirty" furnace was found to be possible when the contaminating components were replaced. The exposed sample tested in such a newly cleaned furnace found almost no contamination.

The oxygen alloyed sample NL 479 showed lower levels of light element contamination as well as metallic contamination. The protected N-doped sample showed higher levels of light element contamination compared to the O-alloyed sample. Both the protected and electropolished N-doped sample and the O-alloyed sample showed mostly sub-ppm levels of metallic contamination. However, the O-alloyed sample was still found to have less metallic contamination.

In general, SIMS analyses showed that the post EP removal of protected samples showed limited contamination remaining for nitrogen doped samples, which is both good and to be expected. However, the experiments performed here showed the presence of contamination on the nitrided surfaces to greatly complicate, even significantly impede the effective "nitrogen doping" of the cavity surface. This variability between details of various furnaces used and even the variability of conduction paths produced by different capping methods presents a significant challenge to reproducible process control needed from reliable production methods for "N-doped" niobium SRF accelerator cavities.

Chapter 8: Conclusion and Future Work

SIMS is a versatile technique, capable of detecting every element on the periodic table. Additionally, its ppb-ppm sensitivity makes this a truly powerful technique. However, the acquisition of accurate and quantitative results for SIMS instrumentation has proven to be difficult for many years. Secondary ion yields for various impurities are strongly dependent on the matrix in which the impurities exist. Therefore, there are nearly an infinite number of combinations to determine RSF values. As a result, traceable implant standards exist for only the most common of SIMS applications. Other standards must be created by ion implantation. In general, the RSF uncertainty for polycrystalline implant standards has ranged from 20% - 60%. This thesis investigated sources of RSF uncertainty for niobium implant standards and proposed mitigation measured to limit known and newly discovered causes that affect the RSF determination. The research topics proposed in Chapter 4 were addressed in the following ways with the findings reported below.

8.1 Investigate implant standard quality and its impact on RSF variation.

The calculation to determine the RSF depends on the known dosage of an impurity, the ratio of impurity and matrix counts, the analysis time, and the sputter rate. Most of the values are fixed; the dosage is a value obtained by the ion implanter, the impurity and matrix counts are data outputs, and the analysis time is an instrument parameter with an exact value. However, the crater depth is the average height difference between the crater and the unsputtered surface. As a result, the crater depth determination is not an exact

value, which can be a source of measurement uncertainty that propagates to the RSF determination. Multiple factors were determined to increase the uncertainty of crater depth determination and subsequent RSF measurement:

1. Grain size: Grains of differing crystallographic orientations sputter at different rates. Therefore, if the average grain size of a material is smaller than the raster of the Cs^+ primary beam, the crater bottom will not be flat. Thus, the standard deviation of the crater depth value is increased. As a result, single crystal implant standards produce the most consistent crater depth values and thus sputter rate determination for a specific profile acquisition.

2. Surface preparation and surface roughness: The flatness of the initial surface is just as important to reducing uncertainty as the flatness of the crater bottom. This surface roughness for a material can be controlled by ensuring the implant standard is polished to yield nearly atomically smooth surfaces. For niobium, electropolishing generated the smoothest surface finishes which correlated to the RSF values with the least uncertainty.

3. Instrument set-up and beam tune: The primary beam must be properly tuned to ensure a concentric beam interacts with the sample surface. If beam astigmatism is present, this leads to uneven sputtering in the crater which results in a rounded crater bottom and poor depth resolution. Additionally, apertures will erode over time and can cause flares in the beam shape that cannot be resolved by tuning. In this case, inadequacies in instrument set-up and maintenance can distort the crater and affect the RSF value and uncertainty.

8.2 Determine the effects of surface topography and its influence on RSF variation. Additionally, suggest instrumental parameters which may mitigate topography as a source of RSF deviation.

Magnetic sector SIMS instruments rely on consistent working distances to make sure that the secondary ion beam remains tuned between analyses. Topographical variations are often a result of differing etch rates for various grains during the polishing process. Therefore, polycrystalline materials are more likely to experience topographical variations compared to single crystals. Inconsistencies in working distance cause the extraction yields to change due to the shifting distance from the immersion lens on a CAMECA instrument, which collects the sputtered secondary ions and directs the beam through the secondary column. The change in the working distance causes a deviation in the beam trajectory which affects the detection of the secondary ions. For analysis of implant standards, this can result in variations in ratio of impurity/matrix counts and affect the RSF determination. Recent CAMECA SIMS instruments have accounted for the trajectory deviation by adding dynamic transfer contrast apertures (DTCAs) to the secondary column to realign the beam as it passes through the contrast and field apertures. This addition is very useful for polycrystalline materials.

8.3 Investigate RSF variation as a function of working distance variation, resulting from sample loading.

The DTCA is useful to correct minor topographical differences, such as grain height variation, but extensive working distance variations cannot be resolved by adjusting the DTCA. Generic sample holders provided by the manufacturer are intended to be versatile and to allow for many different specimen geometries. These sample holders use a large hollow cavity which has a thin faceplate to allow the sample to be mounted. Samples are

held in place by compressing springs between the sample and a backing plate. The analysis of single crystal implant standards showed that the RSF value would change depending on the number of samples loaded, which suggested that variations in the force applied to the faceplate caused the RSF to change.

Static stress simulations of the CAMECA style holder showed that the faceplate could deflect up to 10 μm by the sample loading force, subsequently changing the working distance between the sample and the extracting plate. Therefore, to obtain the most consistent RSF values, sample holders should be designed to allow for minimum faceplate deflection. By adding structural support to the faceplate, it was simulated that faceplate deflection could be effectively nullified. SIMS using the newly designed and reinforced sample holder confirmed that the RSF variation could be reduced by preventing faceplate deflection.

8.4 Determine if certain grain orientation generate differing RSF values.

Grain orientation has been hypothesized to affect RSF determination but the exact cause of its influence has been unclear. It was observed that some grains would exhibit values atypical to the majority of grains on a polycrystalline niobium sample. When this phenomenon occurred, three affects were usually observed. They had very low sputter rates, the matrix counts were nearly an order of magnitude higher than expected, and the impurity signal was lower than expected. If observed in an implant standard, these abnormal grains produced much higher RSF values. EBSD performed on these anomalous grains determined that the grain orientations appeared to be random with respect to normal. Therefore, it was

hypothesized that understanding the grain orientation with respect the primary beam was critical to determining the cause of the grain orientation effect.

An experiment was devised to perform SIMS depth profiles on bicrystal implant standards, determining the RSF values at 15 degree rotational increments. EBSD was performed prior to the analysis and it was determined that a [001] grain and an off axis grain, with respect to normal, could be identified and tested. The experiment showed that at some critical rotation, the RSF value was increased by a factor of 5 for the off-axis grain. The loading alignment of this critical rotational configuration was noted and it was determined the primary beam was offset 23.9 degrees equatorially on the implant standard. Mathematical simulations showed that the grain orientation with respect to the primary beam was the [101] grain orientation. Ion channelling was determined to have caused the increase in RSF for these anomalous grains. FIB confirmed ion channelling was possible for all three cardinal grain orientation.

8.5 Determine if SIMS can be used to identify near surface contamination and to evaluate the effectiveness of furnace caps for SRF cavities. -

Contamination resulting from high temperature baking during the nitrogen doping process has proved to be difficult to avoid. To prevent contamination from the doping process the SRF community uses niobium end caps to place a barrier between the furnace environment and the interior cavity surface. Prior to this study, the effects of these furnace caps have not yet been evaluated and their use scarcely mentioned in literature. XPS survey scans were first acquired of the witness samples both protected from and exposed to the furnace environment. The results showed a very small signal increase where Sn would be found for samples exposed to the furnace environment. Although it is likely that the signal

increase is due to contamination, subsequent SIMS analysis showed that Sn was not present on these samples and indicted that XPS is not sensitive enough to detect furnace contamination.

Magnetic sector SIMS are typically used to generate depth profiles in which a specific mass/charge is monitored as a function time or depth. In this case, the species which are monitored are known to be present. However, these instruments can also vary the mass/charge as a function of time to survey for unknown species in a mass spectrum. The detection sensitivity of non-metals and metals differ according to the type of primary ion beam used to ionize the sample. Therefore, to comprehensively survey a sample all possible unknown species, an O_2^+ beam and a Cs^+ beam were used for metals and non-metals respectively.

Mass spectra were acquired on N-doped witness samples which were protected and exposed to the furnace environment. Initially, samples were tested with the nitride coating intact. The results showed a reduction in carbon and oxygen contamination as well as a reduction in metallic contaminants for samples protected with the furnace caps. To determine if the contaminants would survive the electropolishing process, the experiment was then repeated on samples where the nitride layer was removed. It was found that the metallic contamination was mostly removed via electropolishing. However, carbon and oxygen were found to survive in high concentrations. This was due to these elements ability to diffuse through the interstitial sites of the niobium lattice. Depth profiles showed that carbon contamination would diffuse deeply and reduce the interstitial nitrogen content that would otherwise be produced by the intended process uncontaminated. This study indicated that furnace caps were not only effective, but their use is likely crucial to

producing a high performing SRF cavity. Additionally, the magnetic sector SIMS was found to be an effective tool to identify contaminants which result from the nitrogen doping process with superior sensitivity of this technique allowing for the detection of contaminants in the part-per-billion range.

8.6 Determine if oxygen alloying is less susceptible to surface contamination via SIMS. (IN PROGRESS, SIMS ANALYSIS TO BE PERFOMRED)

Oxygen alloying is emerging as a possible processing technique to replace nitrogen doping as the new state-of-the-art. In this technique, the natural occurring oxide layer is dissolved by heating the cavity to roughly 300˚C allowing the oxide to dissociate and diffuse into the bulk of the material. At this temperature, the diffusivity of carbon and nitrogen are less than oxygen. This information in based on research done by Power et al. (1959) which reported oxygen diffusion coefficients to be 2 to 3 orders of magnitude higher than carbon and nitrogen[87]. The lower furnace temperature also offers less opportunity for metal contaminants to volatilize and deposit on the surface of the niobium. It is for these reasons that oxygen alloying has been theorized to be a cleaner production technique than nitrogen doping.

Using the SIMS mass spectral analysis methods used for detecting furnace contamination, samples which were oxygen alloyed were compared to samples which were nitrogen doped and electropolished. These surfaces were prepared to simulate cavities which were ready for service. The nitrogen doped sample was observed to be mostly free of metallic contamination, having been removed by electropolishing. However, the nitrogen doped sample was found to have high levels of carbon contamination. In general, the

oxygen alloyed sample exhibited lower light element and metallic contamination levels compared to the nitrogen doping sample. This data supports the claim that oxygen alloying is a cleaner processing technique than nitrogen doping.

Acknowledgements

I would like to thank Dr. Eric Lechner, J.K Spradlin, Jay Tuggle, Natalie Sievers, John Will, McAlister Council-Troche, for contributions to this work. I am grateful for support from the Office of High Energy Physics, U.S. Department of Energy under grant DE-SC-0014475 to Virginia Tech. This work was co-authored by Jefferson Science Associates LLC under U.S. DOE contract DE-AC05-06OR23177. This material is based on work supported by the U.S. Department of Science, Office of Science, Office of Nuclear Physics.

I would additionally like to thank the Dr. Michael Kelley, Dr. Charles Reece, Mr. Fred Stevie, Dr. William Reynolds and Dr. Mitsuhiro Murayama for taking part in my Ph. D. committee as well as for the continual wisdom and guidance.

References

[1] E. Rutherford, Philosophical Magazine 21 (1911) 669-688.
[2] E. Rutherford, Proc. R. Soc. Lond. A (1928) 300-316.
[3] M. Vretenar, Radiofrequency for particle acceleratiors - evolution and anatomy of a technology, in: CERN (Ed.) 2007, pp. 1-14.
[4] V. Malka, Short History of Particle Accelerators, in: CERN (Ed.) 2006, pp. 1-24.
[5] P.J. Bryant, A Brief History and Review of Accelerators, in: CERN (Ed.) 1990.
[6] G. Ising, Astronomi och Fysik, 18 (1924) 1-4.
[7] R. Wideroe, Arch. f. Elektrot. 21 (1928).
[8] P. Waloscheck, The Infancy of Particle Accelerators, Life and Work of Rolf Wideroe, in: DESY (Ed.) 1994, pp. 94-139.
[9] M.S. Livingston, 12 (1959) 18-23.
[10] D. H. Sloan, E. O. Lawrence, Phys. Rev. (1931) 2021-2032.
[11] H. Padamsee, J. Knobloch, T. Hays, RF Superconductivity for Accelerators, Wiley-VCH, Germany, 2008, p. 521.
[12] P. Bishop, M. Checchin, H. Conklin, A. Crawford, E. Daly, K. Davis, M. Drury, R. Eichhorn, J. Fischer, F. Furuta, G.M. Ge, D. Gonnella, A. Grassellino, C. Grimm, T. Gruber, D. Hall, A. Hocker, G. Hoffstaetter, J. Kaufman, G. Kulina, M. Liepe, J. Maniscalco, M. Martinello, O. Melnychuk, T. O'Connel, J. Ozelis, A.D. Palczewski, P. Quigley, C. Reece, A. Romanenko, M. Ross, A. Rowe, D. Sabol, J. Sears, D.A. Sergatskov, W. Soyars, R. Stanek, V. Veshcherevich, R. Wang, G. Wu, LCLS-II SRF cavity processing protocol development and baseline cavity performance demonstration, SRF2015, JACoW, Whistler, BC, Canada, 2015.
[13] T.F. Stromberg, The superconducting properties of high purity niobium, Physics, vol Ph.D., Iowa State, 1965, p. 76.
[14] A.D. Palczewski, P. Dhakal, C.E. Reece, Analysis of BCS rf loss dependence on N-doping Protocols, SRF 2015, JaCoW, Whistler, BC, Canada, 2015.
[15] D. Gonnella, R. Eichhorn, F. Furuta, M. Ge, D. Hall, V. Ho, G. Hoffstaetter, M. Liepe, T. O'Connell, S. Posen, P. Quigley, J. Sears, V. Veshcherevich, A. Grassellino, A. Romanenko, D.A. Sergatskov, Journal of Applied Physics 117 (2015).
[16] D. Gonnella, Introduction to SRF and vCM Testing, in: S.N.A. Laboratory (Ed.) 2021, pp. 1-85.
[17] J.T. Maniscalco, D. Gonnella, M. Liepe, Journal of Applied Physics 121 (2017).
[18] A. Grassellino, A. Romanenko, D. Sergatskov, O. Melnychuk, Y. Trenikhina, A. Crawford, A. Rowe, M. Wong, T. Khabiboulline, F. Barkov, Superconductor Science and Technology 26 (2013).
[19] A. Romanenko, A. Grassellino, O. Melnychuk, D.A. Sergatskov, Journal of Applied Physics 115 (2014).
[20] P. Dhakal, Physics Open 5 (2020).
[21] D. Gonnella, S. Aderhold, D. Bafia, A. Burrill, M. Checchin, M. Ge, A. Grassellino, G. Hays, M. Liepe, M. Martinello, A. Palczewski, S. Posen, T. Raubenheimer, C. Reece, A. Romanenko, M. Ross, THE LCLS-II HE HIGH Q AND GRADIENT R&D PROGRAM, 19th Int. Conf. on RF Superconductivity, JACoW, Dresden, Germany, 2019.
[22] A. Grassellino, A. Romanenko, A. Crawford, O. Melnychuk, A. Rowe, M. Wong, C. Cooper, D. Sergatskov, D. Bice, Y. Trenikhina, L. Cooley, C. Ginsburg, R. Kephart, Fermilab experience of post-annealing losses in SRF niobium cavities due to furnace contamination and the ways to its mitigation a pathway to processing simplification and quality factor improvement, in: F. Lab (Ed.) ArXiv, 2013.
[23] S. Posen, A. Romanenko, A. Grassellino, O.S. Melnychuk, D.A. Sergatskov, Physical Review Applied 13 (2020).
[24] H. Ito, H. Araki, K. Takahashi, K. Umemori, Progress of Theoretical and Experimental Physics 2021 (2021).
[25] E.M. Lechner, J.W. Angle, F.A. Stevie, M.J. Kelley, C.E. Reece, A.D. Palczewski, Applied Physics Letters 119 (2021).
[26] G. Ciovati, Appl. Phys. Lett. (2006).
[27] J. Vickerman, G.I. S., Surface Analysis: The Principal Techniques, Wiley, West Sussex, UK, 2009, p. 665.

[28] D. Dowsett, P. Philipp, T. Wirtz, Nuclear Instruments and Methods in Physics Research Section A: Accelerators, Spectrometers, Detectors and Associated Equipment 645 (2011) 120-123.
[29] F.A. Stevie, Secondary Ion Mass Spectrometry Applications for Depth Profiling and surface Characterization, Momentrum Press Engineering, 2016, p. 262.
[30] J.W. Angle, A.D. Palczewski, C.E. Reece, F.A. Stevie, M.J. Kelley, Journal of Vacuum Science & Technology B 39 (2021).
[31] P.K. Chu, Materials Chemistry and Physics 38 (1994) 203-223.
[32] P. MAHESHWARI, Surface Characterization of Impurities in Superconducting Niobium for Radio Frequency (RF) Cavities used in Particle Accelerators, Materials Science and Engineering, vol Ph.D., North Carolina State University, 2012, p. 236.
[33] P. Maheshwari, F.A. Stevie, G.R. Myneni, G. Ciovati, J.M. Rigsbee, P. Dhakal, D.P. Griffis, Surface and Interface Analysis 46 (2014) 288-290.
[34] F.A. Stevie, SRF niobium characterization using SIMS and FIB-TEM, 2015.
[35] J. Tuggle, Advanced Characterization of Materials for Superconducting Radiofrequency Accelerator Cavities, Materials Science and Engineering, vol Ph.D., Virginia Tech, 2019, p. 84.
[36] R.G. Wilson, S.W. Novak, Journal of Applied Physics 69 (1991) 466-474.
[37] A. Laufer, D. Reppin, H. Metelmann, S. Geburt, C. Ronning, T. Leichtweiss, J. Janek, B.K. Meyer, physica status solidi (b) 249 (2012) 801-811.
[38] J. Tuggle, U. Pudasaini, A.D. Palczewski, C.E. Reece, F.A. Stevie, M.J. Kelley, Fundamental SIMS Analyses for Nitrogen-Enriched Niobium, 18th International Conference on RF Superconductivity, JACoW Publishing, Lanzhou, China, 2017, pp. 821-824.
[39] D.S. Simons, K.J. Kim, R. Benbalagh, J. Bennett, A. Chew, D. Gehre, T. Hasegawa, C. Hitzman, J. Ko, R.M. Lindstrom, B. MacDonald, C. Magee, N. Montgomery, P. Peres, P. Ronsheim, S. Yoshikawa, M. Schuhmacher, W. Stockwell, D. Sykes, M. Tomita, F. Toujou, J. Won, Appl. Surf. Sci. (2006) 7232-7235.
[40] A. Budrevich, J. Hunter, Metrology aspects of SIMS depth profiling for advanced ULSI processes, The 1998 international conference on characterization and metrology for ULSI technology, 1998, pp. 169-181.
[41] D.S. Simons, P.H. Chi, K.J. Kim, J. Surf. Anal. 12 (2005) 157-160.
[42] D.S. Simons, R.G. Downing, G.P. Lamaze, R.M. Lindstrom, R.R. Greenberg, R.L. Paul, S.B. Schiller, W.F. Guthrie, Journal of Vacuum Science & Technology B: Microelectronics and Nanometer Structures 25 (2007).
[43] A. Palczewski, K. Umemori, M. Wenskat, WG1 Report, TTC 2020, JACoW, Geneva, Switzlerland, 2020.
[44] J. Tuggle, U. Pudasaini, F.A. Stevie, M.J. Kelley, A.D. Palczewski, C.E. Reece, Journal of Vacuum Science & Technology B 36 (2018).
[45] J.M. Huberty, N.T. Kita, R. Kozdon, P.R. Heck, J.H. Fournelle, M.J. Spicuzza, H. Xu, J.W. Valley, Chemical Geology 276 (2010) 269-283.
[46] N.T. Kita, J.M. Huberty, R. Kozdon, B.L. Beard, J.W. Valley, Surface and Interface Analysis 43 (2011) 427-431.
[47] N.T. Kita, T. Ushikubo, N. Fu, J.W. Valley, Chemial Geology 264 (2009) 43-57.
[48] M.J. Whitehouse, A.A. Nemchin, Chemial Geology 261 (2009) 32-42.
[49] Y. Liu, X.-H. Li, G.-Q. Tang, Q.-L. Li, X.-C. Liu, H.-M. Yu, F. Huang, Journal of Analytical Atomic Spectrometry 34 (2019) 906-914.
[50] G.-Q. Tang, X.-H. Li, Q.-L. Li, Y. Liu, X.-X. Ling, Q.-Z. Yin, Journal of Analytical Atomic Spectrometry 30 (2015) 950-956.
[51] C.E. Reece, H. Tian, Exploiting New Electrochemical Understanding of Niobium Electropolishing for Improved Performance of SRF Cavities, Linear Accelerator Conference 2010, JACoW, Tsukuba, Japan, 2010.
[52] J.K. Spradlin, A.D. Palczewski, H. Tian, C.E. Reece, Analysis of Surface Nitrides Created During Doping Heat Treatments of Niobium, 19th Int. Conf. on RF Superconductivity, JACoW, Dresden, Germany, 2019.
[53] L. Zhao, C.E. Reece, M.J. Kelley, Geneisis of topography in buffered chemical polishing of niobium for application to superconduction radiofrequence accelerator cavities, 18th International Conference on RF Superconductivity, JACoW, Lanzhou, China, 2017.
[54] J. Angle, J. Tuggle, U. Pudasaini, G.V. Eremeev, C.E. Reece, M.J. Kelley, CRYSTALLOGRAPHIC CHARACTERIZATION OF Nb3Sn COATINGS, 19th Int. Conf. on RF Superconductivity, JACoW Publishing, Dresden Germany, 2019, pp. 873-877.

[55] H. Tian, S.G. Corcoran, C.E. Reece, M.J. Kelley, Journal of The Electrochemical Society 155 (2008).
[56] H. Tian, G. Ribeill, C. Xu, C.E. Reece, M.J. Kelley, Applied Surface Science 257 (2011) 4781-4786.
[57] F. Marhauser, J. Follkie, C.E. Reece, Investigation of differential surface removal due to electropolishing at JLAB, IPAC 2015, JACoW, Richmond, VA, USA, 2015.
[58] P. Peres, N.T. Kita, J.W. Valley, F. Fernandes, M. Schuhmacher, Surface and Interface Analysis 45 (2013) 553-556.
[59] J.W. Angle, E.M. Lechner, A.D. Palczewski, C.E. Reece, F.A. Stevie, M.J. Kelley, Journal of Vacuum Science & Technology B 40 (2022).
[60] P. Dhakal, G. Ciovati, W. Rigby, J. Wallace, G.R. Myneni, Rev Sci Instrum 83 (2012) 065105.
[61] G. Ciovati, P. Dhakal, G.R. Myneni, Superconductor Science and Technology (2012).
[62] P. Koufalis, D. Hall, M. Liepe, J. Maniscalco, Effects of Interstitial Oxygen and Carbon on Niobium Superconducting Cavities, arXiv preprint, 2016.
[63] D. Gonnella, B. Clasby, R. Eichhorn, B. Elmore, F. Furuta, M. Ge, A. Grassellino, C. Grimm, D. Hall1, Y. He, G. Hoffstaetter, J. Holzbauer, J. Kaufman, P. Koufalis, M. Liepe, J.T. Maniscalco, O. Melnychuk, T. O'Connell, A. Palczewski, Y. Pischalnikov, C. Reece, P. Quigley, A. Romanenko, D. Sabol, W. Schappert, J. Sears, D. Sergatskov, E. Smith, V. Veshcherevich, Cryomodule Testing of Nitrogen-Doped Cavities, SRF2015, JACoW, Whistler, BC, Canada, 2015, pp. 182-186.
[64] D. Gonnella, T. Gruber, J. Kaufman, P. Koufalis, M. Liepe, J. Maniscalco, Fundamental Studies on Doped SRF Cavities, 18th International Conference on RF Superconductivity, JACoW, Whistler, BC, Canada, 2015, pp. 187-190.
[65] J. Halbritter, Z. Physik 238 (1970) 466-476.
[66] J. Halbritter, Z. Physik 266 (1974) 209-217.
[67] T. Kubo, Superconductor Science and Technology 34 (2021).
[68] F.P.-J. Lin, A. Gurevich, Physical Review B 85 (2012).
[69] M. Checchin, A. Grassellino, Applied Physics Letters 117 (2020).
[70] Y. Trenikhina, A. Grassellino, O. Melnychuk, A. Romanenko, Characterization of Nitrogen Doping Recipes for the Nb SRF Cavities, in: JACoW (Ed.) SRF 2015, Whistler, BC, Canada, 2015.
[71] J. Tuggle, U. Pudasaini, G.V. Eremeev, A.D. Palczewski, C.E. Reece, M.J. Kelley, Materials Characterization for SRF Cavities Gaining Insight into Nb3Sn, IPAC 2017, JACoW, Copenhagen, Denmark, 2017, pp. 1111-1113.
[72] Z.Q. Yang, X.Y. Lu, J.F. Zhao, D.Y. Yang, W.W. Tan, A preliminary Design of a Superconducting Accelerating Structure for Extremely Low Energy Proton Working in TE210 Mode, SRF 2015, JACoW, Whistler, BC, Canada, 2015.
[73] G. Ciovati, P. Dhakal, A. Gurevich, Applied Physics Letters 104 (2014).
[74] D. Gonnella, R. Eichhorn, F. Furuta, G.M. Ge, T. Gruber, G. Hoffstaetter, J. Kaufman, P. Koufalis, M. Liepe, J. Maniscalco, Improved N-Doping Protocols for SRF Cavities, IUPAC 2016, JACoW, Busan, Korea, 2016, pp. 2323-2326.
[75] A.I.H. Committee, ASM Handbook Properties and Selection: nonferrous alloys and special-purpose materials, ASM International, Materials Park, OH, 1990.
[76] A.I.H. Committee, ASM Handbook Properties and selection: irons, steels, and high-performance alloys, ASM International, Materials Park, OH, 1990.
[77] P.A. Carr, M.D. Norman, V.C. Bennett, Chemical Geology 467 (2017) 122-133.
[78] A. Benninghoven, Angewandte Chemie International Edition Angew. Chem. Int. Ed. Engl 33 (1994) 1023-1043.
[79] C. Reece, H. Tian, Exploiting New Electrochemical Understanding of Niobium Electropolishing for Improved Performance of SRF Cavities, LINAC 2010, JACoW, Tsukuba, Japan, 2010, pp. 779-781.
[80] A.V. Eliutin, K.S. Kovalyov, L.I. Voronenko, L.M. Sevryukova, V.G. Kurakin, H.G. Kurschner, G. Muller, H. Piel, J. Pouryamout, D. Reschke, R.W. Roth, B.A. Sokolov, U. Klein, M. Peiniger, Improved High Purity niobium for superconduction accelerator cavities.pdf, SRF 1991, JACoW, Hamburg, Germany, 1991, pp. 426-432.
[81] A. Grassellino, A. Romanenko, Y. Trenikhina, M. Checchin, M. Martinello, O.S. Melnychuk, S. Chandrasekaran, D.A. Sergatskov, S. Posen, A.C. Crawford, S. Aderhold, D. Bice.
[82] E.M. Lechner, J.W. Angle, M.J. Kelley, A. Palczewski, C. Reece, SIMS Investigation of Furace Baked Nb, SRF 2021, East Lancing, MI, USA, 2021.

[83] J.W. Angle, E.M. Lechner, A.D. Palczewski, C.E. Reece, M.J. Kelley, SIMS Sample Holder and Grain Orientation Effects, SRF 2021, JACoW, East Lansing, MI, USA, 2021, pp. 0-4.
[84] M. Martinello, High-Q High-Gradient TTC Report, TTC 2020, Geneva, Switzerland, 2020.
[85] K. Saito, Development of electropolishing technology for superconducting cavities, in: JACoW (Ed.) 2003 Particle Accelerator Conference, JACoW, Portland, Oregon, 2003, pp. 462-466.
[86] A.C. Crawford, Nuclear Instruments and Methods in Physics Research Section A: Accelerators, Spectrometers, Detectors and Associated Equipment 849 (2017) 5-10.
[87] R. Powers, M.V. Doyle, L. Appl. Phys. 30 (1959) 514.